Fatigue analysis for offshore power cable installation

MSc Thesis report

I.Jonoski

Technische Universiteit Delft

DEME OFFSHORE

TU Delft

Fatigue analysis for offshore power cable installation

MSc Thesis report

by

I.Jonoski

to obtain the degree of Master of Science
at the Delft University of Technology,
to be defended publicly on Thursday June 11th, 2020 at 10:00

Student number:	4325222	
Project duration:	August 21st, 2019 – June 11th, 2020	
Thesis committee:	Prof. ir. A. van der Stap,	TU Delft, chairman
	Dr. ir. E. Lourens,	TU Delft, supervisor
	Ir. J. Willems,	DEME Offshore NL, supervisor

This thesis is confidential and cannot be made public until June 11th, 2025

TU Delft

Abstract

FATIGUE ANALYSIS FOR OFFSHORE POWER CABLE INSTALLATION

Master of Science Offshore and Dredging Engineering
by I.Jonoski

Over the last decade, the demand for offshore power cables has increased significantly due to, in particularly, the emergence of offshore wind. Despite, this growth, industry-wide rules and guidelines to analyse fatigue during cable installation operations are yet to be developed, even though fatigue can become an important parameter in the installation design. Gaining knowledge of fatigue in offshore power cable installation will ultimately improve efficiency and safety of operations.

This thesis report presents a methodology for the fatigue assessment in submarine power cables. In similar offshore operations, for example installation of pipelines or umbilicals, fatigue is assessed based on fundamental fatigue theory like rainflow counting, S-N curves and Miner's rule and therefore these principles form the basis of analysis in this research. However, as opposed to pipelines, submarine power cables consist of numerous layers of different materials that result in complex cable cross-sections. The fatigue behaviour of the cross-sectional elements due to external loads has been investigated to determine a maximum stand-by time during installation operations. In this regard, a cross-sectional analysis was performed to establish the stress-strain response of the individual cable components to the global cable deformations. For bending behaviour, the analysis was shown to be consistent with existing test data. However, this type of data is scarce and the analysis was based on a limited sample size. Moreover, geometrical cross-sectional data of submarine cables is rarely provided by suppliers and hence several assumptions were made in the analysis. For future work, it is recommended to develop in-house test data of cables such that the cross-sectional model can be accurately verified and improved.

Thereafter, the cross-sectional stresses were implemented in a fatigue assessment model, in which the local stresses were calculated based on the output of global modelling software OrcaFle and subsequently analysed with rainflow counting and Miner's rule. The model was applied to three cable types and it was found that lead, used for cable sheaths, is the critical cable component in terms of fatigue. When no lead is used in the power cable, the conductors are the critical component. Furthermore, for mild loading scenarios, i.e. waves with significant wave heights $H_s \leq 1.5$m, the model yields components infinite life for all cable components. For higher load cases, i.e. $H_s \geq 2.5$m, the model showed that fatigue mitigation measures are required to stay within the fatigue budget.

Several mitigation methods were implemented, from which it was found that increasing the layback length of the cable combined with adjusting the vessel heading to favourable conditions most effectively reduces fatigue damage as all load cases with $H_s = 2.5$m resulted in maximum stand-by times of $t_{sb} \geq 125$ days. However, for higher loading senarios, i.e. $H_s = 4$m, all researched mitigation measures were insufficient to stay within fatigue budget. For future work, it is therefore recommended to improve the mitigation measures such that severe load cases can be survived.

Lastly, the wave conditions in this study were simulated as JONSWAP waves. These simulations are time-consuming and therefore not many loading scenarios were modelled. It is recommended to research methods to approximate wave conditions with regular waves, as the duration of OrcaFlex simulations will decrease exponentially. An increase in number of load cases will result in more accurate limit states for the cable components.

Preface

This MSc thesis concludes my education in Offshore & Dredging Engineering at the Delft University of Technology. The entirety of the graduation project was carried out during a nine month internship at DEME Offshore Netherlands. I am thankful for the opportunity and topic that DEME Offshore offered me, leading to a very pleasant experience at their engineering department

At the moment of writing, the Netherlands is suffering from the global pandemic known as COVID-19, which has subsequently lead to a lock-down of Dutch society. Due to this pandemic, the last three months of my graduation project were carried out from home. I would like to thank DEME Offshore for making this possible and their support during these peculiar times. In particular, I would like to thank my company supervisor ir. Joost Willems for his endless energy and optimism in guiding me. The weekly discussions I had with Joost provided both insights and motivation, whether it was in the office or from home.

I would also like to thank the additional members of my committee, Dr. Eliz-Mari Lourens and Prof. Andre van der Stap, for sharing their knowledge and sparking discussions.

On a personal note, I would like to thank my family, my girlfriend Gwen and my close friends Arjan and Jesse for their unlimited support during this thesis.

I.Jonoski
Delft, June 2020

Contents

List of Figures

List of Tables

1

Introduction

Throughout history, numerous failures of structural integrity have been caused by fatigue damage. In fact, fracture of structures or machinery during regular operating conditions have most often been due to fatigue [1]. Notorious examples in the Netherlands include the Bijlmerramp in 1992 [2] and the ICE train accident near Enschede in 1998 [1], making it evident that this type of damage can lead to significant financial losses or even human causalties when projects are not properly engineered, monitored or maintained.

The phenomenon has been elaborately analysed since the industrial revolution. Nevertheless, research into fatigue is ongoing and in many fields open questions regarding fatigue still exist. This is also true for offshore cable installation operations, one of the primary activities of DEME Offshore and the main topic of this thesis.

1.1. Background

With the emergence of offshore renewable energy and in particular offshore wind, the demand for offshore power cables has increased significantly during the last decade. Figure 1.1 shows with this increase, naturally, the vessel demand for (installation) operations also increases.

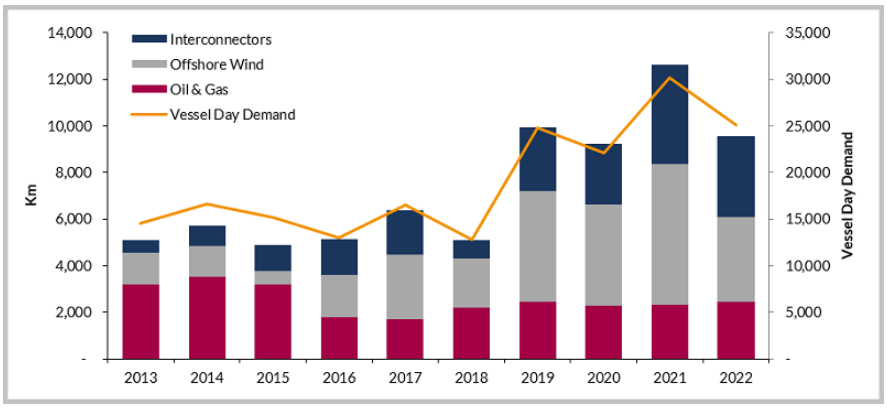

Figure 1.1: Global subsea cable installation outlook by sector and vessel demand, between 2013 and 2022. Image taken from [3]

Despite this growth, industry-wide rules and guidelines to analyse fatigue during cable installation operations are yet to be developed, even though fatigue can become an important parameter in the installation design. During installation, the cable will be free-hanging between the vessel's chute (see section 2.2) and the seabed, resulting in a catenary as can be seen in Figure 1.2. Therefore, it will be subjected to dynamic loading (i.e. waves, currents and vessel motions) for a certain time, and thus exposed to fatigue.
Most commonly, fatigue in installation operation occurs during standby situations, for example when

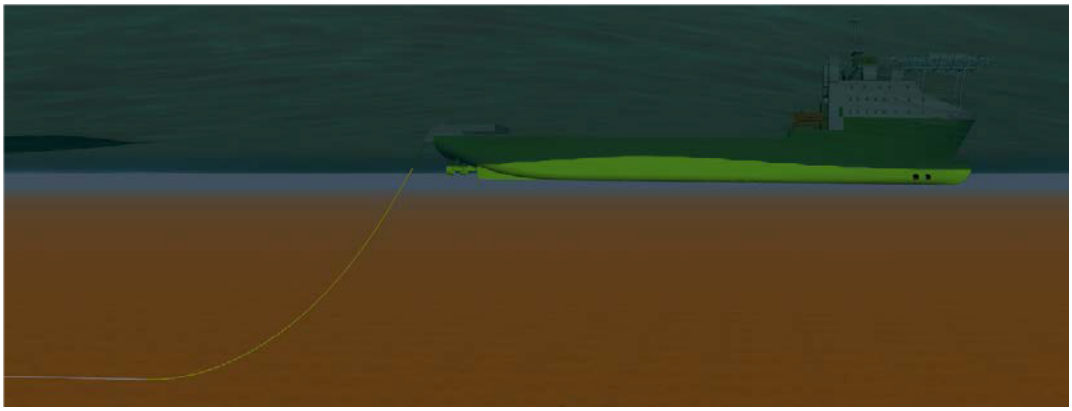

Figure 1.2: Example of a catenary line during cable laying operation. Image taken from [4].

waiting on weather or cable jointing. Needless to say, the fatigue accumulated during these situations must stay within the fatigue budget of the cable and hence a maximum standby period is to be applied. Correlating the loads, type of operations and cable properties to fatigue of the cable is one of the main aims of this thesis and will be elaborated on in the upcoming section.

1.2. Problem statement

As was explained in the previous section, the subsea power cable industry growth calls for insights in fatigue analyses during installation operations. Therefore, the main objective of this thesis is:

To gain both qualitative and quantitative insight in

- *The fatigue limit state during offshore power cable installation,*
- *The mitigation measures to be applied to counter fatigue(i.e. maximize standby time),*

to ultimately establish a methodology for fatigue analyses in cable installation operations.

To fulfill the objective above, a main research question is formulated in the following manner:

Which submarine power cable material properties are limiting from a fatigue point of view and how does this affect cable installation operations?

To succesfully answer this question, the following subquestions have been formulated:

- *How is fatigue assessed in submarine power cable installation operations?*
- *Can a structural model for cross-sectional analysis of a submarine power cable be defined?*
- *Which layer of material of a subsea power cable is most sensitive to fatigue?*
- *Can a model be set up to calculate the maximum standby time dependent on material, operational and environmental properties?*
- *Which fatigue mitigation measures are to be put in place to maximise standby time?*

1.3. Project scope and boundaries

A complete methodology for fatigue assessment in submarine cable would have to take into account all fatigue inducing mechanisms a cable experiences during its lifetime and perform an in-depth structural analysis of the cable with and without mitigation measures. Although the different loading mechanisms (e.g. manufacturing, spooling, hydrodynamic loading, VIV a.o.) and mitigation of fatigue are important aspects for a realistic fatigue assessment, they will be of secondary importance during this thesis project. As Figure 1.3 shows, the main focus of this thesis is understanding fatigue in the cable from a cross-sectional point of view and performing a local structural analysis of the cable. Nevertheless,

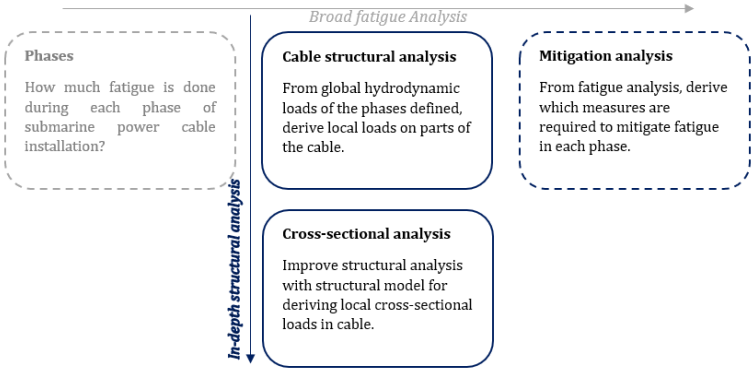

Figure 1.3: The main focus of this thesis will be on the cross-sectional analysis of a submarine power cable.

the local fatigue analysis will subsequently be utilized for defining fatigue limits during global modelling with the software OrcaFlex [5] to relate the local structural model to real-life scenarios and mitigation possibilities.

1.4. Outline

The main structure of this thesis report is based on answering the research subquestions. However, preceding the chapters that will elaborate on the research objective, **Chapter 2** will offer an introduction into submarine power cable installation operations. Its purpose is to familiarize the reader with industry terminology and establish the various parameters that influence operations.

The further outline is as follows:

How is fatigue assessed in submarine power cable installation operations?
Chapter 3 will cover the first subquestion. It will serve as a brief introduction into material science and fatigue and illustrate cable fatigue assessment techniques.

Can a structural model for cross-sectional analysis of a submarine power cable be defined?
The next subquestion is covered in **Chapter 4**. A mechanical cross-sectional analysis is performed, which will form the theoretical base of the structural limits. In addition, the results from the cross-sectional analysis are validated with test data.

Which layer of material of a subsea power cable is most sensitive to fatigue?
Existing fatigue data for various cable materials is examined in **Chapter 5**, which is thereafter combined with the findings from the previous chapters to find the most vulnerable cable material.

Can a model be set up to calculate the maximum standby time dependent on material, operational and environmental properties?
Subsequently, in **Chapter 6** the structural model results will be incorporated in global operational load case models in Orcaflex to be able to answer this subquestion.

Which fatigue mitigation measures are to be put in place to maximise standby time
The final subquestion will be discussed in **Chapter 7**. A mitigation analysis for the most severe operations from Chapter 6 will be performed.

The results of the research are discussed in **Chapter 8** and lastly, conclusions and recommendations are presented in **Chapter 9**.

2

Submarine Power Cable Installation

Submarine power cables have been installed for over a century. In the past, they were mainly used for the power supply to isolated offshore structures like lighthouses or to provide power to near-shore islands. Nowadays, the oil and gas and offshore wind industries give rise to a big part of submarine cable installation activities. Moreover, cable installation projects are very diverse and therefore different types of operations and cables exist . This chapter will serve as an introduction to cable installation projects, touching upon the various operation types, cable types and installation methods.

2.1. Submarine Power Cables

2.1.1. Cable Types

The main difference between cables is the use of either High Voltage Alternating Current (HVAC) or High Voltage Direct Current (HVDC). The advantage of DC cables over AC cables is that they are more efficient for long distance transmission. However, they require an expensive converter at both ends of the cable, making AC cables the typical choice for shorter distances. The breakeven distance between DC and AC is somewhere in the range of 50 to 100 km[6].

Cable Purpose

A cable's design is also determined by its offshore purpose. There are three main types of cable installation projects:

Infield power cables	*The cables used for forming connections between various offshore structures.*
Export power cables	*The cables used for forming a connection between an offshore structure and land.*
Interconnector cables	*The cables used for forming a connection from shore to shore between two land-based electrical systems.*

Infield power cable projects are carried out with HVAC cables due to the relatively short distances between offshore structures, whereas export cables can be HVDC when the offshore structure is far from shore. Although interconnector projects tend to span a long distance and are therefore HVDC, occasionally HVAC cables are used.

2.1.2. Cable Cross-section

Although cable installation projects require specific cable designs, most cables are structured in a similar way. A typical cross-sectional lay-out of AC and DC cables is presented in Figure 2.1. It can be seen that cables have a complex cross-section, consisting of various elements of different materials. These structural elements all serve different functions:

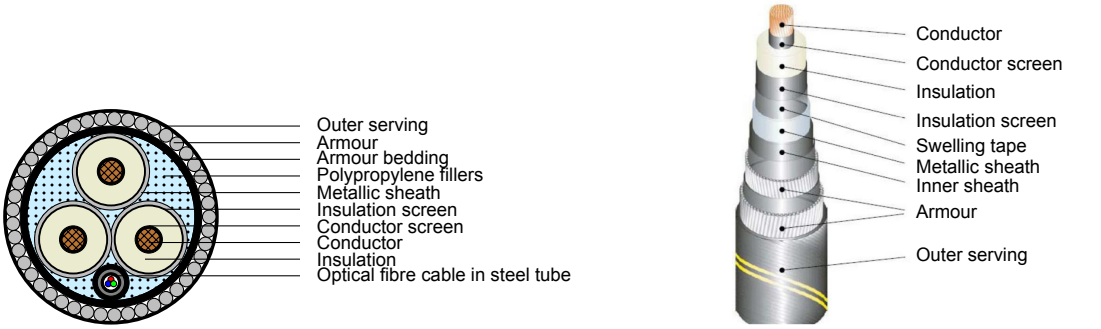

(a) HVAC cable structure

(b) HVDC cable structure. Image taken from [6]

Figure 2.1: Typical cable cross-section of AC and DC cables

Conductor

The conductor is usually comprised of helically wounded stranded wires which are carrying the electrical current. Conductors are made of either copper or aluminium. The main advantage of the more widely used copper conductors is that they have smaller diameters and hence less material in the outer layers is needed. However, copper is heavier and more expensive than aluminium with regards to its current carrying capability and is rapidly being passed in favour of aluminium. For details on the difference between aluminium and copper conductors in submarine power cables and examples of projects with aluminium conductors, see [7]. In HVAC cables, the conductor cores are helically wounded around each other with a certain lay direction (left or right) and lay length, i.e. the length in which the conductor completes one turn. Typical lay lengths for conductor cores are 10 to 30 times the cable diameter.

Insulation

The cable insulation's main purpose is withstanding the potential differences that are present in the cable due to the electrical field. Presently, Cross-Linked Polyethylene (XLPE) is the most popular insulation material for submarine cables. XLPE is preferred over regular polyethylene as the cross-linking of the molecular chains prevents melting at high temperatures.

Conductor & insulation screens

Together with the insulation, the conductor sreen and insulation screen form the dielectric system of the cable. To contain the electric field within the conductor, a layer of semi-conductive tape or extruded XLPE is placed between the insulation and core. Similarly, the insulation screen prevents dielectric losses due to outer layers in contact with the insulation.

Protective sheath

Around the dielectric core of the cable a metallic sheath is applied against water ingression and other mechanical damage and is often combined with water blocking tapes. Additionally, the material of the sheath can influence the dielectric properties of the cable. Due to its straightforward application, guaranteed waterproofing and favourable dielectric properties, lead has become the typical choice of material for sheaths, mostly in the form of thin extruded cylinders. Additionally, lead is heavy, which can sometimes be used to improve cable dynamics. However, lead and its alloys are soft and therefore sensitive to mechanical damages and fatigue. For this reason, increasingly more cables have aluminium or polyethylene sheaths combined with several layers of taping. Nevertheless, for high voltage cables (>150 kV), lead remains the only suitable material due to dielectric properties for containment and alignment of the electric field.

Armour

The cable is surrounded with a metallic armature, providing the cable with tensile stability and mechanical protection. The armour most often consists of stainless steel wires that are helically wounded around the cable. The armouring has great influence on the tensional, torsional and bending stiffness of a cable Typically, armouring wires are 2-8 mm in diameter and the lay length is in the same order of magnitude, but marginally larger than the lay length of the core due to the greater helix radius.

Outer serving
The outer layer of the cable protects the cable from the surrounding environment. It usually consists of polypropylene in combination with bitumen for additional corrosion protection of the armouring. The serving can be either extruded or consist of wound yarn layers.

Fibre optic cable
The cable can have multiple fibre optic cables that are used for data transmission and monitoring purposes (e.g. temperature distribution, cable strain).

The above is based on [8] and [9]

2.1.3. Cable Mechanical Properties

As stated in the previous section, many of the structural elements of a submarine cable are helically wounded around the cable. The helix shapes provide the cable with enough bending flexibility to be capable of absorbing loads due to wave and vessel motions. The helix shapes also invoke a complex dynamic behaviour of the cable due to slipping, see Figure 2.2.

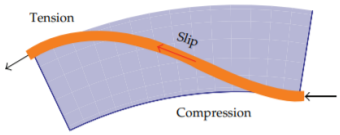

Figure 2.2: Helical geometry slipping around cylinder. Image taken from [10].

Bending stiffness
Namely the bending stiffness of the cable is affected by the helix geometry of the elements. Dominated by stick-slip behaviour between layers, non-linear bending stress vs. curvature hysteresis behaviour is initiated, as seen in Figure 2.3. For low curvatures, the structural components will be subjected to pure

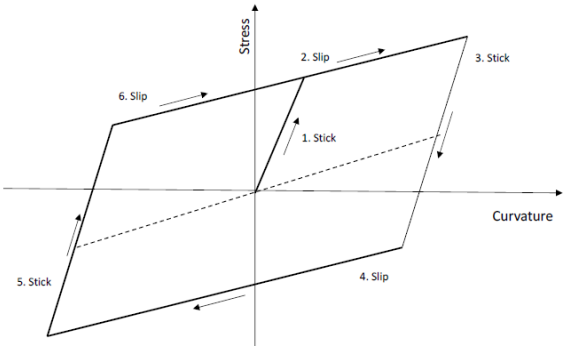

Figure 2.3: Hysteresis shaped bending stress-curvature relationship of a cable composed of helical components. The dotted line represents linear bending. Image taken from [11].

bending stresses and inter-layer friction stresses that result in full stick. As the curvature increases the friction is overcome and the slip regime takes over. When the bending direction is reversed, the same process is repeated. The inter-layer contact friction forces that influence the stick-slip bending behaviour are dependent on the axial tension of the cable and thus bending testing of the cable is needed to describe the bending stiffness.

Axial stiffness
Most of the axial stiffness of submarine cables is determined by the armouring and conductors [8]. While aluminium conductors tend to stay in the elastic region, copper conductors display non-linear stress-strain behaviour under axial tension. Determining the axial stiffness subject to inter-layer contact friction is challenging, especially for copper conductors. However, according to [12], the main contributor to the axial stiffness is the armature: *"Armoured cables can generally be assumed to behave linearly. Both measured cable behaviour and the non-linear governing equations behave in a linear manner over small strains ($\varepsilon < 1\%$) typical of most operating conditions."*

Torsional stiffness
HVAC submarine cables are typically constructed out of three separate conductor cores, which are helically wounded around each other with a given lay direction and length. It is industry practice to wound the likewise helical armour wires in the same lay direction as the cores [8]. This way, when the cable is torqued against the direction of the lay, the armour wires can open up and absorb some of the twisting forces, resulting in a relatively low torsional stiffness. Conversely, when the cable is torqued along the lay direction, the cable will become stiffer, resulting in a torsional stiffness that can be up to three times as high as the stiffness in opposite torque [13]. In some cases, cables have double armatures. The wires in the two layers are then counter rotating for torque balance. A torque-balanced cable will have much less torque developed under tension than a single-armoured cable.

Minimum bending radius
In general, cable manufacturers provide the minimum bending radius (MBR) of the cable. The MBR is the bend radius (Figure 2.4) below which the cable should not be bent to ensure the cable will not be damaged.

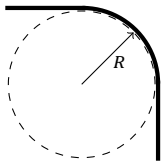

Figure 2.4: Bend radius R of a cable.

Maximum tensile load
When the armour wires are tensioned the radius of the helices reduces and a compressive force is exerted on the layers beneath. A maximum tension should be provided such that no damage to the insulation or conductors occurs.

Side Wall Pressure
The side wall pressure (SWP) on the cable limits its curvature. The side wall pressure is defined as the force the cable is subjected to when being pulled through a bent section and is therefore directly proportional to the tension in the cable. A maximum SWP is generally provided by the cable manufacturer.

2.2. Cable Laying Vessels

Submarine cables are installed by a cable laying vessel (CLV). Cable installation vessels come in many versions, with different cable storage systems and installation methods. A typical layout of a CLV is depicted in Figure 2.5.

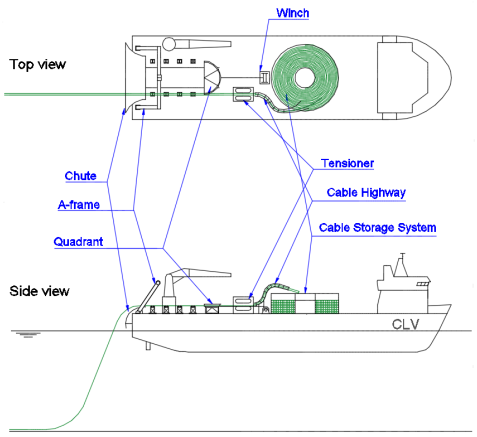

Figure 2.5: Schematical depiction of typical CLV deck layout. Image taken from [6].

2.2.1. Deck Equipment

Cable Storage System

The cable is usually loaded on the vessel by spooling and sometimes by lifting the entire cable at once. The main storage methods are a turntable, carousel, reel or static tank. A turntable is a rotating tank in which the cable is spooled with the help of a load arm, which is the storage system present on DEME Offshore CLV Living Stone. See Figure 2.6. Advantages of the turntable are that is spreads the deck load evenly and the large storage capacity. A carousel is similar to a turntable in storage capacity but

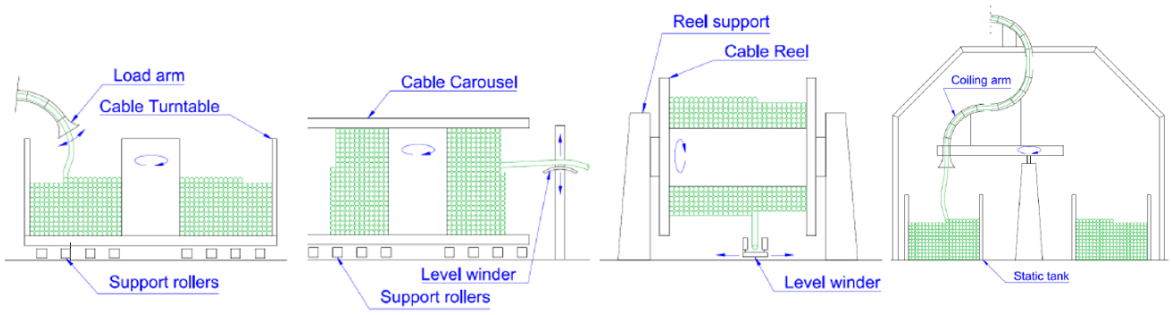

Figure 2.6: Cable storage systems. Image taken from [6].

spooling is more difficult due to gravity. Reels have lower storage capacity and are mostly used for spooling multiple shorter cable segments separately. They can be lifted on the vessel at once and take less deck space. A static tank requires cables that allow torsion and requires a large amount of deck space and is therefore seldomly used.

Cable Highway & Tensioner

The cable highway is used during spooling and unspooling of the cable between the storage system and tensioner to ensure that the MBR-boundary is maintained and no other damage to the cable is done.
A tensioner is required to install the power cable in a controlled manner. The cable is pulled by the tensioner through the highway and controls it during the installation process.

Chute

The chute is a curved guidance rail to overboard the cable from the aft of the vessel without compromising the MBR and the SWP of the cable. The angle at which the cable leaves the chute is an important parameter during installation and is therefore accurately measured during operation: At the departure point from the chute, the cable is not supported anymore and can hence bend around the chute. If not monitored correctly this may lead to cable damage at the departure point.

Quadrant

The quadrant is a half circular device on rails around which the cable can be guided when the power cable needs to lowered to the seabed for safe pull-ins. The quadrant first slides towards the chute and is subsequently turned overboard. It is then lowered to the seabed and tripped to release the cable to the seabed prior to being pulled back up on deck with the help of a crane or A-frame.

2.2.2. Cable Installation

During installation the cable integrity can be ensured by controlling several governing installation parameters, which are defined as:

Chute tension T	*The tension force by the tensioner minus the friction on the cable highway and chute.*
Departure angle α	*The angle at which the cable leaves the chute.*
Touchdown point (TDP)	*The location where the cable touches the seabed.*

The governing parameters can be related to each other by other installation parameters, shown in Figure 2.7. For example, it can be seen that increasing the layback length, the horizontal distance between

the departure point and touchdown point, will increase α and T as well, where α is defined relative to the vertical, as seen in the figure.

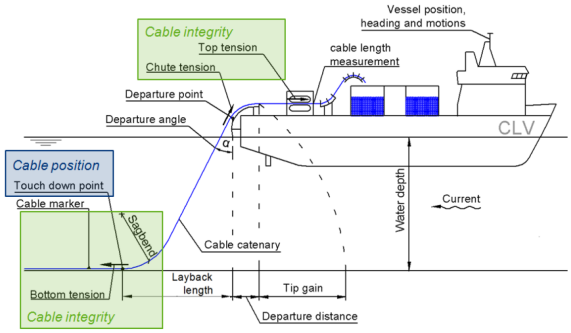

Figure 2.7: Installation parameters overview. Governing parameters are TDP, chute tension and departure angle. Image taken from [6].

2.3. Operation Types

A cable installation project generally consists of several operations, e.g. pull-ins, regular installation, cable jointing, repair etc., varying in required tension and use of the quadrant. The risk of fatigue damage during some of these operations is negligible as the cable is exposed to hydrodynamic loads for a limited time. However, during stand-by periods or breakdowns, one section of the cable is continuously subjected to these loads. The main installation operations that bring risk for fatigue are the jointing of cables and waiting on weather. An elaborated description of all installation operations can be found in [6]

2.3.1. Cable jointing

In some cases two cable ends will have to be jointed together. The cable end is retrieved from the seabed This is done in a jointing container on board of the vessel by a jointing crew from the cable manufacturer. The jointing typically takes up to one week, where the rest of the cable is hanging overboard and is thus subjected to vessel motions.

2.3.2. Waiting on weather

Despite conducting a weather assessment prior to operations, weather can halt the cable installation. Preferably, the CLV will not have to abandon the site and cut the cable but can hold station and continue installing the cable after a certain time period. In this case, the cable will be continuously exposed to hydrodynamic loading. Defining a maximum stand-by time through a fatigue analysis of the cross-section of the cable will optimize the operation when waiting on weather.

2.4. Conclusions

This chapter firstly introduced the interconnector, infield and export submarine power cable types and their corresponding uses. Secondly, the general cross-sectional layout of a submarine power cable was presented, highlighting the most important structural elements.

Thereafter, various mechanical properties of submarine power cables were studied, emphasising the difficulties that arise due to helically wounded geometries, particularly when the cable is subject to bending loads.

Lastly, the operational aspect of cable installation projects was briefly touched upon, presenting a typical Cable Laying Vessel and the operational types that are most likely to induce fatigue damage to a power cable.

3

Fatigue theory

Fatigue has been recognized as an important problem in materials egineering since the early 1800s, when numerous railroad components failed when subjected to repeated loading. Nowadays, it has been estimated that 90% of service failures are caused by fatigue [14] and fatigue research is of greater importance than ever. Therefore, prior to analysing complex cable fatigue, this chapter will serve as a reminder on strength of materials and general introduction to fatigue, providing the reader with an overview of existing fatigue theories and material strength terminology.

3.1. Material properties

3.1.1. Stress-Strain curves

As the name suggests, a material's stress-strain curve gives the relationship between stress and strain. A generic curve for ductile materials is presented in Figure 3.1a. The curve can be divided into two main

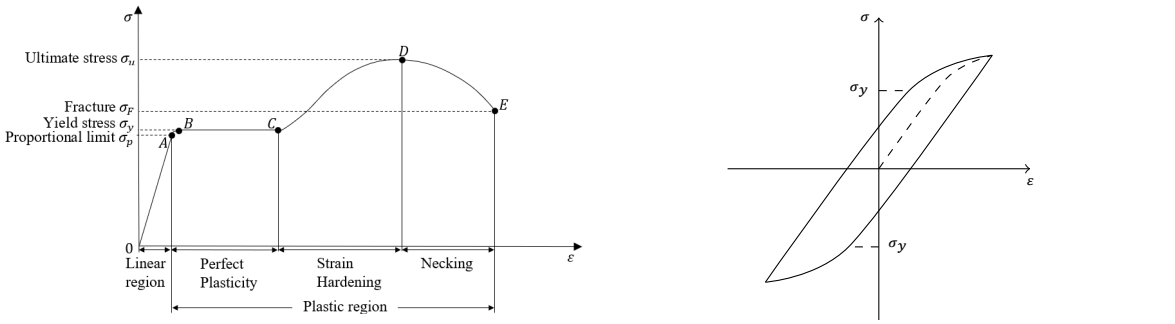

(a) Stress-strain curve, displaying an elastic region (0-B) and a plastic region (B-E). Image taken from [15]

(b) Stress-strain hysteresis loop for a material subject to alternating stress.

Figure 3.1: Stress-strain curves

parts. The first part is called the elastic region, for which the strain of the material will always return to zero over time. The second part is called the plastic region, in which the strain will remain permanent. The point where the curve transitions from the linear to non-linear region is called the proportional limit σ_p. For stresses higher than σ_p yielding occurs. Some materials exhibit a yield stress σ_y for which the strain-stress curve remains horizontal, although this region may also be unnoticeable. The ultimate tensile strength (UTS) σ_u is the maximum tensile stress a material can bear.

Specimens loaded by alternating stresses between tension and compression will exhibit a hysteresis loop when the stresses reach levels above the yield stress, as shown in Figure 3.1b.

3.1.2. Hooke's law

One of the fundamental laws of material science, Hooke's law, has established a linear relationship between the stresses and strains of a material for stresses in the elastic region. For normal stress,

Hooke's law can be written as

$$\sigma = \varepsilon E \tag{3.1}$$

where

- σ Stress [N/m^2].
- E Young's modulus or Modulus of elasticity [N/m^2].
- ε Strain parallel to the axis of material part [-].

Even for low stresses, Hooke's law remains only an approximation as experience has shown that hysteresis always occurs in the stress-strain relationship. Outside of the elastic region the stress-strain relationship becomes non-linear, making it impossible to define a constant Young's modulus and thus, Hooke's law is not applicable.

3.2. Fatigue loading

Following the definition given in [14], fatigue can be defined as:

Fatigue *The process of progressive localized permanent structural change occurring in a material subjected to conditions that produce fluctuating stresses and strains at some point and that may culminate in cracks or complete fracture after a sufficient number of fluctuations.*

The fluctuations described in the above definition can be viewed as cycles. After a certain amount of stress cycles, a crack will start to form in the material. As this process continues, the crack will grow until ultimately the material fractures. Figure 3.2 shows several types of fluctuating stresses, which can be defined by the following terms.

Cyclic stress range $\Delta\sigma$ *The difference between the minimum and maximum stress, i.e.* $\Delta\sigma = \sigma_{max} - \sigma_{min}$

Cyclic stress Amplitude σ_a *Amplitude of the stress cycle, i.e.* $\sigma_a = \frac{\sigma_{max} - \sigma_{min}}{2}$

Mean stress σ_m *Mean stress of the stress cycle, i.e.* $\sigma_m = \frac{\sigma_{max} + \sigma_{min}}{2}$

Stress Ratio R *Ratio between minimum and maximum stress, i.e.* $R = \frac{\sigma_{min}}{\sigma_{max}}$

Most commonly in fatigue theory fully reversed load cycles are used, where the stresses on the material vary periodically and with same amplitude from compression to tension. Sometimes, a mean stress is applied on top of the minimum and maximum stresses, resulting in a repeated stress cycle. The last type of loading shown is an irregular load, which often appears in real-life phenomena.

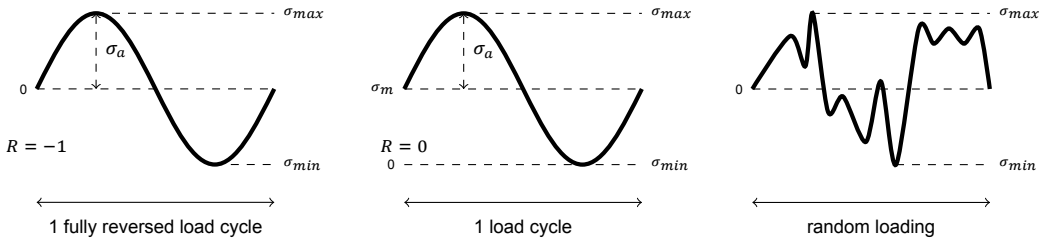

Figure 3.2: Various types of fluctuating stresses.

3.3. Fatigue resistance

3.3.1. S-N curves

Before the study of fatigue had evolved to the microstructural science it is today, engineers were forced to empirically quantify fatigue to formulate design criteria. The single-most important concept that was developed, was the so-called S-N curve or Wöhler curve, named after German railway engineer August Wöhler. S-N curves are derived by applying a constant cyclic stress amplitude σ_a to a material

specimen to determine the amount of cycles N before failure. The fatigue strength σ_{FS} is then defined as the value of stress at which failure occurs after N_F cycles. Two types of S-N curves are shown in Figure 3.3.

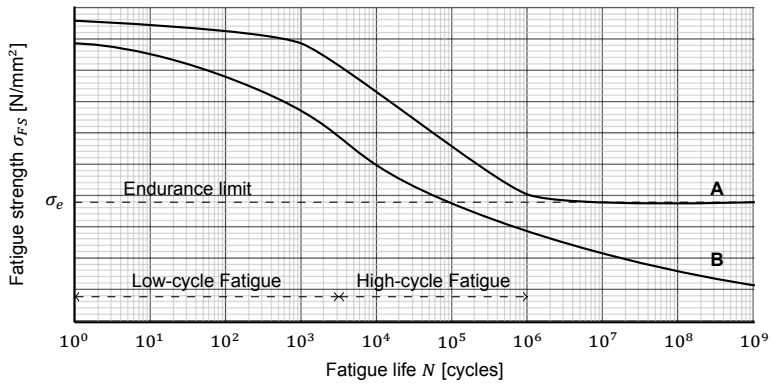

Figure 3.3: Typical S-N curves. Curve A exhibits an endurance limit, below which the material does not fail. Curve B displays continuous decreasing S-N behavior.

Certain materials, most notably ferrous metals like steel, exhibit S-N curves similar to curve A, that flatten out after approximately 10^6 to 10^7 cycles, such that failure will never occur below the so-called endurance limit σ_e. Hence, these materials are said to have infinite fatigue life below the endurance limit. On the other hand, Curve B is characteristic for non-ferrous metals, most notably aluminium and copper, displaying continuously decreasing S-N curves such that no endurance limit can be defined. For these materials the region after $N = 10^6$ is sometimes referred to as the gigacycle fatigue.

3.3.2. Mean-correction criteria

Most S-N curves are derived by applying fully reversed loading on the material component. Consequently, the lifetime of a material will be different when a non-zero mean stress load is applied to it. A negative mean stress (compression) will extend the fatigue life, while a net tension will shorten the fatigue life. Instead of deriving S-N curve data for every load scenario to account for mean stress, the modified Goodman diagram shown in Figure 3.4a has the mean stress plotted against stress and consists of the lines constructed from the mean stress at failure (yielding) to the endurance limit above and below the origin. The bold lines in the diagram thus indicate how the endurance limit changes with increasing mean stress, until it matches the yields. All stress ranges outside the bold parts will invoke finite fatigue life, whereas stress ranges inside it will have infinite life. Thus, using the modified Goodman diagram, a non-zero mean stress history can be related to a zero mean stress history.
Using this, a modified Goodman criterion for failure can be established as

$$\frac{\sigma_a}{\sigma_e} + \frac{\sigma_m}{\sigma_u} = 1 \tag{3.2}$$

where

σ_a Stress amplitude [MPa].
σ_e Endurance limit [MPa].
σ_m Mean stress[MPa].
σ_u Ultimate Tensile Strength [MPa].

The Goodman criterion can be differently visualised in a Haigh diagram, shown in Figure 3.4b, where the mean stress is plotted against the alternating stress amplitude. This gives straight line for the modified Goodman relation, below which a material experiences infinite life. The area above it indicates finite fatigue life.
Furthermore, the figure shows a parabolic criterion called the Gerber failure criterion which can be defined as

$$\frac{\sigma_a}{\sigma_e} + \left(\frac{\sigma_m}{\sigma_u}\right)^2 = 1 \tag{3.3}$$

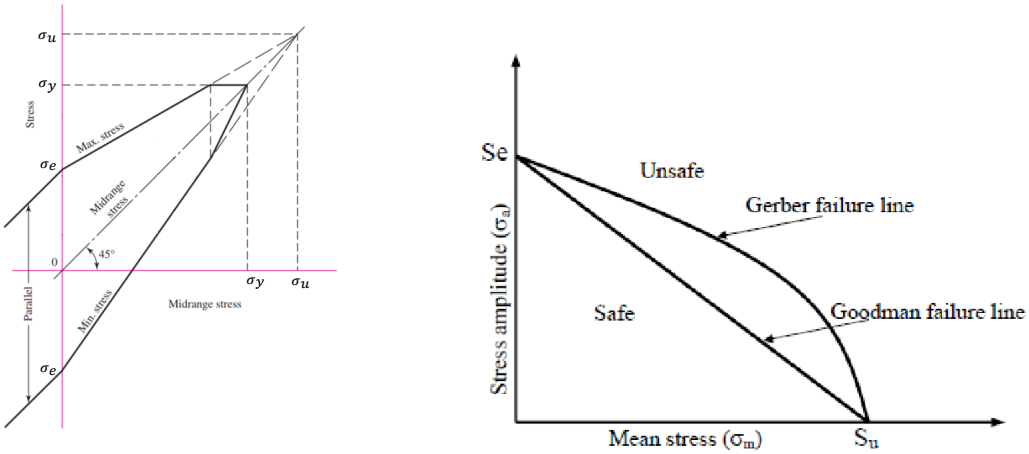

(a) Modified Goodman diagram for mean stress fatigue failure. All stress levels within thick lines have infinite life. Image taken from [16].

(b) Haigh diagram, indicating the Gerber parabolic failure criterion and the Goodman failure criterion. Image taken from [17].

Figure 3.4: Mean stress fatigue failure criteria

Material data tends to fall closer to the Gerber criterion than the conservative Goodman criterion. However, in practice both criteria are widely used due to the linearity of Goodman. There are several other established failure criteria which will not be discussed in this thesis.

It should be noted that the Gerber and Goodman criteria can be used for dealing with a mean stress by correcting the random load to a zero mean stress. This is achieved by defining an effective stress amplitude σ_{eff} and substituting it for the endurance limit σ_e in Equations 3.2 and 3.3, yielding a zero-mean stress with amplitudes

$$\sigma_{eff,Goodman} = \sigma_a \frac{\sigma_u}{\sigma_u - \sigma_m} \tag{3.4}$$

$$\sigma_{eff,Gerber} = \sigma_a \frac{\sigma_u^2}{\sigma_u^2 - \sigma_m^2} \tag{3.5}$$

3.3.3. Basquin's equation

In the above, S-N curves were treated as empirically derived data for materials. However, in 1910 Basquin proposed a mathematical equation to represent the S-N curve part prior to the endurance limit (i.e. $N < 10^6$). Basquin's equation is given by

$$S = aN^b \Leftrightarrow \log(S) = \log(a) + b\log(N) \tag{3.6}$$

where b is the slope of the straight line in the log-log plot and is referred to as the Basquin slope. It can be calculated by

$$b = \frac{-(\log(S_1) - \log(S_2))}{\log(N_2) - \log(N_1)} \tag{3.7}$$

where S_1 and S_2 are two stress values with corresponding cycle values N_1 and N_2. Most often $S_1 = 0.9\sigma_u$ is used as an approximation at $N_1 = 10^3$ and $S_2 = \sigma_e$. As the values for σ_u and σ_e are usually known or can be found relatively easy for materials and structures, Basquin's equation is widely used to establish S-N curves.

3.4. Palmgren-Miner linear damage hypothesis

The previous two sections discussed the types of loads that a material can be subjected to and the material's resistance to these loads, respectively. The next step is to connect the latter and former to determine how much damage is done to the material by a given loading. The Palmgren-Miner linear damage hypothesis or Miner's rule is one of the oldest, simplest and most used methods used to calculate material damage due to fatigue loads. Furthermore, Miner's rule takes into account damage

by different stress magnitudes and accumulates these to a total damage. The hypothesis states that failure will occur when

$$D = \sum_{i=1}^{k} \frac{n_i}{N_i} = 1 \tag{3.8}$$

where

- D Total damage [-].
- k Number of different stress magnitudes [-].
- n_i Number of cycles subject is exposed to at a certain load σ_i [-].
- N_i Number of cycles at a certain load σ_i after which failure will occur [-].

It is evident that D is nothing more than a fraction or percentage of the fatigue life with failure occurring when it reaches 1. The value of N_i is determined with the use of an S-N curve. Given the uncertainty of the curve data, Miner's rule will always have to be employed with a safety factor. In addition to the uncertainty, the rule itself has several limitations. It assumes linearity, such that the damage due to the first cycle is the same as for a cycle occurring at $D = 0.99$. Furthermore, there is not a single definition of failure. Some S-N curves may have been derived by testing until complete fracture, while others maintained a crack growth as definition of failure. Miner's rule does not account for this.

Naturally, D should not become 1 during the installation of the cable. The exact limiting value for D, including safety factor will be further discussed in Chapter 4.

3.5. Rainflow Counting Algorithm

For fully reversed fatigue loading it is straightforward to count the total number of cycles that a structure endures. In real-life phenomena however, the loads on a structure are not often fully reversed but appear to be random and irregular, making cycle counting non-trivial. A method to overcome this problem was proposed in 1968, when T. Endo and M. Matsuishi developed a damage evaluation algorithm for random loading on metals. The basic idea of the algorithm is associating a stress time history to closed hysteresis loops in the stress-strain behaviour of the material in order to define full load cycles. In some cases, hysteresis loops are not closed, resulting in residual half-cycles, as illustrated in Figure 3.5.

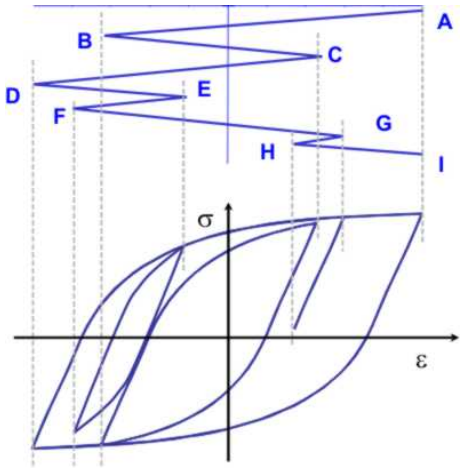

Figure 3.5: RFC is linked to the number of closed stress-strain hysteresis loops. Half-cycle counts correspond to open hysteresis loops. Image taken from [18].

The algorithm is a sequence of rules to find closed hysteresis loops efficiently that was inspired by rain dripping from Japanese pagoda roofs and hence was called Rainflow Cycle Counting (RFC). A detailed definition of RFC, including example, can be found in Figure 3.6.

Rainflow cycle counting algorithm

For a given random load time history execute the following sequence of rules:

1. Reduce the original time history of the loading to a sequence of compressive valleys and tensile peaks.

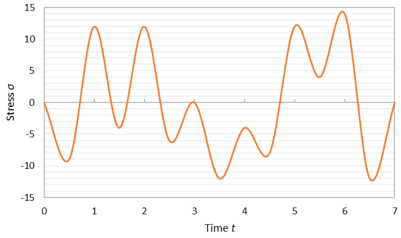

(a) Random load time history

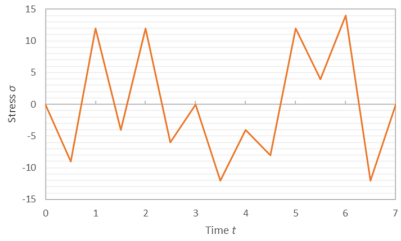

(b) Step 1: Reduce time history to peaks and valleys

2. Rotate the time history 90° such that time is increasing towards the bottom. Imagine each peak and valley is the tip of a pagoda roof from which rain can flow down.

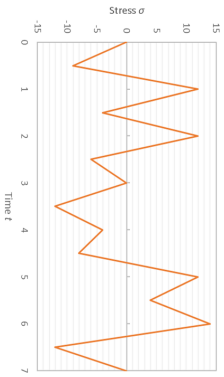

(c) Step 2: Rotate time history 90°

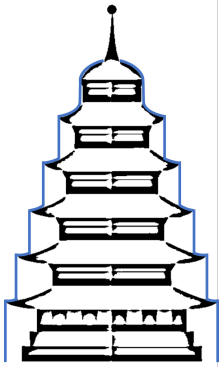

(d) Step 2: The rainflow method was inspired by rain dripping down a Japanese pagoda.

3. Draw rainflow obedient to the following:
   - Flow terminates when an opposite tensile peak has greater or equal absolute magnitude.
   - Flow terminates when it merges with a flow that started at an earlier peak.
   - Flow terminates when it reaches the end of the time history.
4. Repeat step 3 for compressive valleys.

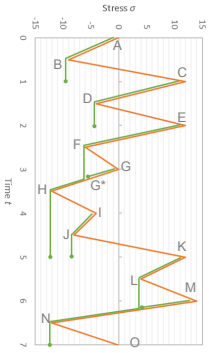

(e) Step 3: Tensile rainflow

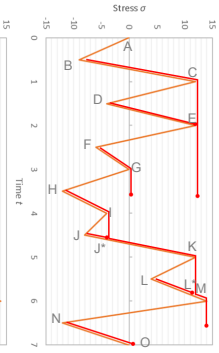

(f) Step 4: Compressive rainflow

5. Determine the magnitude of stress difference between the start and end of a flow.

Tensile Peaks				Compressive Valleys			
From	To	Range [MPa]	Cycles	From	To	Range [MPa]	Cycles
A	B	9	Half	B	C	21	Half
C	D	16	Half	D	E	16	Half
E	H	24	Half	F	G	6	Half
G	G*	6	Half	H	M	26	Half
I	J	4	Half	J	J*	4	Half
K	L	8	Half	L	L*	8	Half
M	N	26	Half	N	O	12	Half

(g) Step 5: Determine flow stress ranges

6. Couple flows of equal magnitude but opposite sense to form full loading cycles. Typically, unpaired reversals will still be present.

Cycle Pairing	
Stress [MPa]	Cycles
4	Full
6	Full
8	Full
9	Half
12	Half
16	Full
21	Half
24	Half
26	Full

(h) Step 6: Couple half-cycles

Figure 3.6: Rainflow Counting algorithm

Miner's rule can be used subsequently to RFC to yield the fraction of damage by the random stress history. There are several techniques for treating the damage contribution by the remaining half-cycles.

While they are sometimes ignored altogether and sometimes counted as full cycles, the recommended practice is to count them as half-cycles [19]. For the half cycles, Miner's rule thus becomes

$$D = \sum_{i=1}^{k} \frac{1}{2N_i} \tag{3.9}$$

RFC is widely regarded as the best estimator of fatigue life and as a consequence there have been several proposals for counting algorithms based on RFC. In 1987, I. Rychlik published a new, analytical definition of rainflow cycle counting [20], which presently is widely implemented and is also used by OrcaFlex [5].

3.6. Fatigue inducing mechanisms

A variety of processes have effect on the fatigue budget of a cable. Apart from installation operations, fatigue may be induced during manufacturing and during the loading of the cable on the vessel due to friction and bending.

Furthermore, vortex-induced vibrations (VIV) due to the current may arise in operations and can have a consequential impact on the fatigue life of the cable; as opposed to manufacturing, onloading and lifecycle loads, it gives rise to high-cycle fatigue. It is recommended by [11] to include VIV in (global) fatigue analyses of submarine cables. However, although VIV fatigue is a risk factor, the main scope of this thesis is the local cross-sectional response of a submarine cable to fatigue which will be derived by considering only loads due to wave, current and vessel motions. Hence, VIV will not be discussed any further.

3.7. Conclusions

In this chapter an introduction to fatigue theory was presented. Basic material science like Hooke's law and stress-strain curves were briefly introduced as the base for fatigue theory. The concepts presented here will be used in the fatigue calculation for cable installation operations in this thesis.

- Existing S-N curves for the various materials in a cable cross section will be used to define material limits for the cable. These can be in tabulated form or defined by Basquin's equation.
- Depending on the S-N data, either the Goodman, Gerber or no mean correction method will be implemented.
- Rainflow cycle counting can be used when analysing irregular wave loads on the cable during installation.
- Miner's rule will be used for determining the total damage done to each of the materials in the cable cross section to determine the weakest link of the cable.

4

Cross-Sectional Analysis

As mentioned earlier, for submarine cables the bending flexibility that is required for smooth operations is achieved by arranging the structural elements in a helix geometry. The helical shapes allow the elements to slip and hence release axial stresses, making the cable compliant in bending while still being stiff in tension. However, the main disadvantage of the helices is that a complete stress analysis of the cable is difficult to perform as the cross-section of the cable is very complex. In addition to helical elements, there are cylindrical elements like the metallic sheath for protection.
This chapter will elaborate on the mechanics of the cable elements. From geometrical properties of helices and cylinders an analytical expression of strains, stresses and moments will be derived for both bending and axial-torsional loading. The resulting expressions will then be used to describe the cross-sectional stresses and moments in the cable. Based on the mechanical description of the cable elements, the parts of the cable that are most sensitive to fatigue will be defined.

4.1. Model Assumptions

The main goal of the cross-sectional analysis performed in this chapter is to determine the stresses in all interior elements of the submarine cables for a given external loading. As a first step, the deformation the cable is exposed to is considered. Three types of strains contribute to the deformation of the cable: Elongation ε, twisting τ and bending curvature κ. The following two main assumptions about these strains form the basis of the cross-sectional analysis presented in this section:

1. Coupling effects of bending to axial and torsional loads are little [21] and thus it is possible to distinguish two separate load models [10], as depicted in Figure 4.1:
    - Bending model, taking into account cross-sectional bending.
    - Axis-symmetrical model, taking into account tension, torsion and contact pressures.
2. Elastic stresses are assumed, i.e. Hooke's law applies.

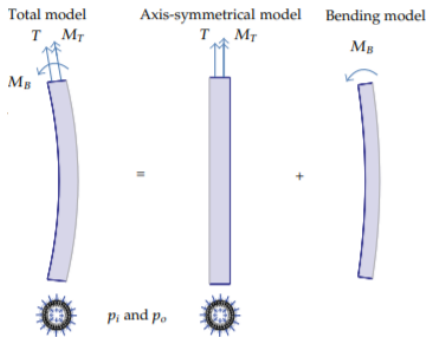

Figure 4.1: The total model composes of an axis-symmetrical and bending model. Image taken from [10]

4.2. Cylindrical elements

4.2.1. Axis-symmetrical model

To determine the stresses and strains on a cylindrical element inside a submarine cable, the approach from [22] will be followed. Figure 4.2 shows a wall section of a cylindrical element of a submarine power cable. When the element is considered to be in an equilibrium in all directions, the equations describing the stresses are given by

$$\begin{aligned} \frac{\partial \sigma_x}{\partial x} + \frac{\partial \tau}{\partial \theta} &= 0 \\ \frac{\partial \sigma_\theta}{\partial \theta} + \frac{\partial \tau}{\partial x} &= 0 \\ \sigma_\theta t_c &= (q_{in} - q_{out})R \end{aligned} \tag{4.1}$$

where

θ	Polar angle for cylindrical elements, positive from y-axis to radial direction [rad].
R	Radius of the cylinder [m].
q_{in}	Inner surface pressure [MPa].
q_{in}	Outer surface pressure [MPa].
t_c	Thickness of the cylinder [m].
σ_x	Axial stress [MPa].
σ_θ	Circumferential stress [MPa].
τ	Shear stress [MPa].

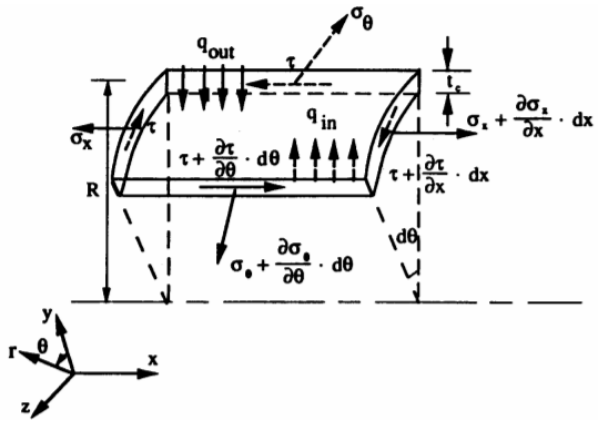

Figure 4.2: Wall section of a cylindrical element. Image taken from [22].

It should be noted that Equation 4.1 was derived under the assumption that there are no internal moments in the wall section. In addition, only first-order terms are taken into account.

Any combination of constant axial, circumferential and shear stress yields a solution to the equation. In the case the cylinder is subject to an axial force F and a twisting moment M_t, the boundary conditions for the stresses are thus straightforwardly given by

$$\begin{aligned} \sigma_x &= \frac{F}{2\pi R t_c} \\ \sigma_\theta &= \frac{q_{in} - q_{out}}{t_c} R \\ \tau &= \frac{M_t}{2\pi R^3 t_c} \end{aligned} \tag{4.2}$$

The stress-strain equations can be expressed by elasticity theory in the form of Hooke's generalised

law for isotropic materials:

$$\begin{aligned}\varepsilon_x &= \frac{1}{E}(\sigma_x - \nu\sigma_\theta - \nu\sigma_r)\\ \varepsilon_\theta &= \frac{1}{E}(\sigma_\theta - \nu\sigma_x - \nu\sigma_r)\\ \varepsilon_r &= \frac{1}{E}(\sigma_r - \nu\sigma_\theta - \nu\sigma_x)\\ \gamma &= \frac{1}{G}\tau\end{aligned} \tag{4.3}$$

where

- ε_x Strain in the axial direction [-].
- ε_θ Strain in the circumferential direction [-].
- ε_r Strain in the radial direction [-].
- γ Shear strain in plane [-].
- σ_r Stress in the radial direction [-].
- E Young's modulus [MPa].
- G Shear modulus [MPa].
- ν Poisson's ratio [-].

When uniform deformations are assumed, the strains of the element can be expressed as

$$\begin{aligned}\varepsilon_x &= \frac{\Delta L}{L}\\ \varepsilon_\theta &= \frac{-\Delta R}{R}\\ \varepsilon_r &= \frac{\Delta t}{t_c}\\ \gamma &= \phi R\end{aligned} \tag{4.4}$$

where

- L Length of the element [m].
- ΔL Axial deformation of the element [m].
- ΔR Constriction of the cylinder [m].
- Δt Change in thickness of the element [m].
- ϕ Twisting angle per unit length [$\frac{\text{rad}}{\text{m}}$].

In the above the radial stress, or out-of-plane stress, σ_r was introduced. As the inner and outer surface pressures q_{in} and q_{out} acting on the element are non-zero, σ_r is zero only when the magnitude of the surface pressures is equal. An analytical derivation of the radial stress in terms of the contact pressures is non-trivial and is therefore assumed to be constant throughout the thickness of the element and equal to the average contact pressure:

$$\sigma_r = \frac{1}{2}(q_{in} + q_{out}) \tag{4.5}$$

Rewriting Equation 4.3 yields the following expressions for the principal stresses in the element

$$\begin{aligned}\sigma_x &= \frac{E(1-\nu)}{(1+\nu)(1-2\nu)}\left[\varepsilon_x + \frac{\nu}{1-\nu}(\varepsilon_\theta + \varepsilon_r)\right]\\ \sigma_\theta &= \frac{E(1-\nu)}{(1+\nu)(1-2\nu)}\left[\varepsilon_\theta + \frac{\nu}{1-\nu}(\varepsilon_x + \varepsilon_r)\right]\\ \sigma_r &= \frac{E(1-\nu)}{(1+\nu)(1-2\nu)}\left[\varepsilon_r + \frac{\nu}{1-\nu}(\varepsilon_\theta + \varepsilon_x)\right]\\ \tau &= G\gamma\end{aligned} \tag{4.6}$$

Subsequently substituting Equations 4.2, 4.4 and 4.5 in Equation 4.6 establishes relations between the

external forces F, q_{in}, q_{out} and M_t and strains on the cylindrical element.

$$\begin{aligned} F &= \frac{2\pi R t_c E(1-\nu)}{(1+\nu)(1-2\nu)}\left[\varepsilon_x + \frac{\nu}{1-\nu}\left(\frac{\Delta t}{t_c} - \frac{\Delta R}{R}\right)\right] \\ q_{out} - q_{in} &= \frac{t_c E(1-\nu)}{(1+\nu)(1-2\nu)}\left[\frac{\Delta R}{R} - \frac{\nu}{1-\nu}\left(\varepsilon_x + \frac{\Delta t}{t_c}\right)\right] \\ q_{out} + q_{in} &= \frac{2E(1-\nu)}{(1+\nu)(1-2\nu)}\left[\frac{\Delta t}{t_c} + \frac{\nu}{1-\nu}\left(\varepsilon_x - \frac{\Delta R}{R}\right)\right] \\ M_t &= 2\pi R^3 t_c G\phi \end{aligned} \tag{4.7}$$

Now that the stress-strain relationship for cylindrical elements has been established for the axis-symmetrical case, the following section will examine the bending stresses on the cylindrical layers.

4.2.2. Bending model

The cylindrical layers of a submarine power cable are in essence hollow cylinders and thus the bending stress can be derived from Euler-Bernoulli beam theory. The general formula for determining the bending stress σ_b in any beam is

$$\sigma_b = \frac{My}{I} = \frac{M}{Z} \tag{4.8}$$

where

- M Bending moment about the neutral axis [Nm].
- y Perpendicular distance to the neutral axis [m].
- I Second moment of area about the neutral axis [m^4].
- Z Section modulus, $Z = \frac{I}{y}$, [m^3].

Equation 4.8 is only valid in the elastic region, i.e. when the stress is below the yield stress. As stated earlier, linearity has been assumed in this chapter, permitting the use of the equation.

It is clear that the bending stress is maximum when the distance to the neutral axis y is at a maximum as well. For a hollow cylinder this distance y_{max} is given by $y_{max} = R = \frac{D}{2}$ where D is the outer diameter of the cylinder, see Figure 4.3. The second moment of area and corresponding section modulus of a hollow cylinder are given by

$$I = \frac{\pi}{64}\left(D^4 - d^4\right) \Rightarrow Z = \frac{I}{y} = \frac{\frac{\pi}{64}\left(D^4 - d^4\right)}{R} \tag{4.9}$$

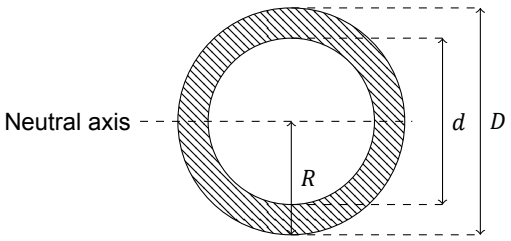

Figure 4.3: Hollow cylinder cross section with outer diameter D and inner diameter d. The maximum distance to the neutral axis is given by $y_{max} = R = \frac{D}{2}$.

The bending moment contributed by the cylindrical layers are linear and given by [23]

$$M = EI\kappa \tag{4.10}$$

where $\kappa = \frac{1}{R_{bend}}$ is the bending curvature. Substituting Equation 4.9 and 4.10 in Equation 4.8 yields the following maximum bending stress for the cylindrical elements of submarine power cables

$$\sigma_{b_{max}} = \frac{My_{max}}{I} = \frac{EI\kappa R}{I} = ER\kappa \tag{4.11}$$

4.3. Helical elements

4.3.1. Helix geometrical configuration

Figure 4.4 depicts the geometrical configuration of a helix element, which can be uniquely defined by the pitch length L_p and helical radius R. The lay angle α can then be defined as

$$\alpha = \arctan\left(\frac{2\pi R}{L_p}\right) \tag{4.12}$$

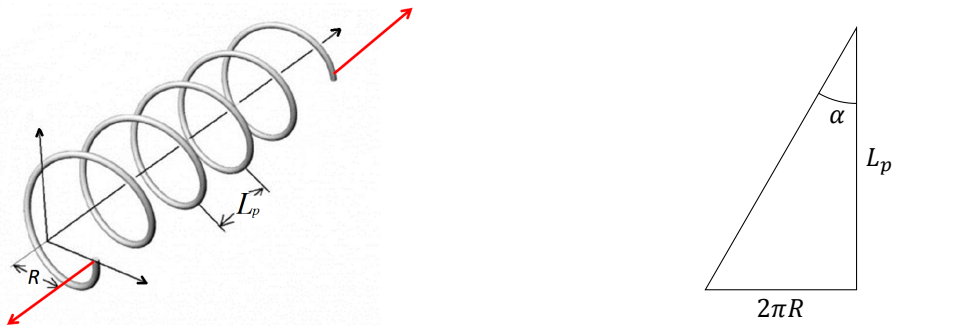

(a) Helix with pitch radius R and pitch length L_p. Image taken from [24]

(b) Lay angle or pitch angle α of a helix. Image taken from [21]

Figure 4.4: Helix geometrical properties

When considering an arbitrary point p on a helical strip as shown in Figure 4.5, its location vector $\mathbf{r}$ can be described as

$$\mathbf{r} = R\cos\theta\hat{\mathbf{x}} + R\sin\theta\hat{\mathbf{y}} + \frac{R\theta}{\tan\alpha}\hat{\mathbf{z}} \tag{4.13}$$

where

$[\hat{\mathbf{x}}, \hat{\mathbf{y}}, \hat{\mathbf{z}}]$ Unit vectors of the coordinate system with origin in the center of the element [-].
θ Polar angle of the considered helix cross-section [rad].

The polar angle θ can be determined by

$$\theta = \frac{2\pi k}{n} + z\frac{\tan\alpha}{R} \quad \text{[25]} \tag{4.14}$$

where

k Index of the helix for which strain is assessed [-].
n Total number of helices in the cable layer considered [-].
z Axial distance of point p from the origin [m].

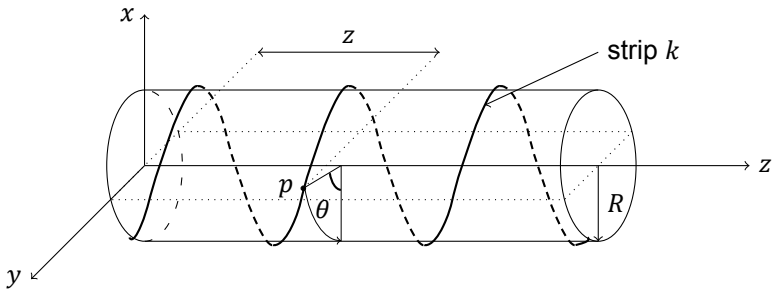

Figure 4.5: Helical strip on a cylinder with arbitrary point p.

Now that the helix geometry and terminology is in place,the axial and torsional strains on helical elements in submarine power cables will be analysed.

4.3.2. Axis-symmetrical model

The content of this section is confidential and will not be made public.

4.3.3. Bending model

The content of this section is confidential and will not be made public.

4.4. Verification and validation

The content of this section is confidential and will not be made public.

4.5. Conclusions

The theoretical analysis performed in this chapter has yielded local loads on the components of a cable cross-section subject to global tension and curvature loads. Under the assumptions of linear stress-strain behaviour and independence of bending and axial/torsional loads, the local stresses and bending moment were derived for cylindrical and helical elements as presented in Table 4.1 and Table 4.2. It was shown that the helical elements do not behave linearly in bending but exhibit a full-stick and full-slip regime, dependent on the cable curvature. The respective loads for full-stick and full-slip are presented in Table 4.2 as well. Furthermore, the expressions for helical elements in bending were fitted against

Table 4.1: Overview of local cross-sectional loads for cylindrical elements in a cable subject to global elongation ϵ, twist τ and curvature κ.

Local load	Cylindrical element	Eq.
Axis-Symmetrical stress	$\sigma_x = \frac{E(1-\nu)}{(1+\nu)(1-2\nu)}\left[\varepsilon_x + \frac{\nu}{1-\nu}(\varepsilon_\theta + \varepsilon_r)\right]$ $\sigma_\theta = \frac{E(1-\nu)}{(1+\nu)(1-2\nu)}\left[\varepsilon_\theta + \frac{\nu}{1-\nu}(\varepsilon_x + \varepsilon_r)\right]$ $\sigma_r = \frac{E(1-\nu)}{(1+\nu)(1-2\nu)}\left[\varepsilon_r + \frac{\nu}{1-\nu}(\varepsilon_\theta + \varepsilon_x)\right]$ $\tau = G\gamma$	4.6
Bending stress	$\sigma_{b,cylinder} = ER\kappa$	4.8
Bending Moment	$M_{b,cylinder} = EI\kappa$	4.10

Table 4.2: Overview of local cross-sectional loads for helical elements in a cable subject to global elongation ϵ, twist τ and curvature κ.

The content of this section is confidential and will not be made public.

available bending moment vs. curvature responses of four HVAC export cables by minimising the RMS error, yielding results listed in Section 4.4. Although the data and theoretical derivations for bending behaviour were consistent with each other, the RMS error was substantial. This is explained by the modelling assumption that only full-stick and full-slip regimes exist, while the test data depicts a smooth transition phase between full-stick and full-slip.

Despite the consistent results in bending behaviour, it must be concluded that more test data of cables is required to sufficiently verify the validity of the cross-sectional axis-symmetrical stresses.

5

Material data

Now that the local stresses in the cable cross-section can be evaluated, they can be linked to fatigue damage through S-N data of the corresponding material. Again, the focus will be on the metallic parts of the cable, i.e. armour wires, conductors and metallic protective sheaths, as their failure is critical for cable function, whereas fracture of fillers and most tapes is less influential on the cable integrity due to their high flexibility. Furthermore, finding data that corresponds to the exact material that is used in a submarine power cable is virtually impossible. Firstly, many manufacturers do not provide details on which metal alloys have been used during fabrication of the cable. Secondly, the probability that S-N data has been derived from a specimen of that material is little. Taking this into consideration, the following will present available S-N data of the cable components.

5.1. Conductor

As mentioned earlier, the two main materials used in submarine power cable conductors are copper and aluminium. Unfortunately, none of the cables used in the bending analysis specify its conductor alloy, which means the S-N curve for aluminium and copper will be based on general material data.

5.1.1. Copper

The most used copper alloys in high conductivity applications are the so-called Electrolytic-Tough-Pitch (Cu-ETP) and Oxygen-Free (Cu-OF) types. Both alloys are high-purity coppers with copper levels of at least 99.9% and 99.95% respectively and their fatigue properties are similar, as demonstrated in [26]. An S-N curve corresponding to the test data of an unnotched specimen of oxygen-free copper is presented in Figure 5.1. which will henceforth be used to define the fatigue limits of the copper conductors in submarine power cables.

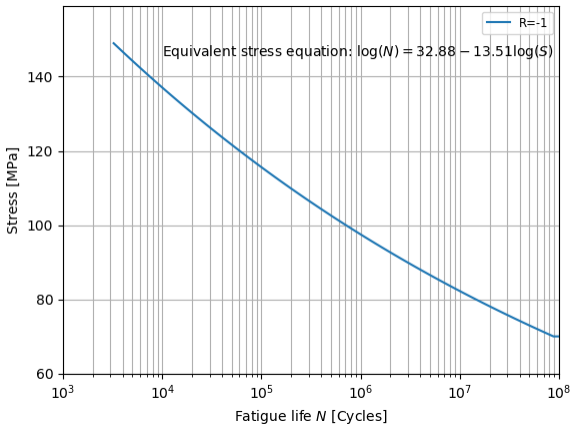

Figure 5.1: S-N curve for oxygen free copper. Data taken from [27].

5.1.2. Aluminium

Aluminium has a wide variety of alloys and applications. For high voltage cable conductors the typical choice is alloy Al-1350, with an Al level of at least 99.5%, due to its high electrical conductivity [7]. Various S-N curves exist for Al-1350 specimens and can be found in [28]. In Figure 5.2, S-N data of an Al-1350-H39 wire specimen is presented, which will be used to determine the fatigue limits of the aluminium conductor.

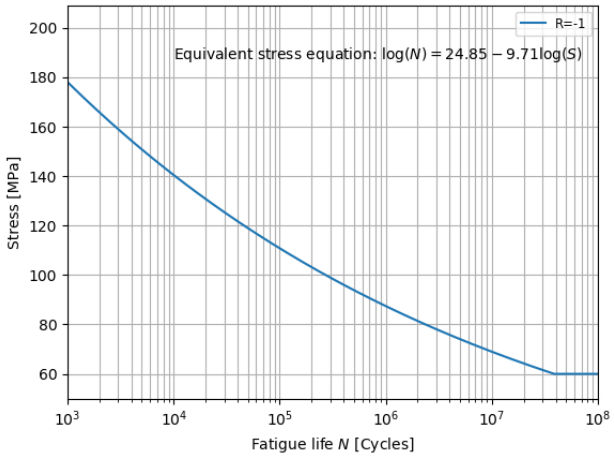

Figure 5.2: S-N curve for smooth Al-H39 wire specimen. Data taken from [28].

5.2. Armour

Most often, armour wires are made out of stainless steel to provide the cable with tensile stability and protect it against mechanical damage. However, to reduce the weight of the cable, in some instances part of the armouring is made out of plastic wires. As can be seen in Table **??**, this is the case for Cable 3 and Cable 4.

5.2.1. Stainless Steel

For Cables 3 and 4, the type of stainless steel used in the armature has been specified as 316L [29]. 316L is one of the commonest austenitic stainless steels and its main constituents apart from iron are chromium, nickel and molybdenum. For other cables, the material type of the armour wires is not provided and thus 316L and its corresponding S-N curve shown in Figure 5.3 will be used as benchmark in the fatigue analysis.

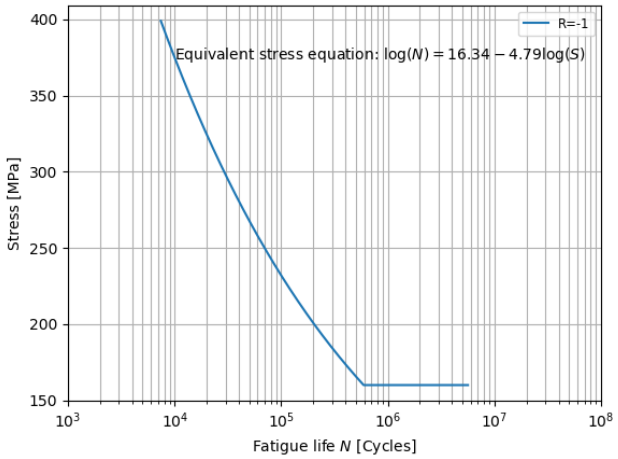

Figure 5.3: S-N curve for stainless steel 316L. Data taken from [30].

5.2.2. HDPE

Since HDPE is a plastic polymer, its low elasticity contributes little to the overall stiffness of a submarine power cable and therefore is expected to experience significantly lesser stresses compared to stainless steel when used in armour wires. However, as can be seen in Figure 5.4, its fatigue life is also considerably worse, making its use in the cable armouring -where local stresses are highest- an interesting study in the fatigue analysis.

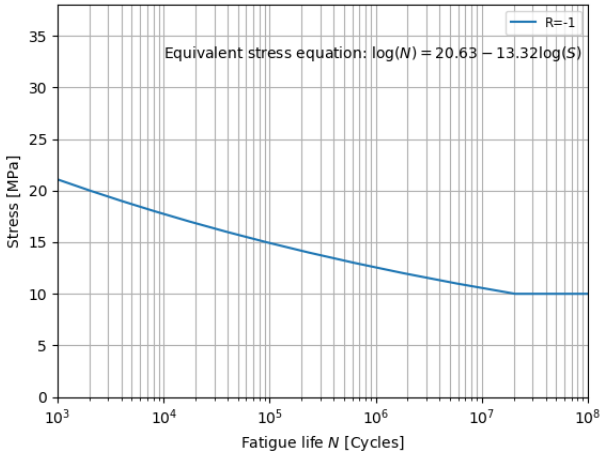

Figure 5.4: S-N curve for HDPE. Data taken from [31].

5.3. Sheath

Lead is the main material that is being used as the metallic protective sheath in submarine power cables. The suitable lead alloys for sheathing are listed in Table 5.1. Although the number of aluminium and

Table 5.1: Lead alloys suitable for metallic sheaths in submarine cables. Data taken from [8].

Type	Alloy elements and percentage (min-max)				
	As	Bi	Cd	Sb	Sn
$\frac{1}{2}C$			0.06-0.09		0.17-0.23
E				0.15-0.25	0.35-0.45
EL			0.06-0.10	0.35-0.45	
F3	0.15-0.18	0.08-0.12			0.10-0.13

copper sheaths have become more frequent, its straightforward application and inexpensiveness make lead the typical choice. Especially for high voltage cables (>150 kV) lead is the best option due to its superior properties with respect to maintaining voltage. In practice, this means that almost all export and interconnector cables are produced with lead sheaths.

Despite being the preferred sheathing material, lead is known to have poor fatigue properties and its application in submarine power cables has been the topic of several (fatigue) studies. However, most of these analyses employ the strain-life method (ε-N), where not the stress but the strain rate is the limiting parameter. See [32] and [33] for examples. Unfortunately, Orcaflex' internal fatigue calculation tool requires S-N curves as input, which are scarcely available for lead. Therefore, as a basis for the fatigue analysis, the S-N curve for lead is defined from material database CES Edupack [34]. The database does not present S-N curves based on specimen tests, but a region in which S-N curves for a specific material tend to fall. Figure 5.5 shows the minimum value of this region for the lead alloy F3.

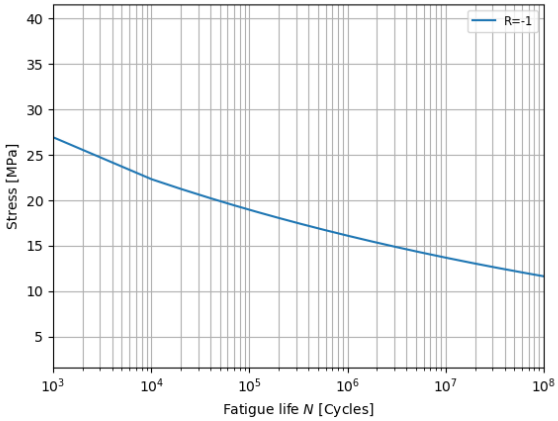

Figure 5.5: S-N curve for lead alloy F3. Data taken from [34].

Moreover, as stated in Chapter 2, increasingly more cables use HDPE or aluminium as sheathing material. Therefore, Figure 5.4 and Figure 5.2 will be used when examining these types of cables.

5.4. Fatigue limits

As mentioned in Chapter 3, the resistance of the various materials to fatigue influences the damage done on the material and can be quantified by Miner's rule, repeated here:

$$D = \sum_{i=1}^{k} \frac{n_i}{N_i} \tag{3.8 revisited}$$

with fracture occurring when $D = 1$. To avoid fracture of any cable elements during the entire lifetime of the cable, the limit for the materials discussed in this chapter should not be set at $D = 1$. However, since fatigue analyses of subsea power cables during installation are not established as a standard practice, there are no fatigue life guidelines developed for them. Hence, in this report, the guidelines for umbilicals, as defined in ISO 13628-5 [35] will be followed:

The umbilical shall be designed with fatigue life that is equal to, or greater than 10 times the service life.

In addition, it is industry practice that up to 10% of the fatigue life of an umbilical shall be consumed during installation. Combining this with the ISO standard for umbilicals, the damage criterion that will be applied for the materials in this report is

$$D \leq 0.01 \tag{5.1}$$

5.5. Conclusions

From the existing S-N curves presented in this chapter, it can be seen that lead and HDPE have significantly worse fatigue life properties than copper, aluminium or stainless steel. Although HDPE is used next to stainless steel in some cable armours, its use in protective sheaths is more sensitive to fatigue damage as there is no stainless steel available to take the main part of the stresses. However, lead - also used in protective sheaths - has a higher Young's modulus than HDPE ($E_{lead} = 14$ GPa, $E_{HDPE} = 1$ GPa). As seen in Chapter 4, the stresses in the cable cross-section elements are all dependent on the modulus of elasticity, meaning that lead will experience significantly higher stresses than HDPE if used in the same purpose, e.g. protective sheaths. Therefore, it can be concluded that lead sheaths are the cable components that are most sensitive to fatigue during installation operations.

6

Cable Fatigue Modelling

With the cable cross-sectional stress analysis in place and the material resistance defined by a set of S-N curves, the next step is to use these theories to determine the fatigue damage of submarine power cables during installation operations.

As numerous load cases with varying environmental conditions will be simulated in the modelling software OrcaFlex to yield the cable response, this chapter will briefly touch upon the models as implemented in the software package. Subsequently, the methods to relate the cable response to fatigue damage in the different cable components will be presented.

Lastly, fatigue damage results for several cables, subject to varying load cases and the corresponding maximum stand-by time due to fatigue will be discussed.

6.1. OrcaFlex model description

As stated before, the cable analysis is performed in the software package OrcaFlex [5], which is regarded as the industry standard time-domain modelling tool for global analysis of marine operations. For the cable installation analyses, OrcaFlex models the vessel and cable response to user-specified environmental conditions and thereby taking into account the mechanical properties of the cable. In the package, the vessel is defined by its geometry and set of RAO's, whereas the submarine power cable is modelled by a non-linear finite element method. If required, the software model can take environmental conditions as current or wind into account. A graphical interface offers a visual representation of the model and enhances efficiency of model set-up.

6.1.1. Conventions

Vessel motions

As for all rigid bodies, vessel motions can be split in three translations and three rotations relative to its Centre of Gravity (CoG). The six motions are defined as shown in Figure 6.1:

Surge X	*Translation along x-axis, positive in positive x-direction.*
Sway Y	*Translation along y-axis, positive in positive y-direction.*
Heave Z	*Translation along z-axis, positive in positive z-direction.*
Roll ϕ	*Rotation around x-axis, positive with starboard down.*
Pitch β	*Rotation around y-axis, positive with bow down.*
Yaw ψ	*Rotation around z-axis, positive with bow to port.*

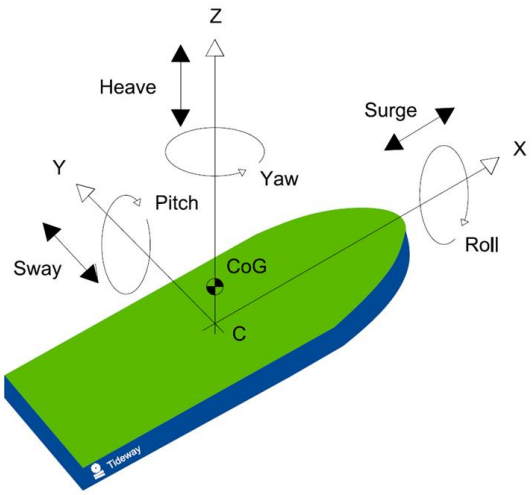

Figure 6.1: Sign conventions for vessel motions. Image taken from [4].

Environmental directional conventions
Environmental forces resulting from wind, current or waves can act on the vessel from various directions. In this research, the directional conventions for the environmental forces in OrcaFlex are defined as depicted in Figure 6.2, although other definitions are possible in the software.

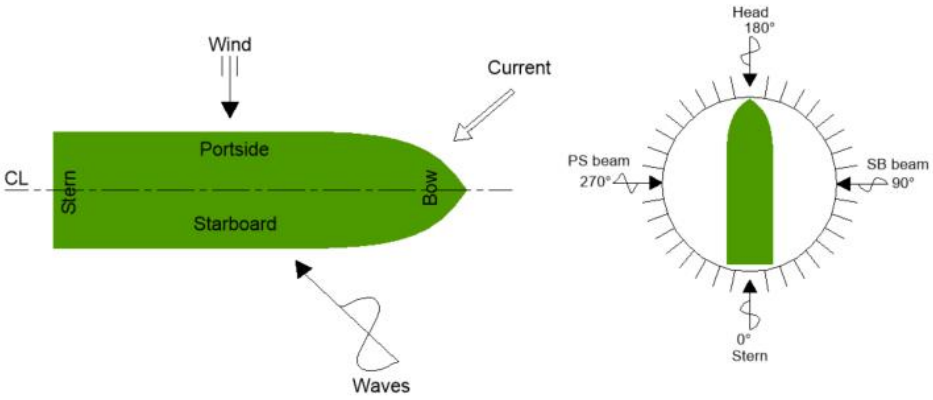

Figure 6.2: Directional conventions for environmental forces

6.1.2. Line model

In OrcaFlex, power cables are defined as line elements, which in turn are modelled by a Finite Element Method. As can be seen in Figure 6.3a, in the discretised model, the line is divided in a finite number of massless segments with a node at both ends. The segments and nodes are numbered such that segment n is the link between nodes n and $n+1$. Additionally, the first and last nodes of the line element are referred to as End A and End B, respectively.
As segments are massless, only the axial, torsional en bending properties of the line are modelled by them. All other cable properties (e.g. mass, buoyancy, drag) are lumped to the nodes, such that each node represents half of each adjacent segment.
Figure 6.3b shows the OrcaFlex line segment model in greater detail. It can be seen that each segment can be thought of as two rods subject to three spring-dampers:

1. An axial spring-damper in the middle of each segment is used to model the axial stiffness and damping properties of the line by applying an equal and opposite effective tension force to the nodes at the segment ends.

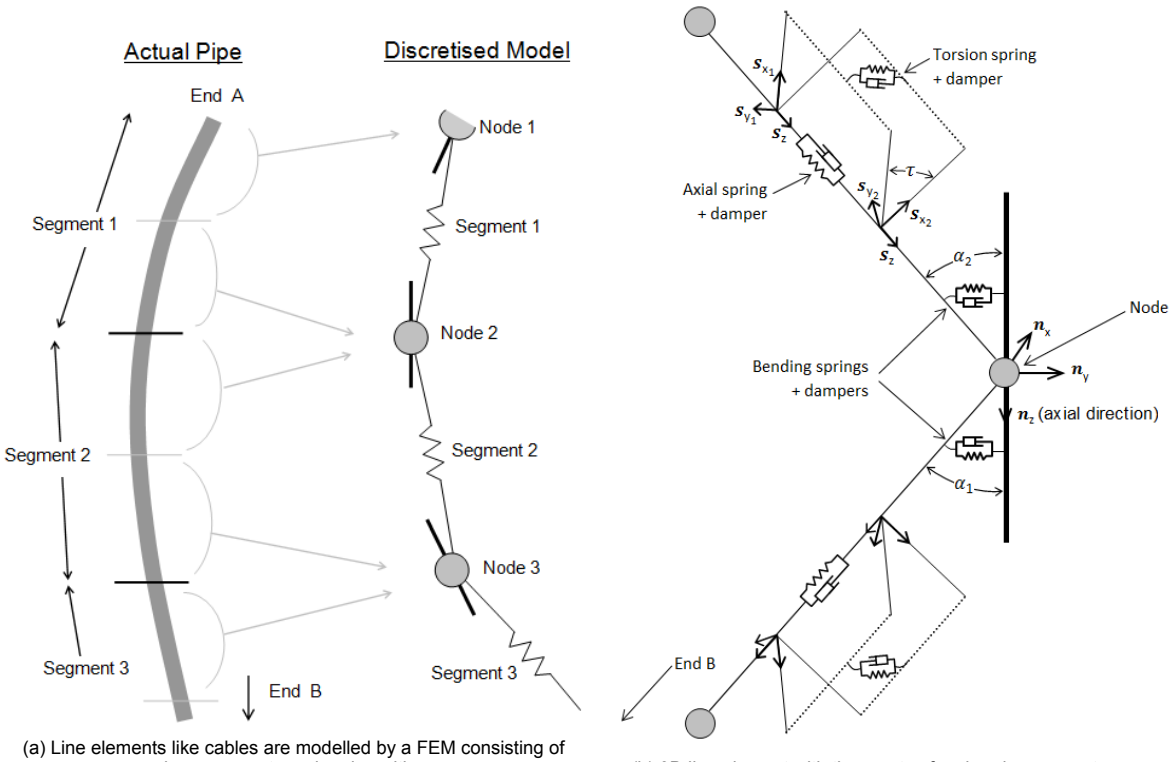

(a) Line elements like cables are modelled by a FEM consisting of massless segments and nodes with mass.

(b) 3D line element with three sets of spring-damper systems.

Figure 6.3: OrcaFlex line model

2. Rotational spring-dampers that connect a node's axial direction n_z and a segment's axial direction s_z is representative for the line's bending properties.

3. A torsional spring-damper in the middle of each segment is used to model the torsional properties of the line by applying equal and opposite torque moments to the nodes at the segment ends. However, it is possible to not include torsion in the model and thus allowing the two halves of the segment to twist freely.

After having defined the cable by its properties and number of segments, a set of discrete equations of motion are derived for each cable node that can be solved in the time-domain by means of a finite difference method to calculate the forces and moments working on the cable. The details of the equations of motion, boundary conditions and time integration method are not of primary importance for the results of this thesis and will therefore not be elaborated on any further. Details can be found in the OrcaFlex manual [5].

6.2. Fatigue calculation in OrcaFlex

The content of this section is confidential and will not be made public.

6.3. Test case discussion

Prior to examining various cables and load cases, the methodology described above is applied on Cable 1, as this cable has most complete data for the cross-sectional analysis. A 100 m cable was modelled in 30 m water depth with three JONSWAP load cases, specified in Table 6.1.
The direction of $60°$ was chosen since it is most limiting for the CLV during installation operations. The influence of the vessel heading to fatigue damage will be analysed, along with other mitigation measures, in Chapter 7.

The fatigue analysis was performed on a single cable node, at a cable arc length of 53 meter. This node

Table 6.1: Three JONSWAP wave loadings that were simulated on Cable 1 to determine fatigue damage.

Loading type	Duration	Direction Θ[°]	Significant wave height H_s [m]	Peak period T_p[s]
JONSWAP	3 hours	60	2	5
JONSWAP	3 hours	60	3	7
JONSWAP	3 hours	60	4	9

is in the touchdown zone of the cable and is therefore expected to experience more fatigue damage than other nodes. The results of this fatigue analysis are listed in Table 6.2

Table 6.2: Fatigue damage due to bending and tension for Cable 1 under three JONSWAP loading scenarios.

Loading	Bending Fatigue Damage D_b			Tensile Fatigue Damage D_t		
	Sheath [Pb]	Conductor [Al]	Armour [SS]	Sheath [Pb]	Conductor [Al]	Armour [SS]
$\begin{cases}\Theta = 60^\circ \\ H_s = 2m \\ T_p = 5s\end{cases}$	1e-5	0	0	0	0	0
$\begin{cases}\Theta = 60^\circ \\ H_s = 3m \\ T_p = 7s\end{cases}$	2e5	0	0	0	0	0
$\begin{cases}\Theta = 60^\circ \\ H_s = 4m \\ T_p = 9s\end{cases}$	1e7	2e-5	0	0	0	0

The table indicated that, even for higher loading scenarios, the tensile stresses do not contribute to fatigue damage. For the two load cases with $H_s = 3$m and $H_s = 4$m, the MBR of the cable is exceeded and failure of the cable due to extreme bending loads will have occurred before tensile stresses can fatigue the cable components. Hence, damage due to bending will be approximated to be the total damage, $D_b \approx D$.

Furthermore, the table shows that the lead sheath is most sensitive to fatigue, as expected from the material data analysis. It can be seen that the fatigue damage for the lead sheath increases significantly for higher loading scenarios, up to unrealistic values. This is due to:

1. The slope of the S-N curve for lead is very steep, causing unstable fatigue behaviour: minor increases of stress magnitude cause excessive increases in fatigue damage. Uncertainty in the cross-sectional stress analysis or in the S-N data are therefore enlarged in the fatigue damage.

2. Peak periods around 8 and 9 seconds are near the peak RAO for roll motion of CLV Living Stone, such that the motions of the vessel and thus the motions of the cable are increased.

3. For higher loading scenarios, the stresses in the sheath will have already exceeded yield stresses or the cable will have exceeded its extremes limits by e.g. breach of MBR. Therefore, it is not surprising to see that cable elements show fracture when subjected to these loadings.

Consequently, quantifying the fatigue damage to the lead sheath (and thus the maximum stand-by time of installation operations) is difficult. However, for conductor materials, the fatigue assessment can be quantified more accurately.

Moreover, as mentioned in Section 6.2, the results of the internal OrcaFlex fatigue assessment tool have proven to not be physically comparable with the damage resulting from the developed algorithm (see Appendix B for details), such that no verification of the method is possible based on a comparative analysis. increasing the the results from the external fatigue assessment method is.

6.4. Base loading cases

In this section, fatigue analyses of various cables in existing cable installation projects are performed. Cables for each project purpose (infield, export, interconnecting) are examined. Contrary to the previous section, the fatigue analysis will be performed on the full cable length to determine which parts of the cable will be most severely affected by fatigue loads.

Two base loading scenarios were chosen to determine fatigue damage, which will be expanded with mitigation measures in Chapter 7. The loading scenarios will be equal for all types of cables and are listed in Table 6.3.

Table 6.3: Base case loading scenarios to determine fatigue damage for infield, export and interconnector power cables.

Loading type	Duration	Direction Θ [°]	Significant wave height H_s [m]	Peak period T_p[s]
JONSWAP	3 hours	60	1	4
JONSWAP	3 hours	60	1	5
JONSWAP	3 hours	60	1.5	5
JONSWAP	3 hours	60	1.5	6
JONSWAP	3 hours	60	2.5	7
JONSWAP	3 hours	60	2.5	8
JONSWAP	3 hours	60	4	9
JONSWAP	3 hours	60	4	10

The wave loading direction of $60°$ was chosen because the CLV experiences least favourable installation conditions under this incoming wave direction. Furthermore, a set of four wave heights was chosen, $H_s \in [1, 1.5, 2.5, 4]$, where $H_s = 1$ and $H_s = 1.5$m are typical favourable loading condition for which cable installation operations are carried out. For the case where $H_s = 2.5$m, installation operations can still be carried out, although the conditions may be limiting for certain cables. $H_s = 4$m is a higher loading case, which can for example be thought of as a storm scenario, where no installation operations are carried out. Lastly, for each load case, a set of two peak periods was examined.

As will be demonstrated in Chapter 7, one of the fatigue mitigation measure possibilities is increasing the bottom tension in the cable, which is defined as

Bottom Tension *The tension in the cable part in contact with the seabed, during the static state of the cable (i.e. no external environmental loading)*

In the following, the base cases for an infield, export and interconnector cable will be presented, specifying the corresponding model parameters.

6.4.1. Infield cable

The infield cable that was examined during this thesis is a three-core HVAC cable. See full cable specifications in Appendix A. The specific model parameters are listed in Table 6.4 and Figure 6.4 provides a graphical representation of the cable catenary model that was used for the infield cable.

Table 6.4: Model parameters infield cable.

Parameter	Value
Cable length	190 m
Total number of nodes	550
Bottom Tension	3 kN
Water depth	80 m

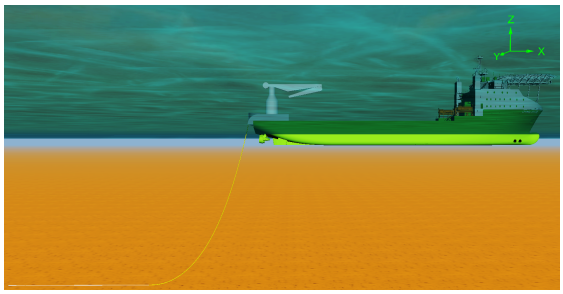

Figure 6.4: Shaded graphics view of OrcaFlex cable catenary model for the infield power cable.

The end of the cable that is connected to the chute of the vessel is defined to be at arc length $s = 0$m, whereas the end that is anchored to the seabed is at $s = 190$m. Furthermore, the max water depth for

many North Sea wind farms is approximately 40-70 m. Water depth of 80 m was chosen to research the boundaries of the cables.

6.4.2. Export cable

The export cable that was examined during this thesis is a HVAC cable. See full cable specifications in Appendix A. The specific model parameters are listed in Table 6.5. Figure 6.5 provides a graphical representation of the cable catenary model that was used for the export cable.

Table 6.5: Model parameters for export cable

Parameter	Value
Cable length	140 m
Total number of nodes	484
Bottom Tension	3 kN
Water depth	30 m

Similarly to the infield power cable, the water depth is chosen to be realistic for North Sea wind farms. Again, the end of the cable that is connected to the chute of the vessel is at $s = 0$m, whereas the end that is anchored to the seabed is at arc length $s = 145$m.

6.4.3. Interconnector cable

The interconnector cable that was examined during this thesis is a HVDC cable. See full cable specifications in Appendix A. The specific model parameters are listed in Table 6.6. Figure 6.6 provides a graphical representation of the interconnector cable catenary model.

Table 6.6: Model parameters for HVDC interconnector cable.

Parameter	Value
Cable length	500 m
Total number of nodes	967
Bottom Tension	10 kN
Water depth	200 m

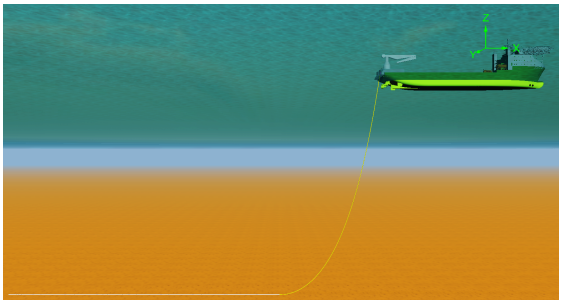

Figure 6.6: Shaded graphics view of OrcaFlex cable catenary model for the HVDC export power cable.

The total length of the cable spans from $s = 0$m at the chute to $s = 500$m at the seabed. For this cable, the modelled water depth of 200 m is not representative for North Sea projects. Additionally, it should be stated that it is a lightweight cable that has low bending stiffness (see cable properties in Appendix A) and has not been designed for installation at a water depth of 200m. Consequently, excessive bending motions may occur. However, the interconnector analysed in this text is one of the few HVDC cables with elaborate geometrical specifications that can be used in deep water. Therefore, this cable was chosen to analyse a deep water fatigue case.

6.5. Results

6.5.1. Infield Cable

Sheath

Figure 6.7 shows the fatigue damage of the HDPE protective sheath of the HVAC infield power cable due to the wave loadings described in Table 6.3 On the horizontal axis, the cable arc length s is depicted, ranging from end A at $s = 0$m to $s = 190$m at end B. At the vertical axis, the fatigue damage is shown. As stated in Chapter 5, the fatigue budget for cable installation operations is 10^{-2}, implying that all damage values below this are within budget for the 3-hr JONSWAP load cases.

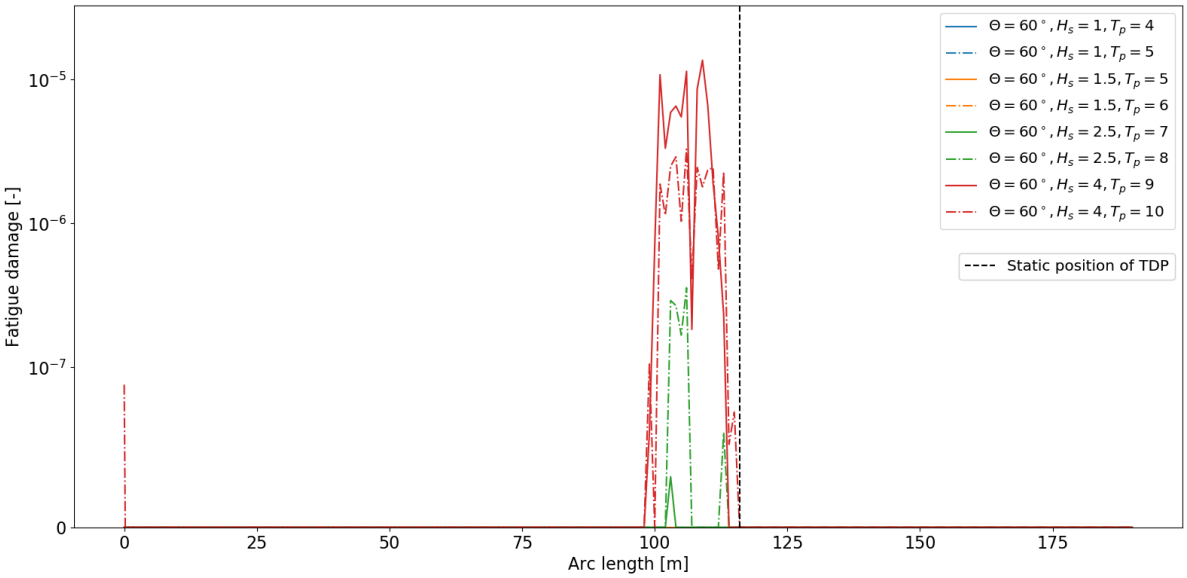

Figure 6.7: Fatigue damage of HDPE infield power cable sheath, due to the base load cases. Fatigue damage vs. cable arc length.

Two peaks are clearly visible in the figure. However, the peak in the origin, at End A of the cable, is due to how the end of the cable is modelled in OrcaFlex at its connection with the chute. The second peak, at approximately $s = 100$m is wider and corresponds to the touchdown zone of the cable. In this region, the fatigue damage D varies between $D = 0$ and $D = 10^{-5}$, depending on the load case, with the maximum fatigue damage is occurring in the case where $H_s = 4$m and $T_p = 10$s. Since each load case duration is three hours, the maximum stand-by time t_{sb} for this case is up to 3000 hours, or $t_{sb} =$ 125 days, which can be regarded as an infinite fatigue life in terms of cable installation operations. Furthermore, it is seen that no fatigue damage occurs when $H_s = 1$m or $H_s = 1.5$m

The RFC stress-history of the cases with $H_s = 4$m and $T_p = 10$s is depicted in Figure 6.8. On the horizontal axis, the stress magnitudes that are present in the time-history are depicted, whereas the vertical axis shows the corresponding amount of cycles that the HDPE sheath is subjected to. It can be seen that the time-history is dominated by stress cycle magnitudes of $\Delta\sigma =$ 0-6 MPa. From Figure 5.4, it is seen that these stress magnitudes do not contribute to the fatigue damage of HDPE components.

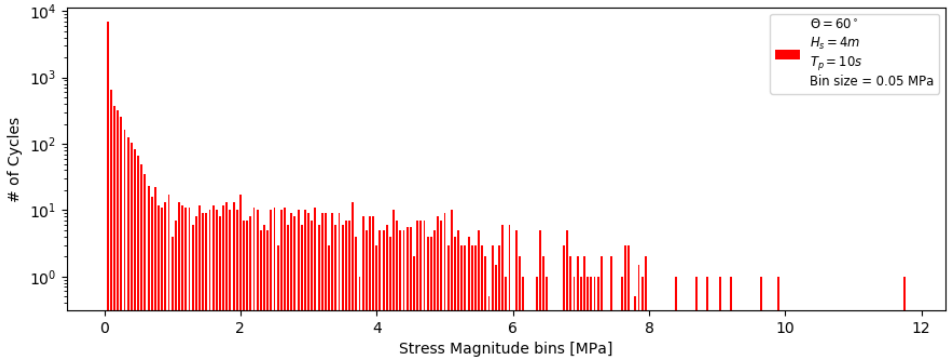

Figure 6.8: Sheath: Number of cycles vs. stress magnitude for $[\Theta = 60°,\ H_s = 4\text{m},\ T_p = 10\text{s}]$. Histograms are shown for the point along the cable at which damage was most severe, $s = 109$m

Conductor

Figure 6.9 shows the fatigue damage of the Aluminium conductor of the infield power cable.
For the conductor, additional peaks of damage are observed at $s =$10-15m, corresponding to the de-

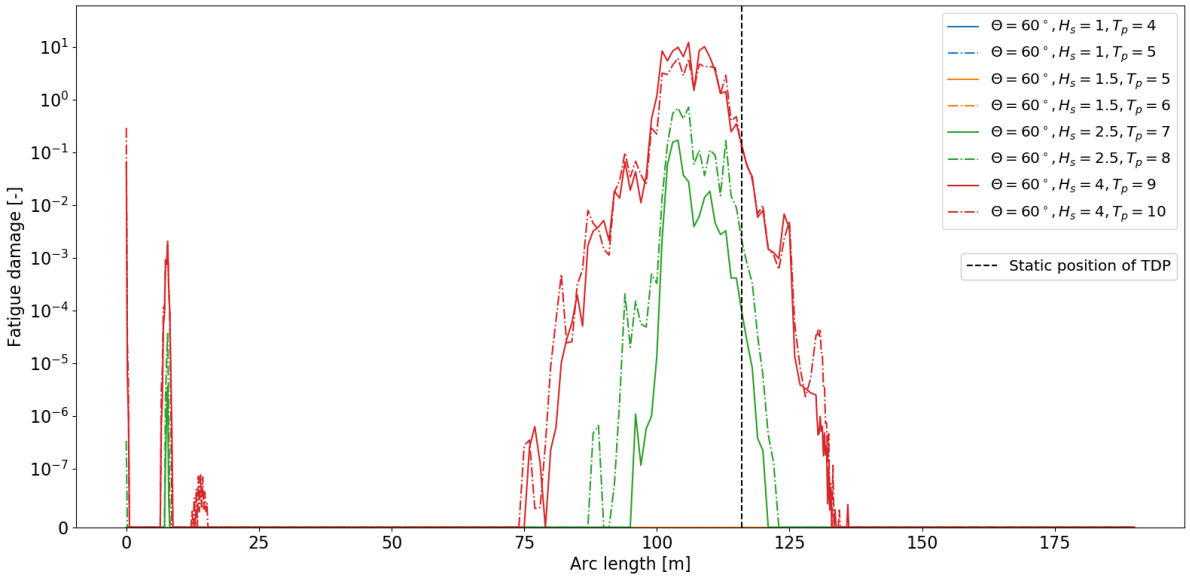

Figure 6.9: Fatigue damage of Al infield power cable condctor, due to the base load cases. Fatigue damage vs. cable arc length.

parture point of the cable. However, the damage at the departure point is within the fatigue budget as $D < 0.01$ and the touchdown zone is again the critical part of the cable. At the touchdown zone, the fatigue budget of the conductors is exceeded by significant margin for all cases where $H_s \geq 2.5$m. However, for these cases, it was found that the MBR of the cable was breached since the maximum curvature $\kappa_{max} \geq 0.56\text{m}^{-1} \geq \frac{1}{\text{MBR}} = 0.51\text{m}^{-1}$ and hence extreme stresses are present in the stress-time history. This is also evident from Figure 6.10, where the stress-time history of the case where $H_s = 4$m and $T_p = 10$s is shown. At the arc length $s = 109$m, where the fatigue damage is maximum, the conductors endure stress cycle magnitudes up to 210 MPa, which equals the yield stress of aluminium that was assumed for this cable, see Appendix A.

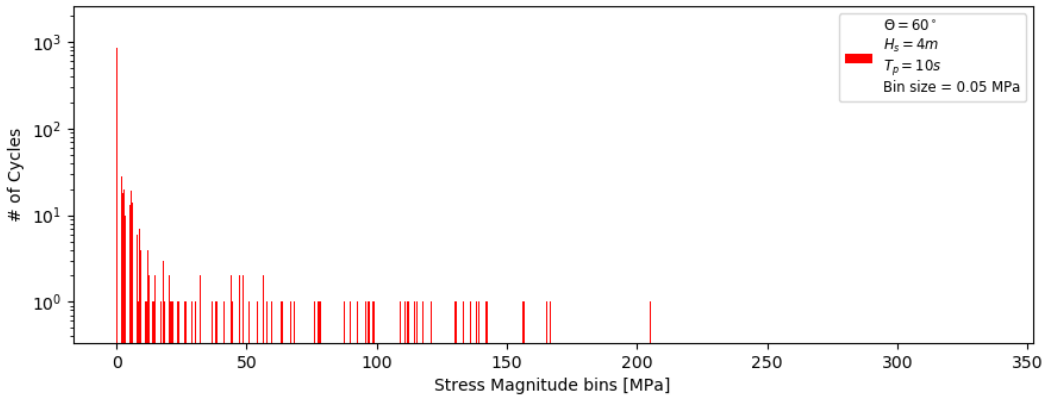

Figure 6.10: Conductor: Number of cycles vs. stress magnitude for $[\Theta = 60°,\ H_s = 4\text{m},\ T_p = 10\text{s}]$ Histograms are shown for the the point along the cable at which damage was most severe, $s = 109$m.

For the conductors to be able to withstand these loads, mitigation measures are to be applied, which will be discussed in Chapter 7.

Armour

The stainless steel armour wires of the infield power cable are not subjected to any fatigue damage for the base cases. It can be observed from Figure 6.11 that the maximum stress magnitude the armour wires endure is one full cycle at 160 MPa. As can be seen from the S-N curve for stainless steel in

Chapter 5, this equals the endurance limit of stainless steel and therefore no damage is done to the armour wires.

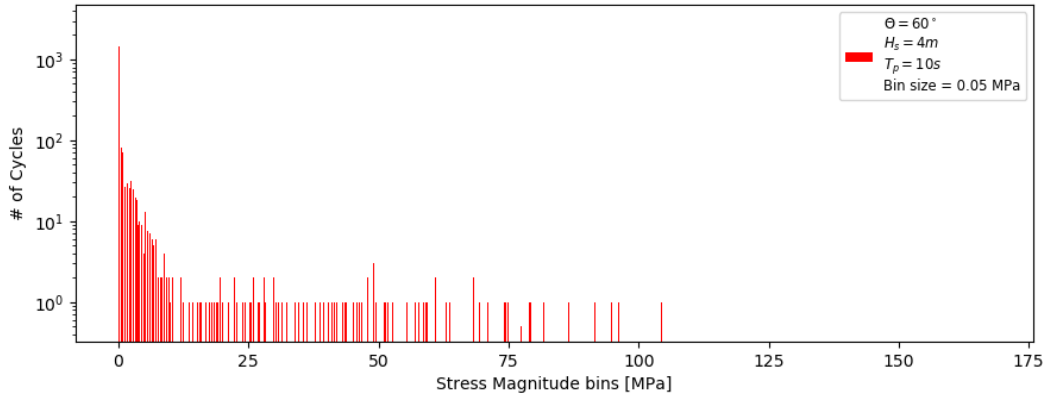

Figure 6.11: Armour: Number of cycles vs. stress magnitude for $[\Theta = 60°,\ H_s = 4\text{m},\ T_p = 10\text{s}]$. Histograms are shown for the the point along the cable at which damage was most severe, $s = 109\text{m}$.

6.5.2. Export cable

Sheath

Figure 6.12 shows the fatigue damage of the lead protective sheath of the export power cable due to the wave loadings described in Table 6.3

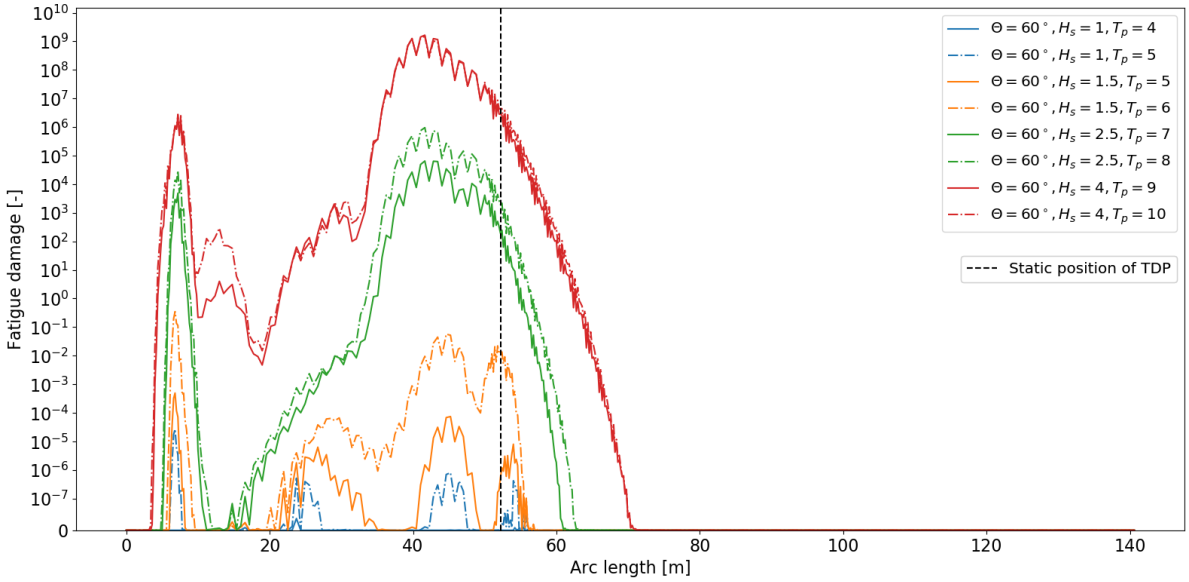

Figure 6.12: Fatigue damage of export power cable sheath, due to the base load cases. Fatigue damage vs. cable arc length.

There are significant differences between the HDPE infield sheath and the lead export sheath fatigue behaviour. First of all, due to the shallow water depth of 30m, the two damage peaks corresponding to the departure point and TDP are less distinguishable than in the case of the infield power cable and thus the full free-hanging part of the cable is subject to fatigue loads. In addition, the magnitude of fatigue damage for the lead sheath is extreme for the higher loading scenarios. The lower loading scenarios have maximum fatigue damage ranging between $D = 10^{-6}$ and $D = 10^{-4}$, corresponding to maximum stand-by times of $t_{sb} = 300\text{h}$ or 12 days.

As was the case for the infield power cable, for the load cases where $H_s \geq 4\text{m}$, the MBR of the cable is breached and thus extreme loads are present in the time-history. However, for the load cases where $H_s = 2.5\text{m}$, this is not the case as it was found that $\kappa_{max} = 0.2\text{m}^{-1} < 0.23\text{m}^{-1} = \frac{1}{\text{MBR}}$. Despite this,

it is seen that for these cases the fatigue damage is $D \approx 10^5$. As mentioned earlier, the instability of the S-N curve for lead results in inflated fatigue damage. Moreover, due to the maximum curvature being close to breaching the MBR of the cable, the yield stress of lead is exceeded and hence plastic deformation occurs.

Lastly, the load case with $H_s = 1.5$m, $T_p = 8$s results in fatigue damage of $D = 0.8$. Although the fatigue budget is exceeded, Figure 6.13 demonstrates that the maximum stress magnitude the lead sheath is subject to is $\sigma = 18.5$MPa (half-cycle). From the S-N curve for lead in Figure 5.5 it can then be seen that the fatigue behaviour corresponding to this stress-history is entirely in the high-cycle fatigue regime.

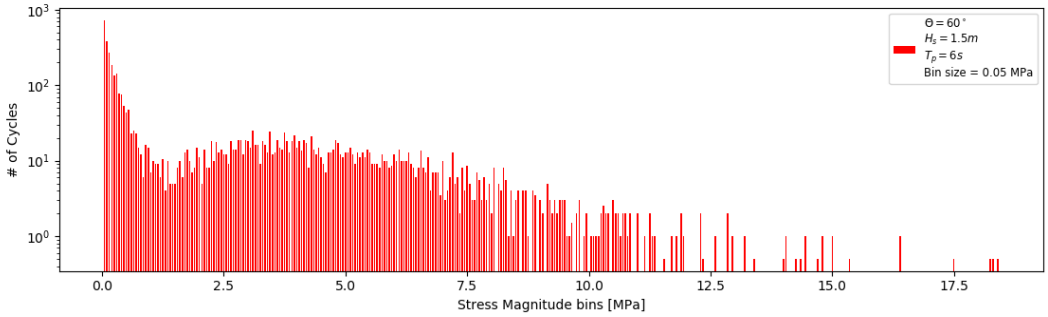

Figure 6.13: Sheath: Number of cycles vs. stress magnitude for $[\Theta = 60°,\ H_s = 1.5\text{m},\ T_p = 6\text{s}]$. Histograms are shown for the the point along the cable at which damage was most severe, $s = 41.6$m respectively.

Conductor

Figure 6.14 shows the fatigue damage of the Aluminium conductor of the HVAC export power cable.

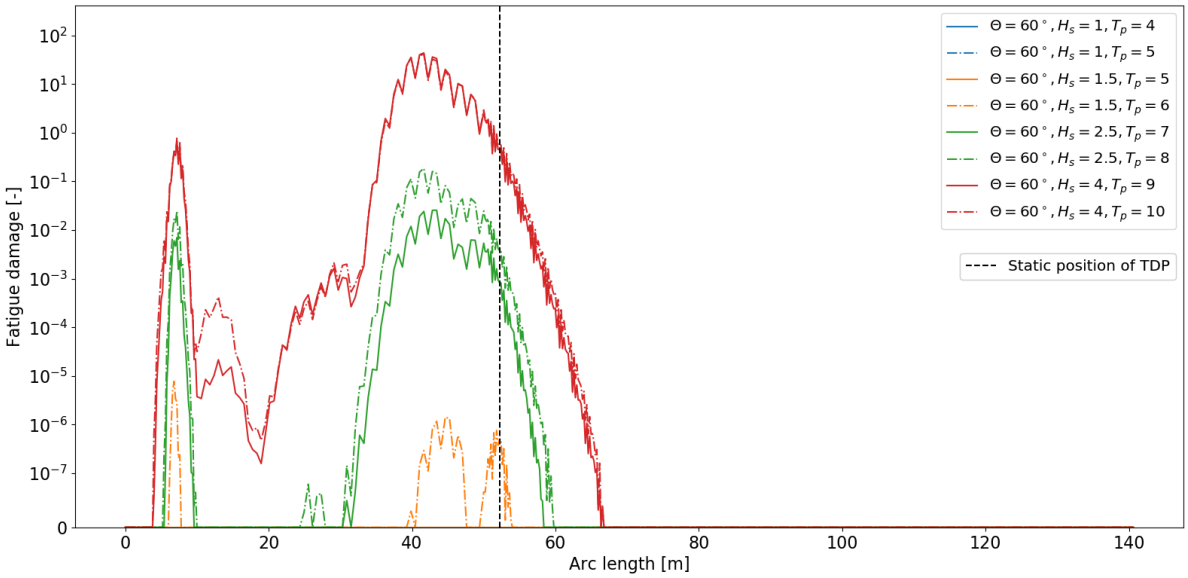

Figure 6.14: Fatigue damage of export power cable conductor, due to the base load cases. Fatigue damage vs. cable arc length.

It is observed that the fatigue behaviour of the aluminium conductors is similar to that of the infield power cable. However, in this case, it was found that the loading scenarios with $H_s = 2.5$m do not cause a breach of MBR, whilst the fatigue budget is exceeded. From Figure 6.15, it can be concluded that all stress magnitudes present in the time-history for loading scenario $H_s = 2.5$m, $T_p = 8$s are in the elastic regime of the stress-strain curve for aluminium since $\sigma_{max} = 140$ MPa < 210 MPa $= \sigma_{y,Al}$.

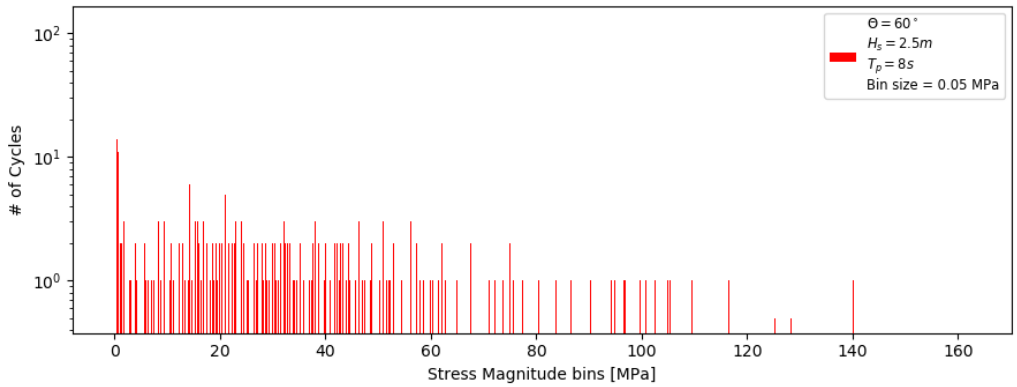

Figure 6.15: Conductor: Number of cycles vs. stress magnitude for $[\Theta = 60°,\ H_s = 2.5\text{m},\ T_p = 8\text{s}]$. Histograms are shown for the the point along the cable at which damage was most severe, $s = 41.6\text{m}$.

Armour

The stainless steel armour wires of the export power cable are not subject to any fatigue damage for the base cases. It can be seen from Figure 6.16 that the maximum stress magnitude the armour wires endure is one full cycle at 153 MPa, under wave loads with $H_s = 4\text{m}$, $T_p = 10\text{s}$. Since $\sigma_{max} = 153\text{MPa} < 160\text{MPa} = \sigma_{e,st}$, no fatigue damage occurs in the armour wires of the export cable.

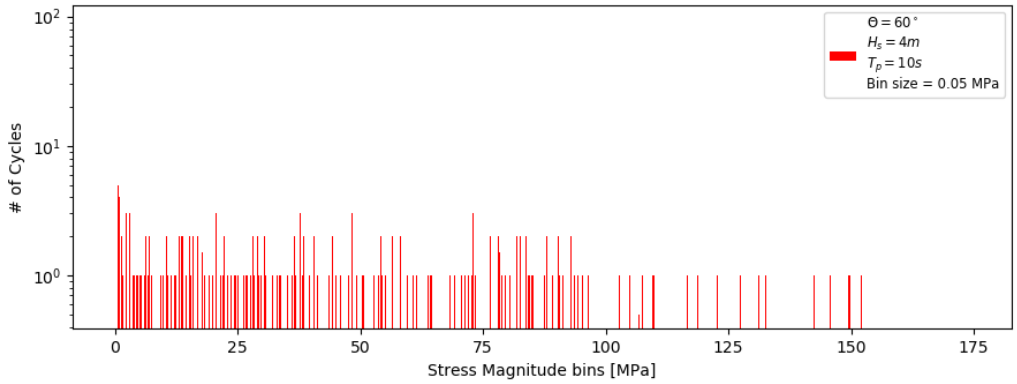

Figure 6.16: Armour: Number of cycles vs. stress magnitude for $[\Theta = 60°,\ H_s = 4\text{m},\ T_p = 10\text{s}]$ Histograms are shown for the the point along the cable at which damage was most severe, $s = 41.6\text{m}$.

6.5.3. Interconnector Cable

Sheath

Figure 6.17 shows the fatigue damage of the lead protective sheath of the interconnector power cable due to the wave loadings described in Table 6.3

Again, it can be seen that the departure point and TDP are the critical positions of the cable. However, it is also evident that the 200m water depth invokes excessive bending motions in the cable. For the mild ($H_s = 2.5\text{m}$) and severe ($H_s = 4\text{m}$) load cases, fatigue damage magnitudes in the range of $D = 10^{12}$-10^{14} are observed. In the time-histories, curvatures up to $\kappa_{max} = 0.7\text{m}^{-1} \leq \frac{1}{\text{MBR}} = 0.36\text{m}^{-1}$ are present and thus the MBR is breached by significant margin. These load cases will be further examined with the implementation of mitigation measures.

On the other hand, the figure shows that for the loading scenarios with $H_s = 1\text{m}$ or $H_s = 1.5\text{m}$ the fatigue damage of the lead sheath is within budget, with corresponding maximum standby time $t_{sb} = 3\text{h}$. For this load case, the stress-history is depicted in Figure 6.18

It can be seen that the maximum stress magnitude in the stress history is 27.5 MPa. Based on the S-N curve for lead, the transition from elastic to plastic fatigue regime (assumed to occur at $N = 10^3$), occurs at $\sigma_{y,Pb} = 25$ MPa. Therefore, some plasticity may occur in the lead sheath, but most damage is done due to high-cycle fatigue.

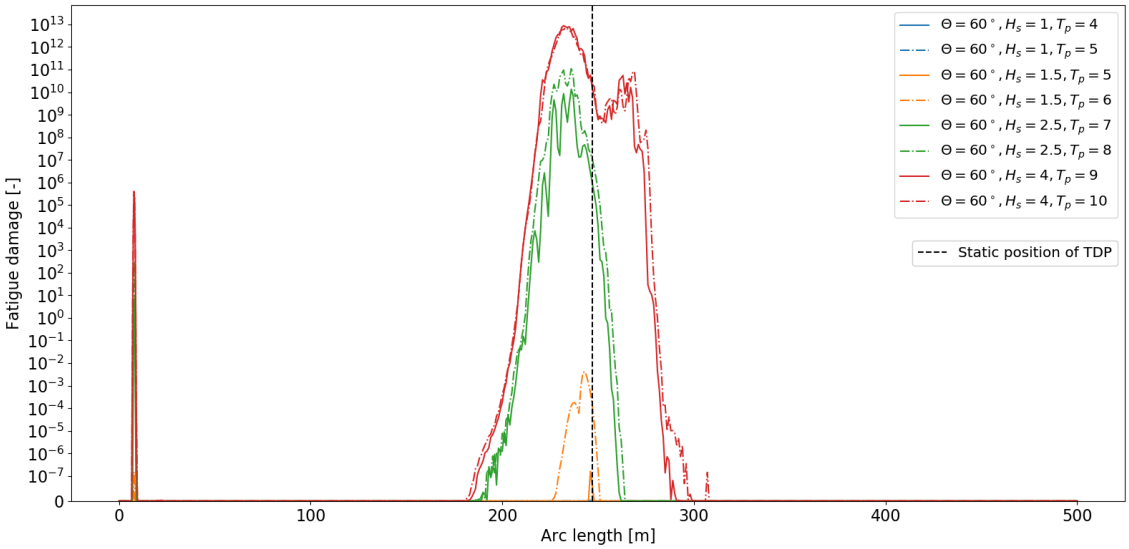

Figure 6.17: Fatigue damage of interconnector power cable sheath, due to the base load cases. Fatigue damage vs. cable arc length.

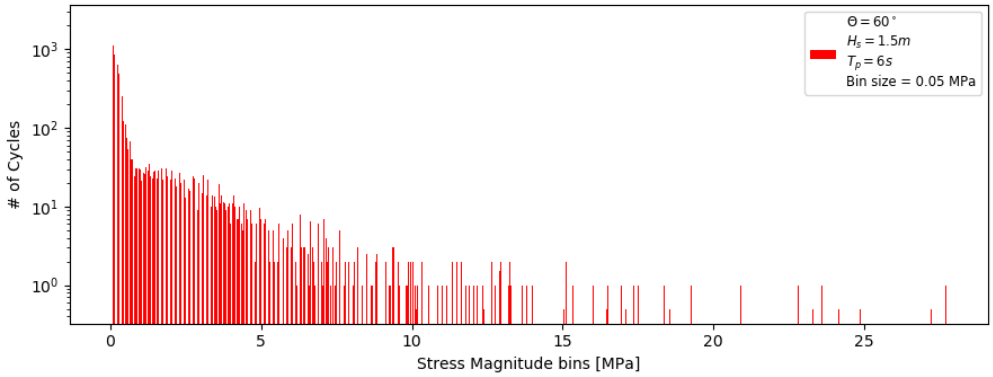

Figure 6.18: Sheath: Number of cycles vs. stress magnitude for $[\Theta = 60°,\ H_s = 1.5\text{m},\ T_p = 6\text{s}]$. Histograms are shown for the the point along the cable at which damage was most severe, $s = 243\text{m}$.

Conductor

Figure 6.19 shows the fatigue damage of the copper conductor of the HVDC interconnector power cable.

Similarly to the lead sheath fatigue behaviour, it is seen that the damage of the copper conductor is significant due to the combination of cable properties and deep water. However, as opposed to the lead sheath, all loading scenarios with $H_s \leq 1.5\text{m}$ do not give rise to conductor damage. Furthermore, it can be seen that the conductor damage at the departure point has a magnitude of $D = 10^{-1}$ for high loading scenarios and it was found that at the departure point no breach of MBR occurs. The stress-history of the departure point, depicted in Figure 6.20, shows that all stress magnitudes are below the yield strength of copper $\sigma_{y,Cu} = 140$ MPa and thus the copper conductor exceeds the fatigue budget at the departure point by damage due to elastic loads.

Armour

Despite the cable being exposed to significant motions, the armour wires of the cable show fatigue damage only at the cable node at $s = 243\text{m}$, when subject to loading scenarios with $H_s = 4\text{m}$. The corresponding fatigue damage at this node is found to be $D = 2 \cdot 10^{-5}$. The stress-history of this node is depicted in Figure 6.21.

It is seen that all stress magnitudes are below the endurance limit of steel $\sigma_{e,St} = 160$ MPa, except one full load cycle with magnitude $\sigma = 180$ MPa and one residual half-cycle with magnitude $\sigma = 185$ MPa.

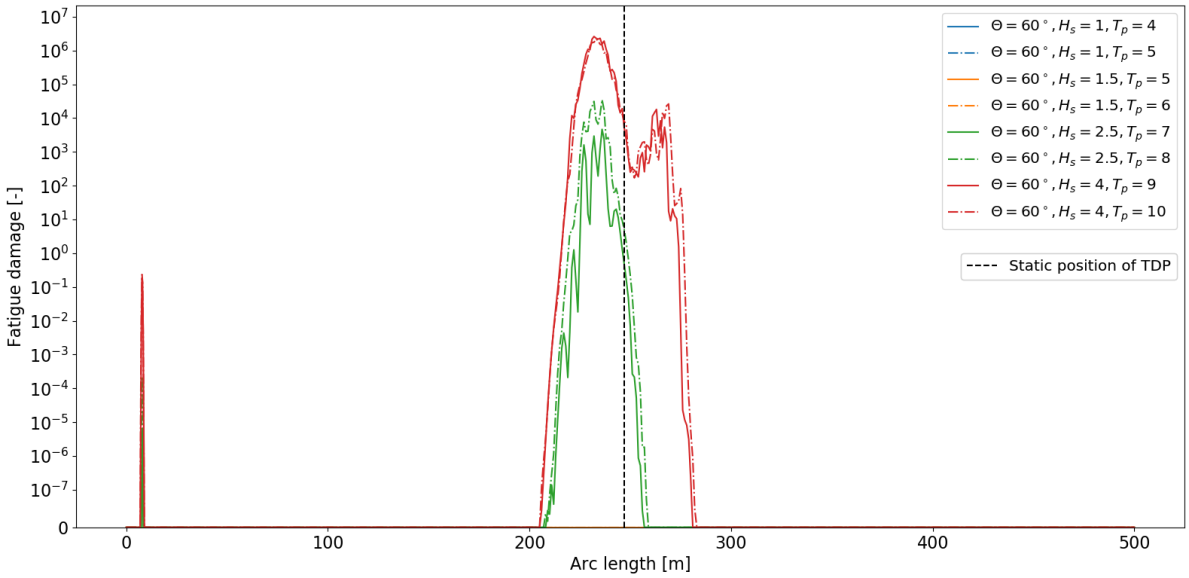

Figure 6.19: Fatigue damage of interconnector power cable conductor, due to the base load cases. Fatigue damage vs. cable arc length.

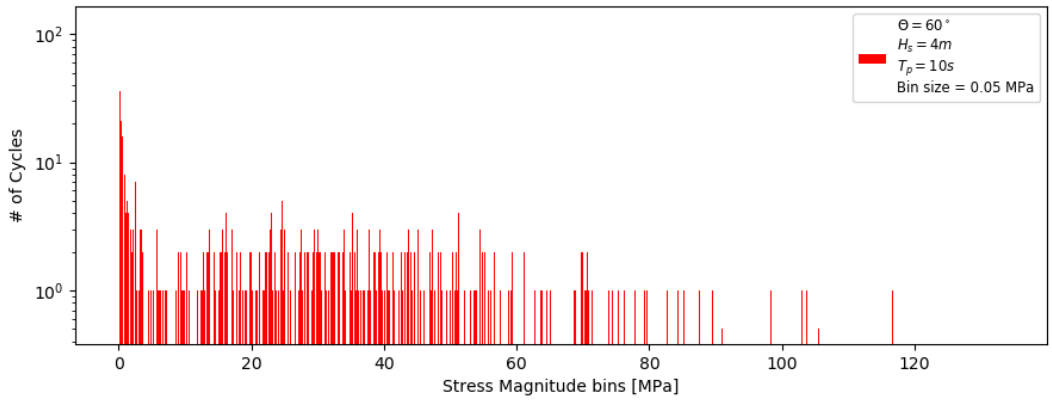

Figure 6.20: Conductor: Number of cycles vs. stress magnitude for $[\Theta = 60°,\ H_s = 4\text{m},\ T_p = 10\text{s}]$. Histograms are shown for the departure point, $s = \text{m}$ respectively.

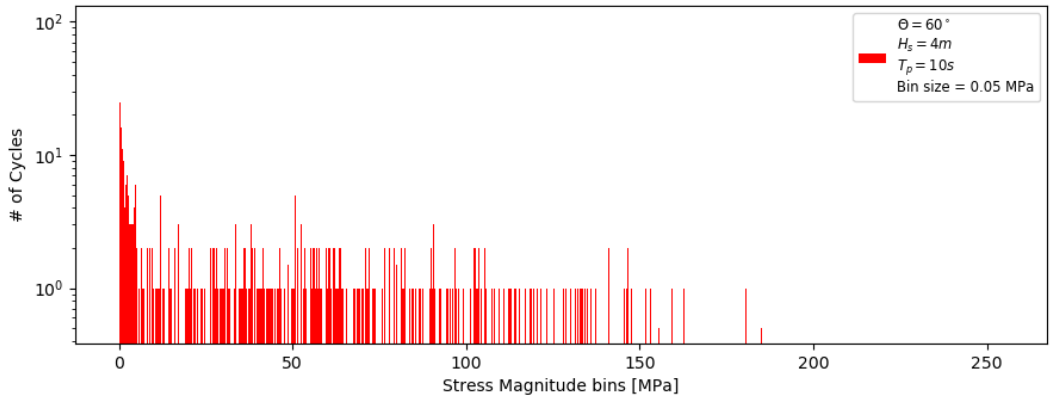

Figure 6.21: Armour: Number of cycles vs. stress magnitude for $[\Theta = 60°,\ H_s = 4\text{m},\ T_p = 10\text{s}]$. Histograms are shown for the the point along the cable at which damage was most severe, $s = 243\text{m}$.

6.6. Conclusions

In this chapter, results of the fatigue assessment of typical infield, export and interconnector cables, subject to various worst-case scenario load cases were presented. An overview of the load cases is

provided in Table 6.3.

6.6.1. Sheath

The load case simulations were not bounded to the MBR of the cables and hence in several cases, the MBR of the cable was breached. The results from the fatigue analysis are consistent with this, as in many cases the stress magnitudes exceed the yield stress of the material. This is mostly the case for lead sheaths. However, it was also shown that lead sheaths exhibit excessive fatigue damage even when the cable's MBR is not breached. Additionally, uncertainty in the S-N curve for lead causes a significant instability in the fatigue assessment method, adding to the difficulty of quantifying fatigue damage for lead sheaths. As a consequence, the lead sheath of the HVAC export cable exhibited fatigue damages ranging from $D = 0$ for loading scenarios where $H_s \leq 1.5$m to $D_{lead} = 10^{14}$ for loading scenarios where $H_s = 4$m. This is further discussed in Chapter 8.
For the infield power cable, the protective sheath is made of HDPE, for which the fatigue analysis yields standby times $t_{sb}^{HDPE} \geq 125$ days for all load cases. In terms of cable installation operations, the HDPE sheath has infinite fatigue life.

6.6.2. Conductors

Aluminium conductors were analysed in the infield and export cable. It was observed that for severe loading scenarios ($H_s = 4$ m), the MBR of the cable was breached and the fatigue budget was exceeded, with maximum damage magnitudes of $D_{Al} = 10^2$. Additionally, it was shown that for the aluminium conductors the load cases where $H_s = 2.5$m are limiting from fatigue point of view as the MBR was not necessarily breached, but the fatigue budget was exceeded. Nevertheless, the aluminium elements did not enter the plastic stress-strain region and hence, with the addition of mitigation measures, it is expected that the aluminium conductors will not be critical from fatigue point of view. Lastly, the interconnector HVDC cable with single copper conductor core exhibited disproportionate fatigue damage due to excessive cable motions in deep water and will therefore be a main point of interest during the mitigation analysis.

6.6.3. Armour

All cables that were studied make use of stainless steel armour wires. In all load cases, no fatigue damage occurred to the armature of the cables. Therefore, it may be concluded that the stand-by time for stainless steel armour wires is $t_{sb}^{steel} = \infty$

Although not all cable elements show well-defined fatigue limits and standby times, it is interesting to see if fatigue damage is mostly dominated by the severity of the load cases and excessive bending motions, or by the material properties of the elements. In that regard, the next chapter will present mitigation measures to be applied to the cables to reduce fatigue damage, which will subsequently be compared to the non-mitigated results. In Chapter 8, the results from both chapters will be elaborately discussed.

7

Mitigation Load cases

In the previous chapter, a fatigue analysis was performed for three different cables for a set of load cases, with the wave direction chosen in a way such that the most severe vessel motions are invoked. These base cases will be further analysed in this chapter. In particular, it will be analysed which types of mitigation measures are applicable for countering fatigue and what their effect on the total fatigue damage on the cable will be. Firstly, a brief introduction to the various countermeasures is presented. Subsequently, the load cases from the previous chapter will be modified according to the mitigation specifications, whereafter a fatigue analysis will be performed on the mitigated load cases.

7.1. Mitigation possibilities

This section will present the various possibilities for fatigue mitigation and the load cases that are analysed for each mitigation measure. Since the load cases with favourable conditions (i.e. $H_s =\leq 1.5$m) were shown to not do damage to the various components, the focus of this chapter will be on the severe load cases, i.e. $H_s \geq 2.5$m.

7.1.1. Vessel Heading

The most straightforward method of mitigating cable motions is reducing vessel motions by positioning the vessel in a way that its response to the waves is minimised. When this is done purposely, it is also referred to as weathervaning. To analyse the effect of vessel heading variation, the base load cases from Chapter 6 will be varied in loading direction. For the Living Stone, DEME Offshore has found that wave direction $\Theta = 0^\circ$ (see Figure 6.2 for direction conventions) are most favourable in terms of vessel motions. Therefore, the mitigated load cases to study vessel heading effects have been modified as specified in Table 7.1. It can be seen that the only difference with the base cases is that the wave directions have been adjusted from $\Theta = 60^\circ$ to $\Theta = 0^\circ$ and hence, the vessel heading model is still represented by the parameters listed in Tables 6.4 - 6.6.

Table 7.1: Loading scenarios for infield, export and interconnector power cables under vessel heading variation.

Loading type	Duration	Direction Θ [°]	Significant wave height H_s [m]	Peak period T_p[s]
JONSWAP	3 hours	0	2.5	7
JONSWAP	3 hours	0	2.5	8
JONSWAP	3 hours	0	4	9
JONSWAP	3 hours	0	4	10

7.1.2. Layback length increase

As mentioned before, another method to mitigate cable motions is the increase of the overall tension in the cable such that the system becomes stiffer and therefore less cable motions are expected. This can easily be achieved by increasing the layback length, which results in higher bottom tension and thus causing the cable to become more stiff. In the following, the mitigated load cases for each of the studied cabeles will be detailed.

Infield cable

The specific layback model parameters are listed in Table 7.2.

Table 7.2: Model parameters for the infield cable with increased bottom tension.

Parameter	Value
Cable length	190 m
Total number of nodes	550
Bottom Tension	19 kN
Water depth	80 m

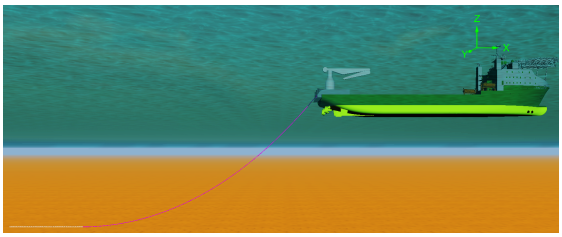

Figure 7.1: Shaded graphics view of OrcaFlex cable catenary model for the infield power cable with increased layback length.

The layback length d_l has been increased from $d_l^{base} = 59$ m to $d_l^{mitigated} = 160$ m, causing the bottom tension to become six times higher than in the base catenary model.

Export cable

The specific layback model parameters are listed in Table 7.3.

Table 7.3: Model parameters for the export cable with increased bottom tension.

Parameter	Value
Cable length	140 m
Total number of nodes	484
Bottom Tension	45 kN
Water depth	30 m

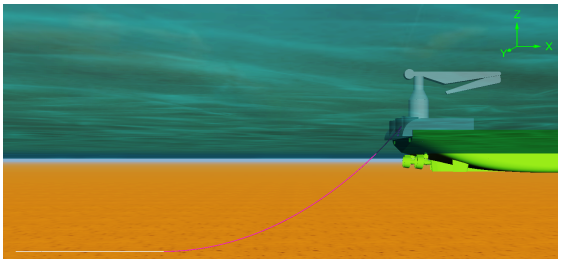

Figure 7.2: Shaded graphics view of OrcaFlex cable catenary model for the export power cable with increased layback length.

The layback length d_l has been increased from $d_l^{base} = 25$ m to $d_l^{mitigated} = 77$ m, resulting in a bottom tension that is 15 times higher than in the base catenary model.

Interconnector cable

The specific layback model parameters are listed in Table 7.4.

Table 7.4: Model parameters for the interconnector cable with increased bottom tension.

Parameter	Value
Cable length	500 m
Total number of nodes	967
Bottom Tension	48 kN
Water depth	200 m

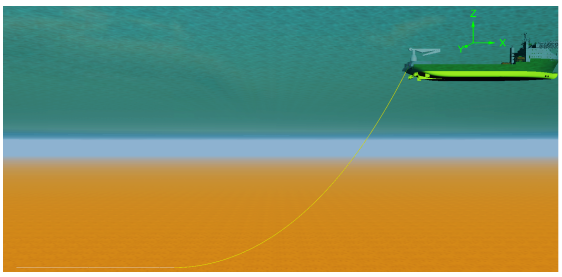

Figure 7.3: Shaded graphics view of OrcaFlex cable catenary model for the interconnector power cable with increased layback length.

The layback length d_l has been increased from $d_l^{base} = 100$ m to $d_l^{mitigated} = 250$ m, resulting in a bottom tension that is 15 times higher than in the base catenary model.

7.1.3. Lazy wave configuration

The base cases in the previous chapter were all modelled with the cable in a free-hanging catenary configuration, see left side of Figure 7.4. Another possible cable configuration is the so-called lazy wave configuration, seen on the right side of the figure. In this configuration, the cable is forced into the wave shape by the use of buoyancy tanks that are placed around the cable. This way, the installation operation is terminated and thus the lazy wave configuration is only used during weather survival.

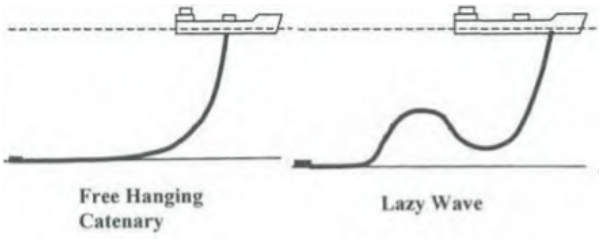

Figure 7.4: Free-hanging catenary configuration vs. Lazy wave configuration. Image taken from [36]

When a cable is configured in a lazy wave shape, the middle section of the cable is bent and will therefore partially damp the motions in the cable that arise from the vessel motion and therefore decreasing the motions at the touchdown point. On the other hand, the bending motions in the bent part will increase. However, as opposed to the TDP, the cable does not have a clamped boundary in this section of the cable and as long as the MBR of the cable is preserved, the bending motions of the middle section are tolerable.

Typically, buoyancy tanks are cable-type specific and have maximum outer cable diameter limitations. In this research, all three cables are modelled with equal buoyancy tanks, specified by data provided by [4].

In this thesis, the buoyancy tanks have been modelled as buoyant line elements with flexural properties of the cable, and not as separate buoyancy tanks, see model specifications below.

Infield cable

The specific lazy wave model parameters for the infield cable are listed in Table 7.5.

Table 7.5: Model parameters for the infield cable with lazy wave configuration.

Parameter	Value
Cable length	190 m
Total number of nodes	590
Buoyant section start	$s = 80$m
Buoyant section end	$s = 90$m
Water depth	80 m

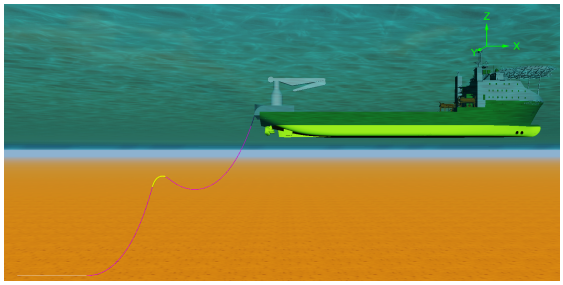

Figure 7.5: Shaded graphics view of OrcaFlex cable catenary model for the infield power cable with lazy wave configuration.

In Figure 7.5, the buoyant section of the cable is indicated in yellow.

Export cable

The specific lazy wave model parameters for the export cable are listed in Table 7.6.

Table 7.6: Model parameters for the export cable with lazy wave configuration.

Parameter	Value
Cable length	142 m
Total number of nodes	472
Buoyant section start	$s = 40$m
Buoyant section end	$s = 52$m
Water depth	30 m

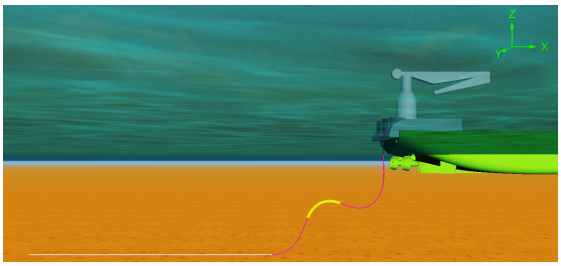

Figure 7.6: Shaded graphics view of OrcaFlex cable catenary model for the export power cable with lazy wave configuration.

In Figure 7.6, the buoyant section of the cable is indicated in yellow.

Interconnector cable
The specific lazy wave model parameters for the interconnector cable are listed in Table 7.7.

Table 7.7: Model parameters for the interconnector cable with lazy wave configuration.

Parameter	Value
Cable length	500 m
Total number of nodes	944
Buoyant section start	$s = 220$m
Buoyant section end	$s = 260$m
Water depth	200 m

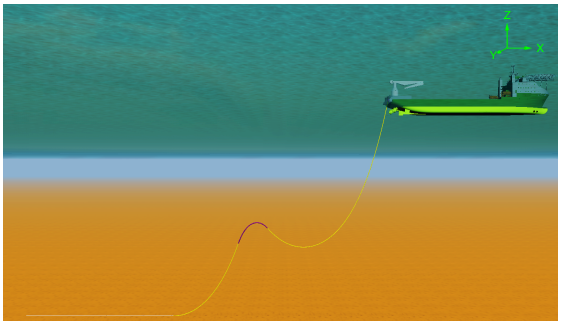

Figure 7.7: Shaded graphics view of OrcaFlex cable catenary model for the interconnector power cable with lazy wave configuration.

In Figure 7.7, the buoyant section of the cable is indicated in purple.

7.1.4. Cable Protection System

The last mitigation measures that are analysed, are Cable Protection Systems (CPS). CPS are used to limit the cable bending motions to a specified maximum curvature. The two main types of CPS are the bend stiffener and the bend restrictor.

Bend restrictor
A bend restrictor is a CPS that is applied around the cable, which limits the cable to a maximum curvature. A restrictor is typically a chain of knuckle-shaped sections that mechanically lock up when bending, as depicted in Figure 7.8.

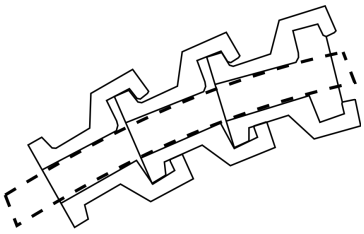

Figure 7.8: Schematic representation of bend restrictor sections mechanically locking up and restricting cable curvature. Cable depicted by dashed lines.

Bend restrictors, like cables, can be modelled in OrcaFlex as line elements. The bending properties

of the CPS can then be defined by a user-specified bending stiffness, i.e. up to κ_{max}, the bending stiffness equals that of the cable, when κ_{max} is exceeded, the bending stiffness is steeply increased.

Bend stiffener

A bend stiffener is a CPS that can be applied around the cable and is made of a material with high bending stiffness. It is mostly used during cable pull-in operations. It can be either of uniform thickness or of progressive thickness. A bend stiffener is not further analysed in this thesis since its application for maximum curvatures is less straightforward than is the case for bend restrictors.

In the simulation models for the infield, export and interconnector cables, a bend restrictor was implemented at both the departure point and TDP, see restrictor properties and model parameters below.

Infield cable

The specific bend restrictor model parameters for the infield cable are listed in Table 7.8.

Table 7.8: Model parameters for the infield cable with bend restrictors.

Parameter	Value
Cable length	190 m
Total number of nodes	590
Restrictor 1 section start	$s = 8$m
Restrictor 1 section end	$s = 13$m
Restrictor 2 section start	$s = 83$m
Restrictor 2 section end	$s = 113$m
κ_{max}	$s = 0.4\text{m}^{-1}$
Water depth	80 m

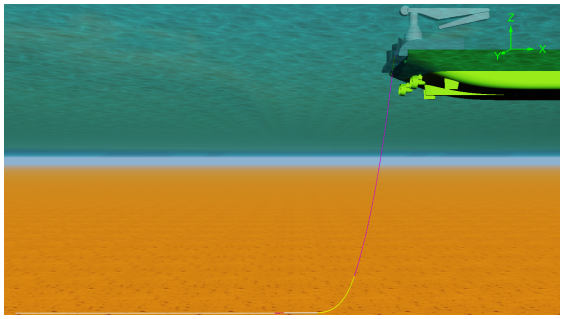

Figure 7.9: Shaded graphics view of OrcaFlex cable catenary model for the infield power cable with bend restrictors.

In Figure 7.9, the restrictors are indicated in yellow.

Export cable

The specific bend restrictor model parameters for the export cable are listed in Table 7.9.

Table 7.9: Model parameters for the export cable with bend restrictors.

Parameter	Value
Cable length	142 m
Total number of nodes	472
Restrictor 1 section start	$s = 8$m
Restrictor 1 section end	$s = 13$m
Restrictor 2 section start	$s = 38$m
Restrictor 2 section end	$s = 58$m
κ_{max}	$s = 0.2\text{m}^{-1}$
Water depth	30 m

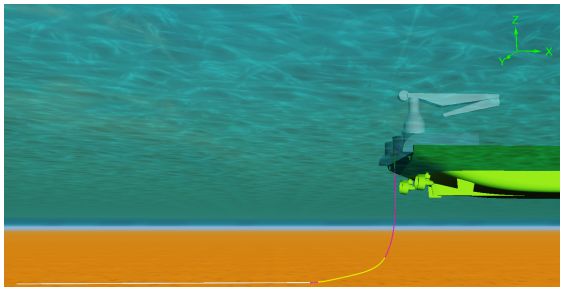

Figure 7.10: Shaded graphics view of OrcaFlex cable catenary model for the export power cable with bend restrictors.

In Figure 7.10, the restrictors are indicated in yellow.

Interconnector cable

The specific bend restrictor model parameters for the interconnector cable are listed in Table 7.10.

Table 7.10: Model parameters for the interconnector cable with bend restrictors.

Parameter	Value
Cable length	500 m
Total number of nodes	944
Restrictor 1 section start	$s = 8$m
Restrictor 1 section end	$s = 13$m
Restrictor 2 section start	$s = 239$m
Restrictor 2 section end	$s = 269$m
κ_{max}	$s = 0.35\text{m}^{-1}$
Water depth	200 m

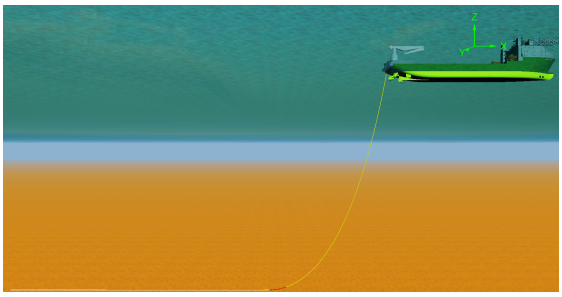

Figure 7.11: Shaded graphics view of OrcaFlex cable catenary model for the interconnector power cable with bend restrictors.

In Figure 7.11, the restrictors are indicated in red.

7.2. Results

The following sections present the results of the fatigue analysis for the mitigated load cases. It is noted here that the fatigue of the armour wires of the cables will not be analysed for these cases, as they were found to have infinite stand-by time for the worst-case loading scenarios. Moreover, for clarity, in the next sections only the mitigated load cases with $H_s = 2.5$ m will be presented. The results for load cases with $H_s = 4$m can be found in Appendix D.

Furthermore, it is noted that the figures in the following sections include the damage curves from the base loading scenarios, depicted in grey, such that the effect of the mitigation measure is clearly visible. In the below, fatigue damage $D \leq 10^{-6}$ will be said to have infinite standby time, since the corresponding stand-by time for three hour JONSWAP simulations is $t_{sb} = 3 \cdot 10^4 = 30000\text{h} = 1250$ days

7.2.1. Vessel heading

Firstly, the cable fatigue damage is analysed for load cases which are mitigated by a variation in vessel heading. Results for the infield power cable are shown in Figure 7.12, whereas Figure 7.13 corresponds to the export power cable. The fatigue behaviour of the interconnector is seen in Figure 7.14.

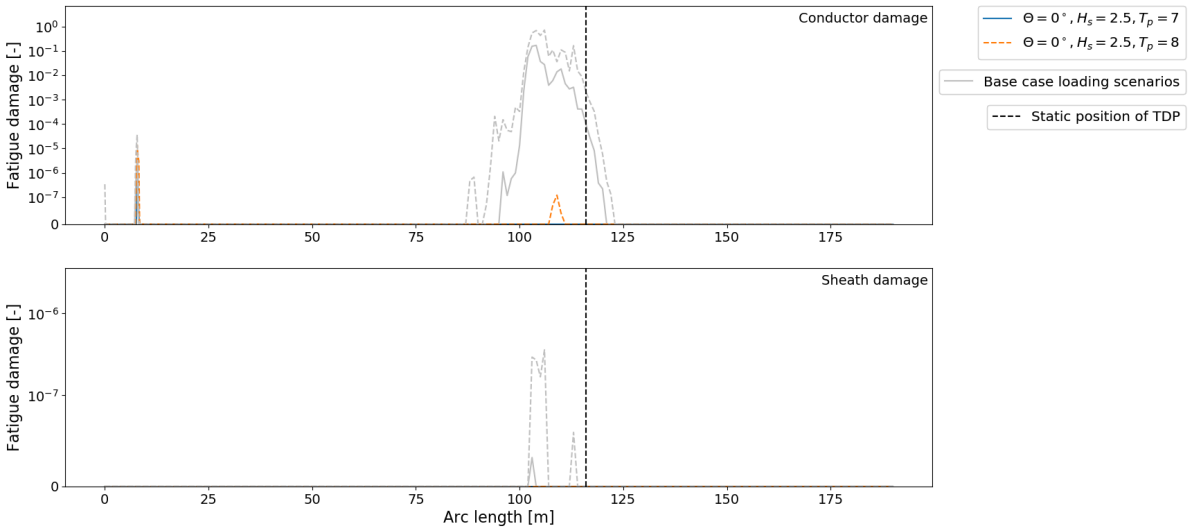

Figure 7.12: Vessel heading: Fatigue damage vs. cable arc length for HVAC infield power cable Al conductor (top) and HDPE sheath (bottom). Wave loading direction $\Theta = 0°$. Grey lines correspond to base case damage curves.

It is clearly visible in the figures that the vessel heading variation has positive effect on cable damage.

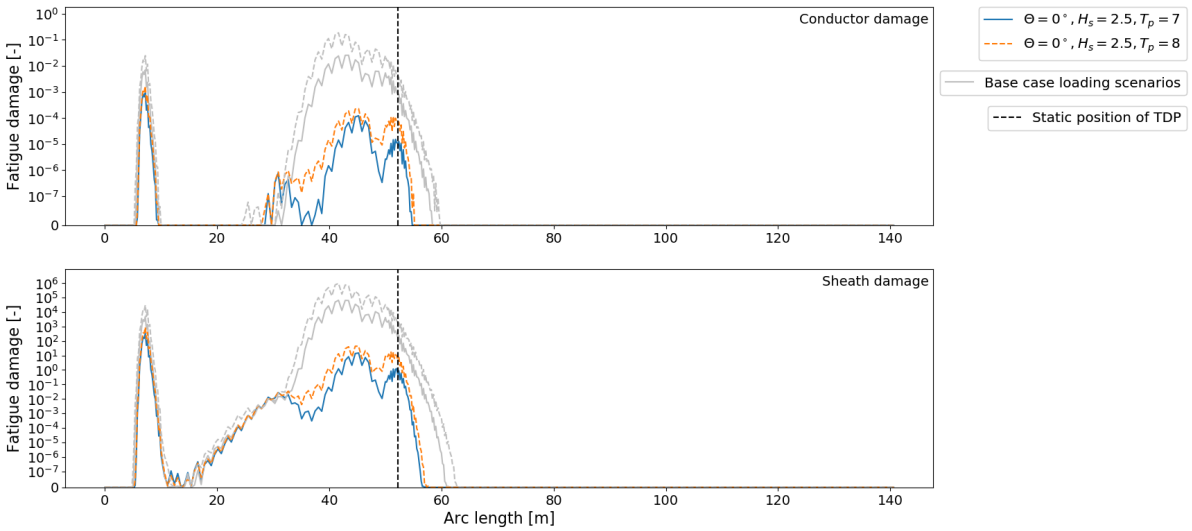

Figure 7.13: Vessel heading: Fatigue damage vs. cable arc length for HVAC export power cable Al conductor (top) and Pb sheath (bottom). Wave loading direction $\Theta = 0°$. Grey lines correspond to base case damage curves.

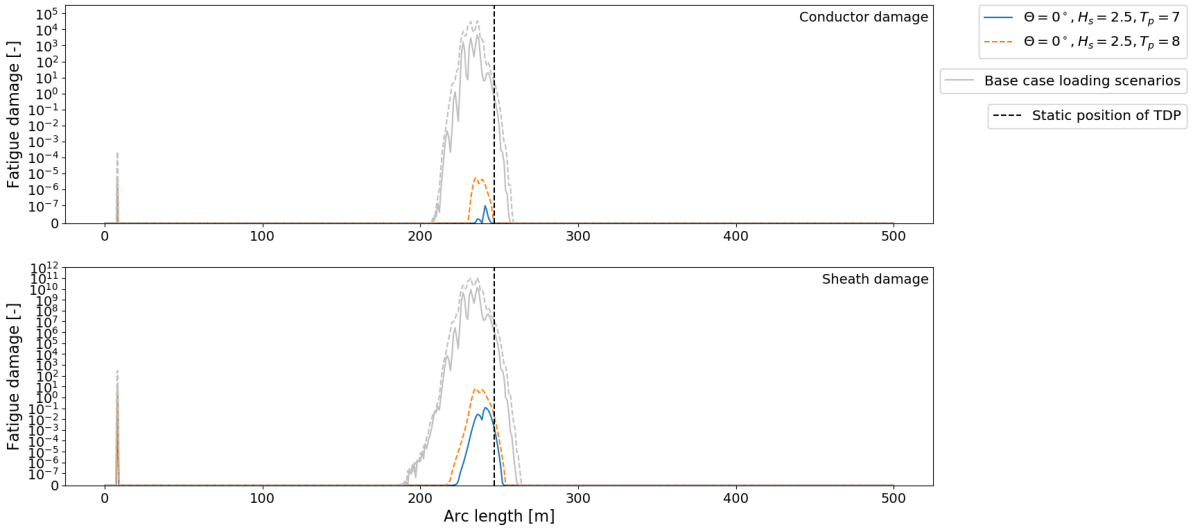

Figure 7.14: Vessel heading: Fatigue damage vs. cable arc length for HVDC interconnector power cable Cu conductor (top) and Pb sheath (bottom). Wave loading direction $\Theta = 0°$. Grey lines correspond to base case damage curves.

The three cables all show conductor damage that is within the fatigue budget. Furthermore, it can be seen that varying the vessel heading is most effective in deep water, as the reduction in damage increases with greater water depth. However, it is also clear that fatigue mitigation by vessel heading variation only is not sufficient to decrease lead sheath fatigue below the fatigue budget. The findings from the fatigue analysis for the conductor and sheath components are summarised in Table 7.11 and Table 7.12, respectively.

Table 7.11: Vessel heading mitigation for cases where $H_s = 2.5$m for infield, export and interconnector conductors.

Cable	D_{max}^{base}[-]	t_{sb}^{base}[days]	$D_{max}^{heading}$[-]	$t_{sb}^{heading}$[days]
Infield (Al)	10^{0}	0	$5 \cdot 10^{-7}$	∞
Export (Al)	10^{-1}	0	10^{-4}	12.5
Interconnector (Cu)	10^{5}	0	10^{-5}	125

Lastly, the damage curves for load cases with $H_s = 4$m can be found in Appendix D.1. However, despite

Table 7.12: Vessel heading mitigation for cases where $H_s = 2.5$m for infield, export and interconnector sheaths.

Cable	D_{max}^{base}[-]	t_{sb}^{base}[days]	$D_{max}^{heading}$[-]	$t_{sb}^{heading}$[days]
Infield (HDPE)	$5 \cdot 10^{-7}$	∞	0	∞
Export (Pb)	10^{6}	0	10^{3}	0
Interconnector (Pb)	10^{12}	0	10^{1}	0

the change in vessel heading, the cable responses are severe and the mitigation has little effect.

7.2.2. Layback length increase

In this section, cable fatigue damage is analysed for load cases which are mitigated by a variation in cable tension. The infield, export and interconnector cable correspond to 7.15, Figure 7.16 and Figure 7.17, respectively.

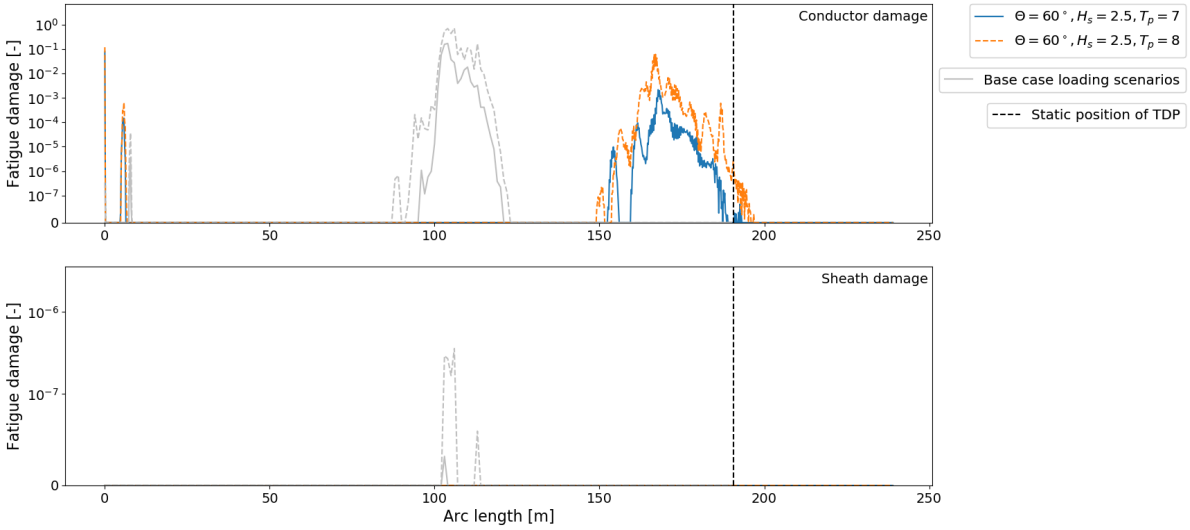

Figure 7.15: Layback increase: Fatigue damage vs. cable arc length for HVAC infield power cable Al conductor (top) and HDPE sheath (bottom). Wave loading direction $\Theta = 60°$. Grey lines correspond to base case damage curves.

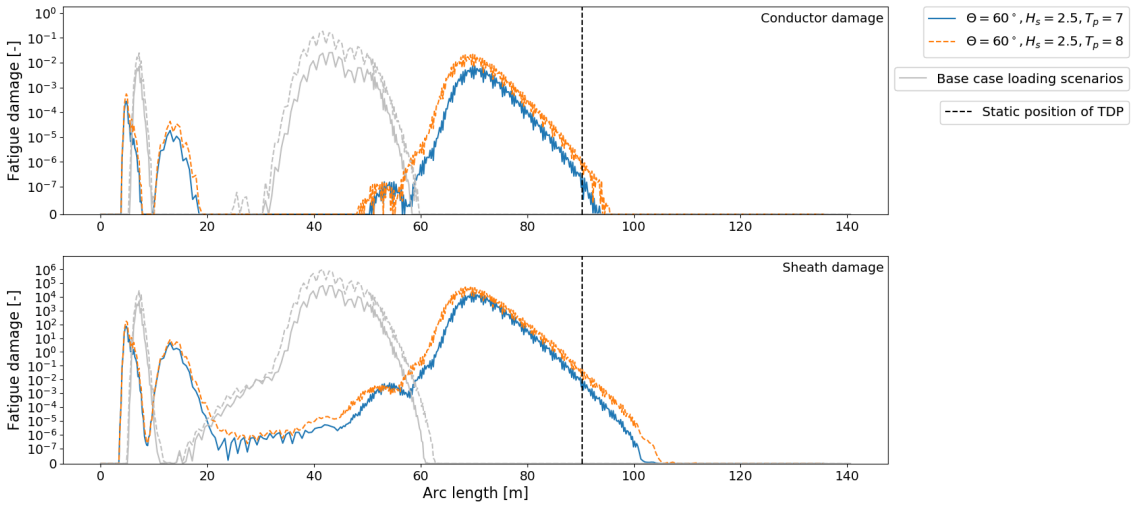

Figure 7.16: Layback increase: Fatigue damage vs. cable arc length for HVAC export power cable Al conductor (top) and Pb sheath (bottom). Wave loading direction $\Theta = 60°$. Grey lines correspond to base case damage curves.

The increased layback length implies that a longer part of the cable is free-hanging. This is supported

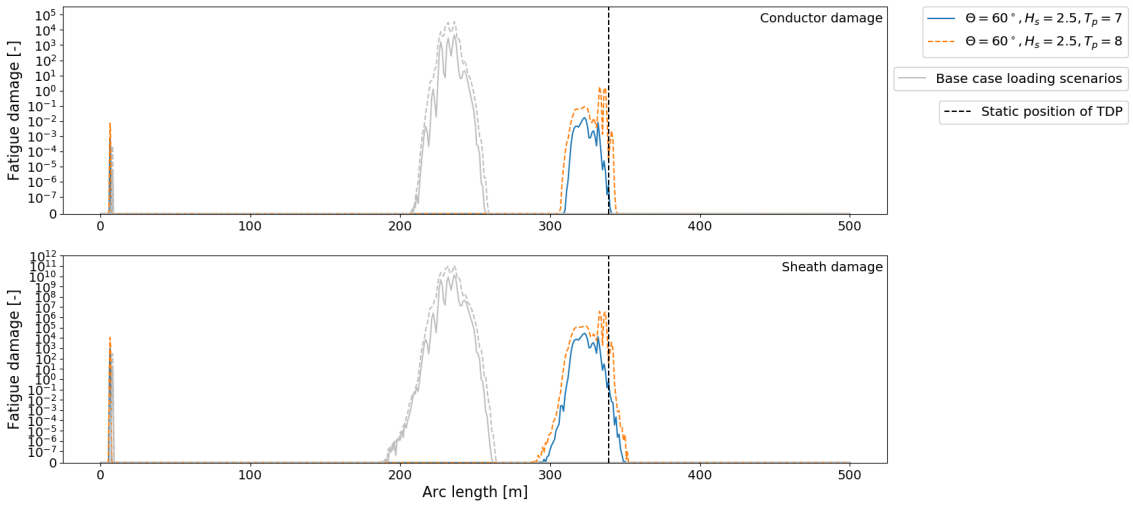

Figure 7.17: Layback increase: Fatigue damage vs. cable arc length for HVDC interconnector power cable Cu conductor (top) and Pb sheath (bottom). Wave loading direction $\Theta = 60°$. Grey lines correspond to base case damage curves.

by the data in the figures as all TDP damage peaks are shifted towards the anchored end of the cable. Furthermore, from the figures it can be seen that the increased system tension leads to a reduction in component damage. However, the reduction is significantly smaller in comparison to the vessel heading mitigation. In addition, like in the case of vessel heading mitigation, the figures show that mitigation is most effective in deep water. Out of the three cables, the interconnector bottom tension was increased the least, but the conductor damage is mitigated the most. The findings from the conductor and sheath fatigue analysis are summarised in Table 7.13 and Table 7.14.

Table 7.13: Layback increase mitigation for cases where $H_s = 2.5$m for infield, export and interconnector conductors.

Cable	D_{max}^{base}[-]	t_{sb}^{base}[days]	$D_{max}^{heading}$[-]	$t_{sb}^{heading}$[hours]
Infield (Al)	10^{0}	0	10^{-2}	3
Export (Al)	10^{-1}	0	10^{-2}	3
Interconnector (Cu)	10^{5}	0	10^{1}	0

Table 7.14: Layback increase mitigation for cases where $H_s = 2.5$m for infield, export and interconnector sheaths.

Cable	D_{max}^{base}[-]	t_{sb}^{base}[days]	$D_{max}^{heading}$[-]	$t_{sb}^{heading}$[hours]
Infield (HDPE)	$5 \cdot 10^{-7}$	∞	0	∞
Export (Pb)	10^{6}	0	10^{5}	0
Interconnector (Pb)	10^{12}	0	10^{7}	0

Similarly to the vessel heading mitigation measure, the increased layback length does not significantly influence the damage curves for load cases where $H_s = 4$m, see Appendix **??**.

7.2.3. Lazy wave configuration

In this section, cable fatigue damage is analysed for load cases which are mitigated by a lazy wave configuration. The infield, export and interconnector cable correspond to corresponds to Figure 7.18, Figure 7.19 and Figure 7.20, respectively.

All three cables exhibit different behaviour when the lazy wave configuration is applied. The infield power cable, modelled in 60m water depth, shows a significant decrease in the part of the cable that is subject to fatigue, with no damage occurring in the touchdown zone. However, the part of the cable that forms the bend in the lazy wave, is subject to fatigue damage (in the conductor). It can be concluded that the lazy wave shape indeed provides an additional damping to the cable response at the TDP.

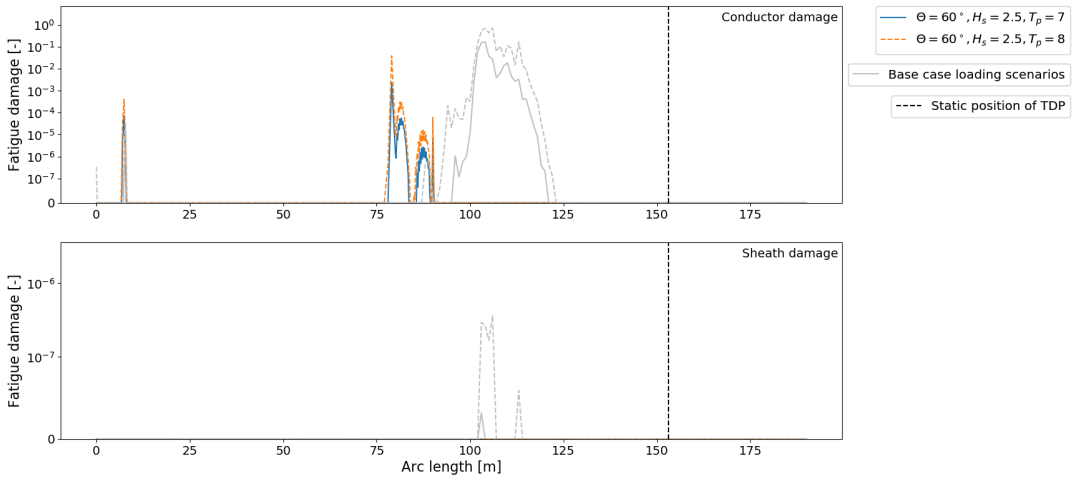

Figure 7.18: Lazy wave: Fatigue damage vs. cable arc length for HVAC infield power cable Al conductor (top) and HDPE sheath (bottom). Wave loading direction $\Theta = 60°$.

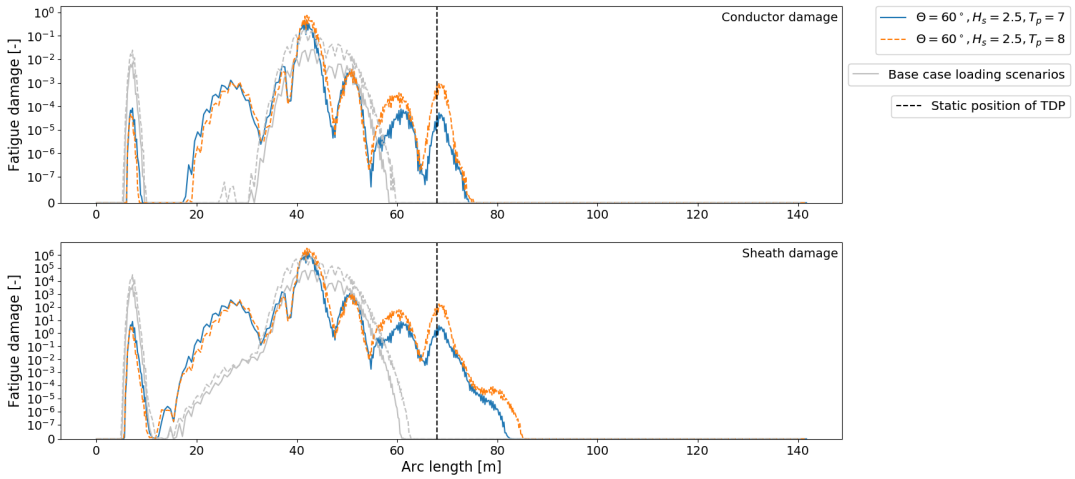

Figure 7.19: Lazy wave: Fatigue damage vs. cable arc length for HVAC export power cable Al conductor (top) and Pb sheath (bottom). Wave loading direction $\Theta = 60°$.

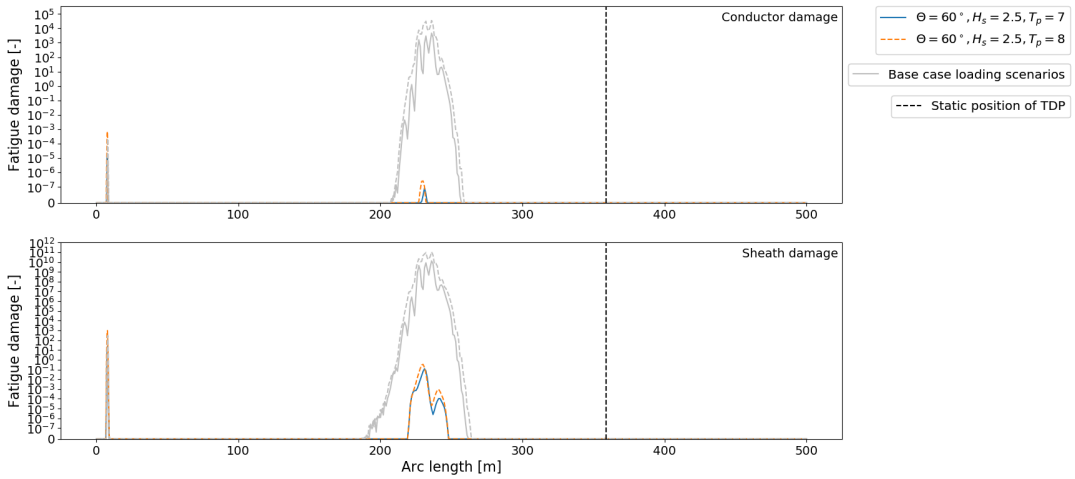

Figure 7.20: Lazy wave: Fatigue damage vs. cable arc length for HVDC interconnecting power cable Cu conductor (top) and Pb sheath (bottom). Wave loading direction $\Theta = 60°$.

However, in magnitude, the fatigue damage in the lazy wave bend exhibits a peak that is still significant and will cause fracture.
Contrary to the infield cable, the export cable exhibits worse fatigue behaviour when in lazy wave configuration in comparison to the free-hanging catenary. Although the magnitude of the fatigue damage is slightly improved at the departure point, the lazy bend causes fatigue damage over the entire length of the cable, whilst not mitigating the TDP fatigue. Due to being modelled in shallow water, the export cable lazy bend cannot freely move along with the wave loading and is held back by the clamped boundary conditions of the nearby TDP and departure point. It follows that a lazy wave configuration requires intermediate to deep water to effectively mitigate fatigue damage. This is further illustrated by the interconnector cable, which is modelled in 200m water depth. Here, the fatigue damage has significantly decreased in both magnitude and over the length of the cable, such that only two narrow peaks at the departure point and in the lazy wave bend remain. The findings from the lazy wave fatigue analysis are summarised in Table 7.15 and Table 7.16 for the conductor and sheath components respectively.

Table 7.15: Lazy wave configuration mitigation for cases where $H_s = 2.5$m for infield, export and interconnector conductors.

Cable	D_{max}^{base}[-]	t_{sb}^{base}[days]	$D_{max}^{heading}$[-]	$t_{sb}^{heading}$[hours]
Infield (Al)	10^{0}	0	10^{-2}	3
Export (Al)	10^{-1}	0	10^{0}	0
Interconnector (Cu)	10^{5}	0	10^{-7}	∞

Table 7.16: Lazy wave configuration mitigation for cases where $H_s = 2.5$m for infield, export and interconnector sheaths.

Cable	D_{max}^{base}[-]	t_{sb}^{base}[days]	$D_{max}^{heading}$[-]	$t_{sb}^{heading}$[hours]
Infield (HDPE)	$5 \cdot 10^{-7}$	∞	0	∞
Export (Pb)	10^{6}	0	10^{5}	0
Interconnector (Pb)	10^{12}	0	10^{-1}	0

As opposed to other mitigation measures, wave loads with $H_s = 4$m are also mitigated by a lazy wave configuration in deep water. For the interconnector cable, the conductor damage was reduced to $D = 10^{-3}$ by applying the lazy wave configuration, see damage curve in Appendix D.2.

Lazy wave and vessel heading mitigation
Table 7.16 indicates that in deep water, a lazy wave configuration is nearly sufficient to mitigate the fatigue of the interconnector lead sheath. Given that lead sheaths are the critical component from fatigue point of view, the lazy wave mitigation measure is combined with the vessel heading mitigation in this section in order to check if lead sheath fatigue can indeed be mitigated. In this regard, Figure 7.21 depicts the fatigue damage curve for the interconnector lead sheath when the cable is configured in lazy wave shape and the incoming wave direction is $\Theta = 0°$.
It can be seen that the lead sheath fatigue has been mitigated such that $D = 10^{-5}$, with corresponding maximum stand-by time $t_{sb} = 125$ days.

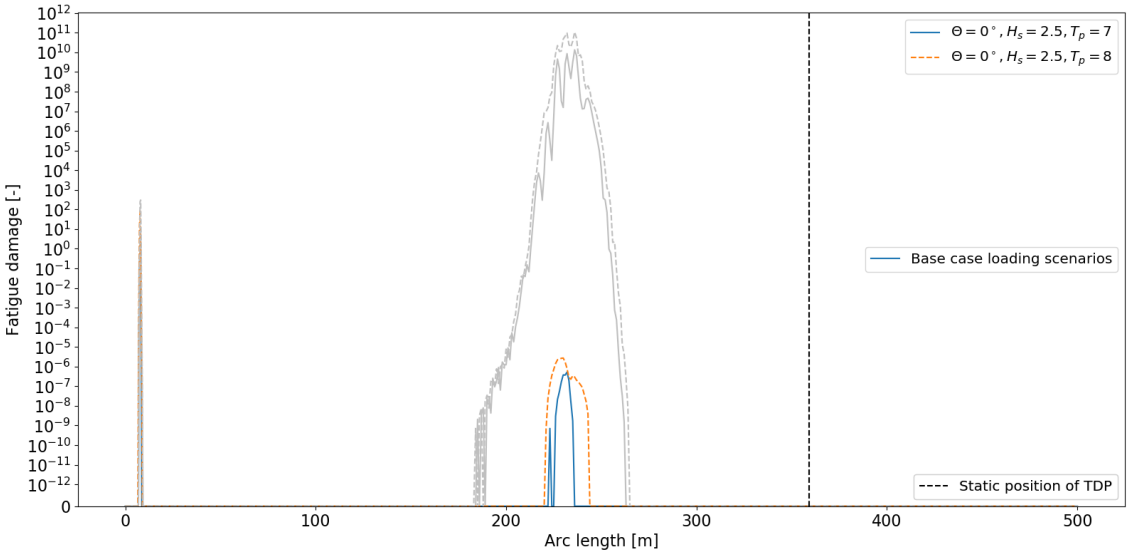

Figure 7.21: Lazy wave: Fatigue damage vs. cable arc length for HVDC interconnecting power cable sheath (Pb). Wave loading direction $\Theta = 0°$.

7.2.4. Bend restrictor

The last mitigation measure that is discussed in this chapter is the bend restrictor. Figures 7.22, 7.23 and 7.24 show the damage curves for the infield power cable, the export power cable and the interconnecting power cable respectively.

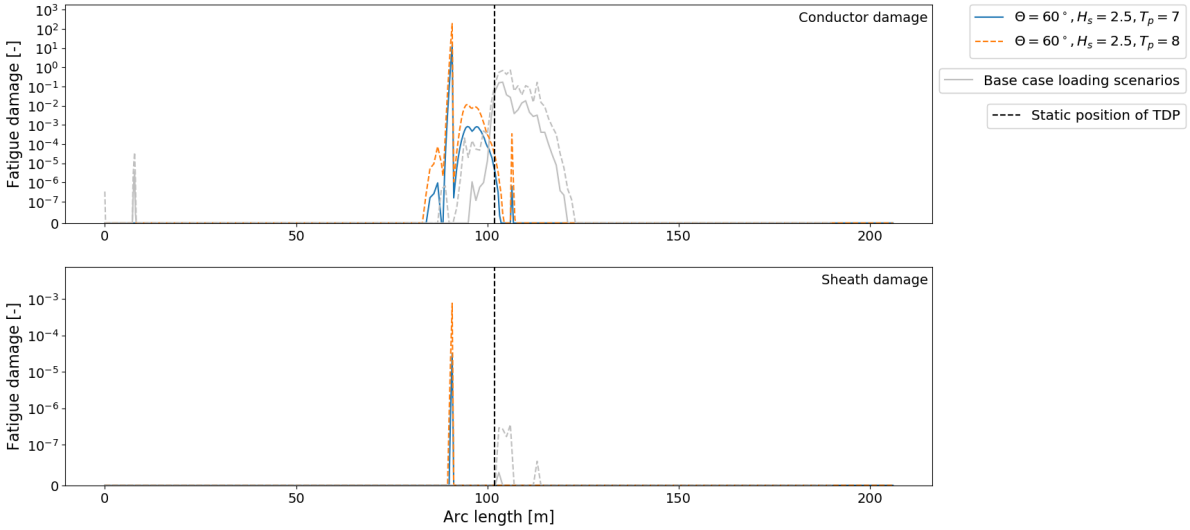

Figure 7.22: Bend restrictor: Fatigue damage vs. cable arc length for HVAC infield power cable Al conductor (top) and HDPE sheath (bottom). Wave loading direction $\Theta = 60°$. Grey lines correspond to base case damage curves.

From Figure 7.22, the position of the bend restrictor at the TDP can be seen as the arc length between the two damage peaks at $s = 83$m and $s = 113$m., as was stated in 7.8. Within this region, the conductor damage is reduced in comparison to the non-mitigated case. However, due to the presence of the bend restrictor, the cable parts exiting the bend restrictor show increased fatigue. At these positions, the bend restrictor becomes a buckling point for the rest of the cable, when the MBR of the cable is breached. Mitigation of the TDP is therefore only possible if the full span of the touchdown zone is covered by the bend restrictor. For the case of the infield power cable, this implies that a 50-60m bend restrictor would have to be installed, which is not a realistic option during cable installation operations. Contrary to the TDP, the departure point of the cable shows decreased fatigue damage due to the implementation of the bend restrictor.

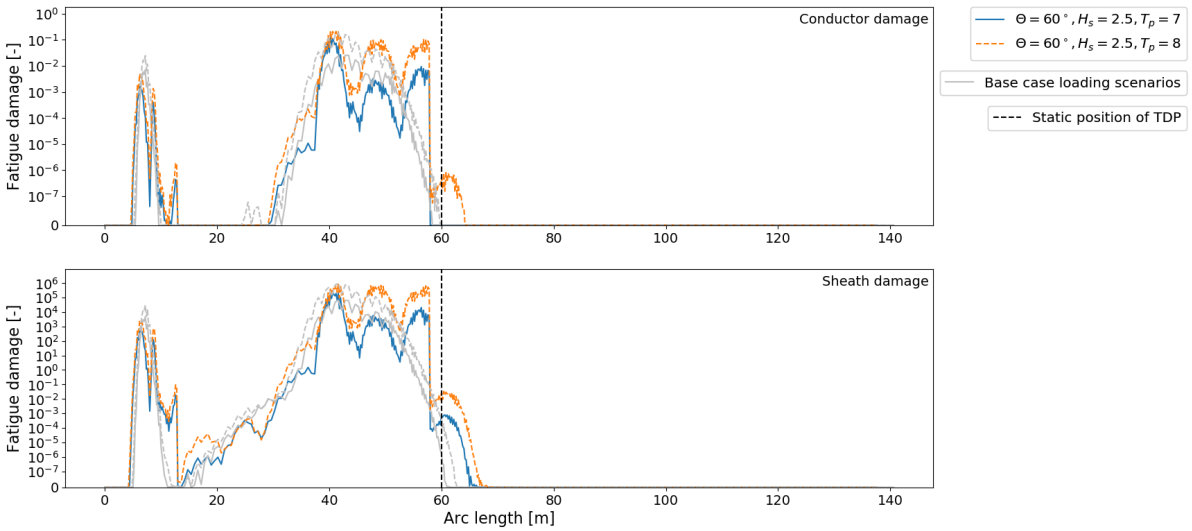

Figure 7.23: Bend restrictor: Fatigue damage vs. cable arc length for HVAC export power cable Al conductor (top) and Pb sheath (bottom). Wave loading direction $\Theta = 60°$. Grey lines correspond to base case damage curves.

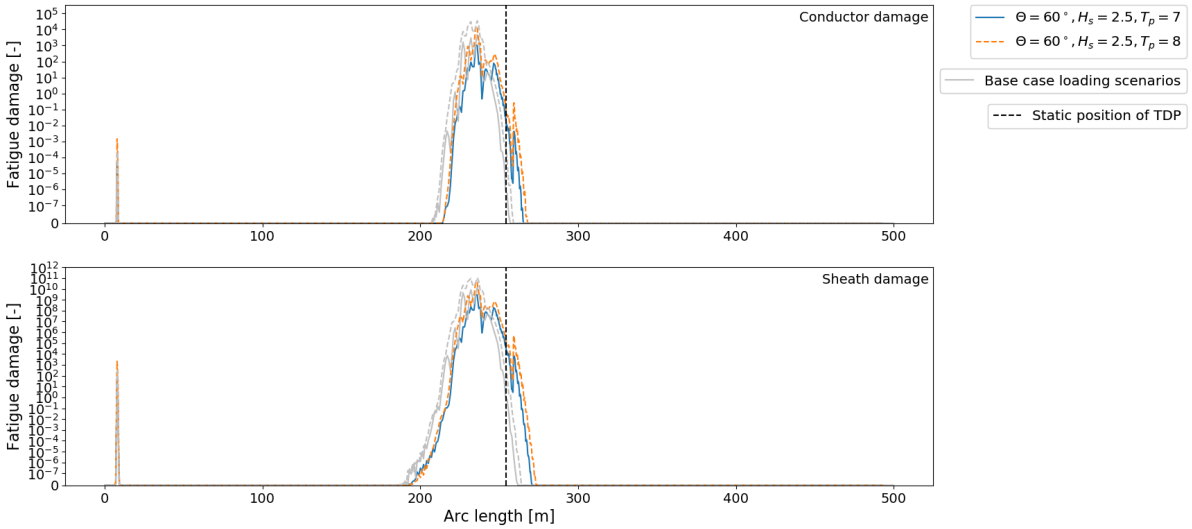

Figure 7.24: Bend restrictor: Fatigue damage vs. cable arc length for HVDC interconnector power cable Cu conductor (top) and Pb sheath (bottom). Wave loading direction $\Theta = 60°$. Grey lines correspond to base case damage curves.

The export power cable shows similar behaviour as the infield power cable. Figure 7.23 indicates that the bend restrictor is placed between arc lengths $s = 38$m and $s = 58$, at which the increased damage peaks due to the buckling motion of the cable are clearly visible. Within the bend restrictor range and the departure point, a slight decrease of conductor damage is observable.
Lastly, in the damage curve for the interconnector cable conductor, seen in Figure 7.24, the employment of the bend restrictor is not clearly noticeable and nearly identical fatigue damage magnitudes are found as in the base cases due to the deep water conditions and broad touchdown area.

It can be concluded that a bend restrictor is only suitable as mitigation method when applied at the departure point, or other narrow cable parts that are subject to fatigue. In Appendix D.3 the damage curves for the cable sheaths and higher wave heights are presented.

7.2.5. Layback increase and vessel heading

This far, it has been shown that the vessel heading, increase of the tension in the cable and a lazy wave configuration have positive effect on the fatigue behaviour of cross-sectional cable components. However, it was also found that mitigation by vessel heading and layback increase are not always sufficient measures to force the fatigue damage within its installation budget. Additionally, configuring a cable in lazy wave shape takes time and puts a stop to installation operation. Therefore, this section will include a mitigation method which combines the layback increase and vessel heading.
Figures 7.25, 7.26 and 7.27 show the damage curves for the infield power cable, the export power cable and the interconnecting power cable respectively. It is seen in the figures that the combined

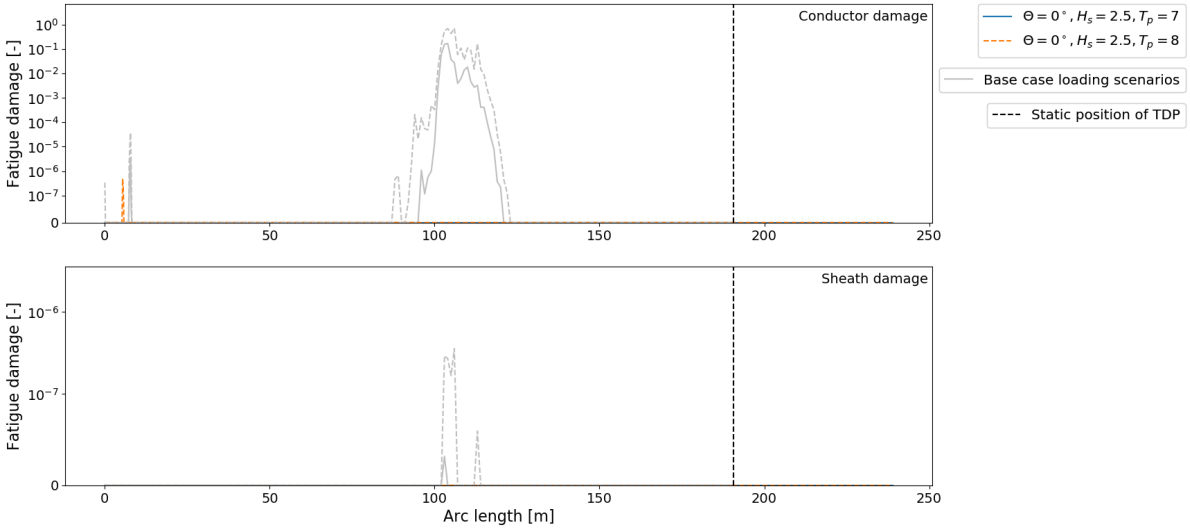

Figure 7.25: Layback increase: Fatigue damage vs. cable arc length for HVAC infield power cable Al conductor (top) and HDPE sheath (bottom). Wave loading direction $\Theta = 0°$.

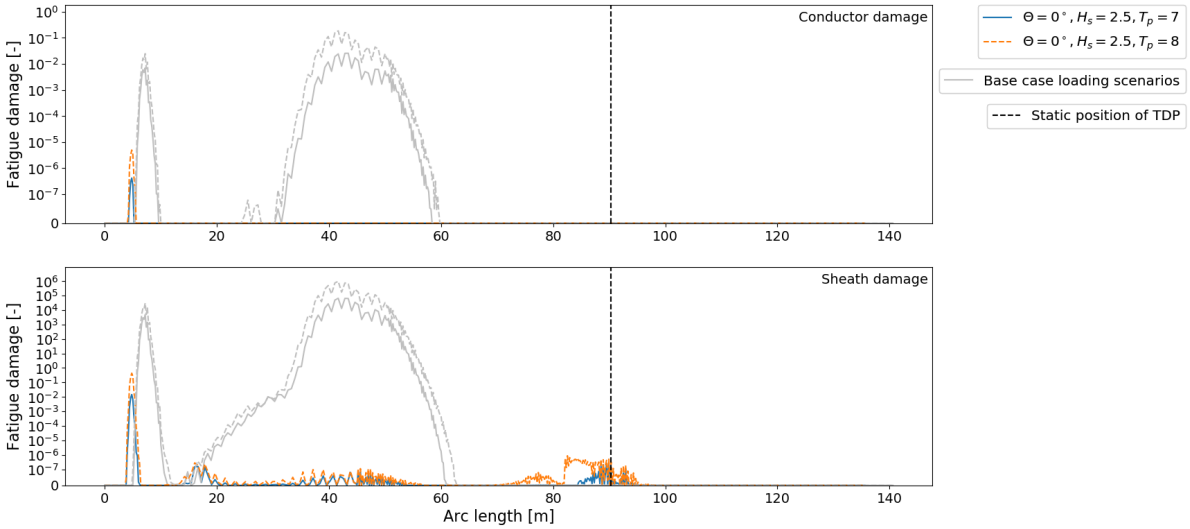

Figure 7.26: Layback increase: Fatigue damage vs. cable arc length for HVAC export power cable Al conductor (top) and Pb sheath (bottom). Wave loading direction $\Theta = 0°$.

mitigation method yields very favourable results. No damage occurs at the touchdown point anymore and the damage at the departure point is decreased beyond the fatigue budget of 10^{-2}, even in the lead sheath cases. The findings from the damage analysis are summarised in Table 7.17 and Table 7.18. Lastly, it is noted that the higher loading scenarios were also significantly mitigated, although damage still exceeds the fatigue budget. See Appendix D.4 for details on the damage curves.

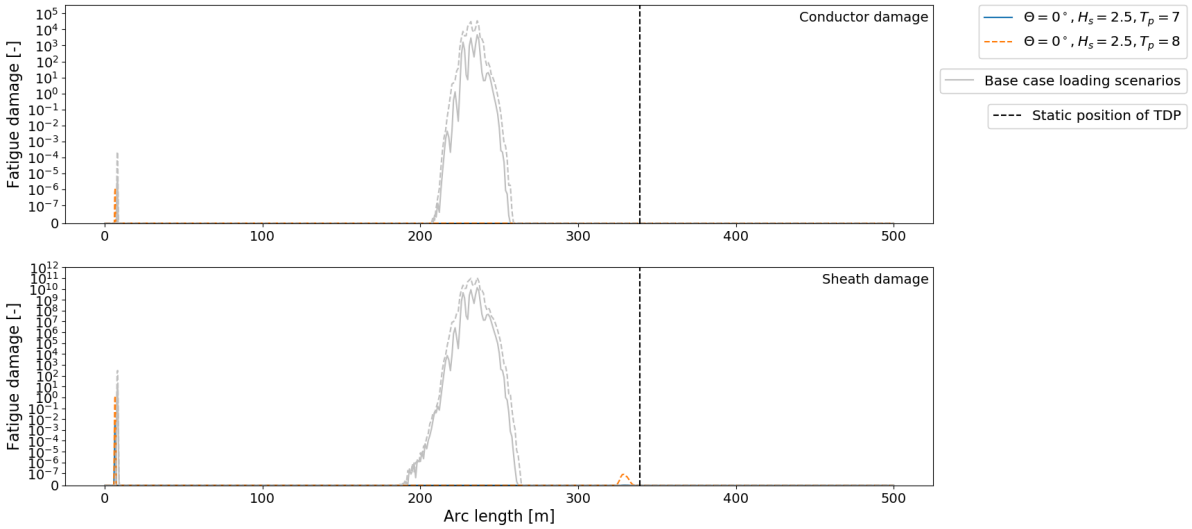

Figure 7.27: Layback increase: Fatigue damage vs. cable arc length for HVDC interconnector power cable Cu conductor (top) and Pb sheath (bottom). Wave loading direction $\Theta = 0°$.

Table 7.17: Layback increase with adjusted vessel heading mitigation for cases where $H_s = 2.5$m for infield, export and interconnector conductors.

Cable	D_{max}^{base}[-]	t_{sb}^{base}[days]	$D_{max}^{heading}$[-]	$t_{sb}^{heading}$[days]
Infield (Al)	10^{0}	0	10^{-6}	∞
Export (Al)	10^{-1}	0	10^{-5}	125
Interconnector (Cu)	10^{5}	0	10^{-6}	∞

Table 7.18: Layback increase with adjusted vessel heading mitigation for cases where $H_s = 2.5$m for infield, export and interconnector sheaths.

Cable	D_{max}^{base}[-]	t_{sb}^{base}[days]	$D_{max}^{heading}$[-]	$t_{sb}^{heading}$[days]
Infield (HDPE)	$5 \cdot 10^{-7}$	∞	0	∞
Export (Pb)	10^{6}	0	10^{-1} (only at the departure point)	0
Interconnector (Pb)	10^{12}	0	10^{-7}	∞

7.3. Conclusions

In this chapter, an overview of mitigation measures for cable fatigue was presented. Vessel heading variation, layback increase, lazy wave cable configuration and bend restrictor mitigation measures were added to the base loading case models and subsequently, fatigue analyses of the three cable types subject to the mitigated load cases were performed.

Firstly, it was found that loading scenarios where $H_s = 4$ m, are difficult to mitigate due to the severity of the loads. In fact, most cable elements fracture under these loads, with the exception of the HDPE sheath that is used in the infield HVAC power cable and certain combinations of mitigation measures, e.g. vessel heading and layback increase or vessel heading and lazy wave (in deep water only). However, all other loading scenarios, with $H_s = 2.5$m were mitigated accordingly, to ultimately reach fatigue damage levels that are below the fatigue budget.

Additionally, it was shown that for the vessel heading mitigation, where the wave direction was chosen to be $\Theta = 0°$, and layback increase, there is a significant decrease in cable fatigue, but the failure of lead sheaths could not be countered by vessel heading alone. Therefore combined mitigation measures were introduced. In particular, the combination of lazy wave configuration and vessel heading was shown to be well suited to counter (lead sheath) fatigue, although sufficiently deep water is re-

quired for the lazy wave configuration to be effective, as it was found that in shallow water, the cable experiences high fatigue loads over the full length of the cable.

The combination of layback increase and vessel heading was also researched, as this method does not require a stop of installation operations, whereas the installation of buyancy tanks or a bend restrictor takes time. Results of this combined mitigation measure showed very favourable down-time conditions, as all components had stand-by times of the order $t_{sb} = 10^2$ days or greater for wave loads with $H_s \leq 2.5$m, except the lead sheath of the export cable - which is still critical at the departure point.

The last mitigation method introduced in this chapter was the bend restrictor, for which it was shown that it is only suitable for mitigating fatigue at the departure point, since the broad span of the touchdown zone may give rise to buckling motions of the cable around the bend restrictor, or needs to become very long.

8

Discussion

In this chapter, an elaborate discussion of both the theoretical findings and modelling results that were obtained during this research is presented. The structure of the chapter will be based on the content relating to the research questions that were defined in Chapter 1.

8.1. Fatigue and material theory

In the fatigue theory overview, a method to assess fatigue in subsea marine power cables was presented. The most important concepts of the method were the rainflow counting algorithm to analyse irregular load time-histories and S-N curves that define material resistances to fatigue. The former and latter concepts were subsequently related to each other by Miner's rule. Rainflow counting, S-N curves and Miner's rule are widely established concepts in fatigue assessment theory and are available in software packages like OrcaFlex.

Despite this, fatigue life time is difficult to analyse for materials that have steep S-N curves. In particular lead, the material that was found to be most sensitive to fatigue in submarine power cable cross-sections, exhibits steep fatigue resistance curves. Typically, the S-N approach is not accurate for materials with S-N curves that have slope larger than seven. The slope of the S-N curve that is used in this research for lead can be approximated by $b_{lead} \approx 13$. Although other materials also have S-N curves with high slopes, lead also has weak fatigue life properties, causing an unstable fatigue life time behaviour, as was seen in the lead sheath fatigue analyses of Chapters 6 and 7. An alternative method to the S-N approach would be the infinite life criterion [37]. In this method, fatigue is not quantified, but determined qualitatively by the so-called life criterion. Stress magnitudes that exceed this line caue fracture, whereas stress magnitudes beneath the life criterion are said to have infinite life. However, by using this method, one loses information about fatigue life times of materials, which is one of the main goals of this thesis.

In addition, the S-N curves for all materials were defined for the high-cycle, elastic fatigue regime and were extrapolated for stress magnitudes in the low-cycle, plastic regime. As plastic stress magnitudes did occur in the fatigue analysis, S-N curves with separate low-cycle fatigue parts would enhance the accuracy of the fatigue analysis. Moreover, S-N curves are derived empirically and are therefore test and material dependent. S-N curves specifically for subsea power cable materials are hence very rare and therefore many S-N curves correspond to materials that only approximate the materials in power cable cross sections. An alternative method would be the strain-life approach, in which the material fatigue resistance is based on the strain. Especially for lead applications in submarine cable, there have been several cable-specific tests for the derivation of strain-life curves. For future work, it is recommended to develop a strain-life based fatigue assessment method to be able to compare fatigue results.

8.2. Cross-sectional analysis

The cross-sectional model that was derived in this thesis was shown to be consistent with test data for bending moments. However, the sample size of cables for which test data and/or cross-sectional properties is available is very small, which creates the necessity of making various assumptions for fatigue analyses on different types of cables. In fact, no existing test data for tensile cross-sectional stress-strain behaviour was available, although it should be noted that results showed that fatigue damage due to tensile stresses are negligible.

Future fatigue studies would improve significantly if more cross-sectional cable data, test data and submarine power cable fatigue assessment tools would be available to develop well-defined models and compare these to existing data.

Furthermore, one of the main assumptions that was made in this work is that the cross-section materials are always within the elastic stress-strain limit However, results showed several load cases where the yield stress of a material was exceeded. Most of these cases also caused a breach of cable MBR. Therefore, during installation, this will not be a problem, as the MBR is always maintained during operations.

8.3. Results

Most of the cases where plasticity occurred were in lead sheaths, which proved to be the most critical cable component from fatigue point of view. When this is combined with its inaccurate application of the S-N approach, it can be concluded that lead is also the component for which it is most difficult to define maximum stand-by times based on fatigue damage.

For future work in lead sheath fatigue assessment it is interesting to research a strain-life fatigue analysis performed for the HVDC interconnector cable that was analysed in this work, found in [38]. By means of a strain-life analysis the maximum stand-by time for the interconnector cable was found to be 3 hours for waves with 6 second peak periods, in 30 m water depth. This work can be used as reference or comparative data for a strain-life fatigue assessment method.

For aluminium and copper conductors, it was found that as long as the MBR of the cable is not breached, installation operations will not be limited from fatigue point of view. Moreover, the HDPE sheath used in the infield power cable was found to have superior fatigue behaviour to lead, surviving load cases for which the MBR was breached. It is interesting to continue developing HDPE as a sheathing material such that in the future it can be applied in high-voltage cables and lead can be ultimately eliminated.

Lastly, it is noted that armour wires experience little to no fatigue damage during installation operations, which was expected based on the cross-sectional and S-N data analyses due to the high elastic modulus and fatigue resistance of stainless steel

8.4. Mitigation analysis

The four mitigation measures that were studied, vessel heading, layback increase, lazy wave configuration and bend restrictors all proved to have positive effect on the fatigue life of cable materials. Weathervaning is the most straightforward mitigation measure and can be combined with any additional mitigation measures. In this research, it was combined with the lazy wave configuration and the layback increase. Both combinations mainly mitigate the cable response at the TDP, so the departure point becomes the critical point in terms of fatigue. However, the lazy wave configuration should only be applied in deep water, as the free movement of the cable is limited in shallow water and fatigue may become apparent once more. Additionally, the lazy wave configuration is only applied for weather survival, i.e. installation operations come to a stop. For these reasons, it is recommended to always mitigate by the combination of increasing the layback length and a favourable vessel heading. Furthermore, the bend restrictor was found to be inadequate for mitigation of cable motions at the TDP due to the broad span of the touchdown zone. Contrary to the TDP mitigation, bend restrictors showed significant decreases in cable damage at the departure point. In severe loading conditions, a bending

restrictor could be installed at the departure point, as the other mitigation methods primarily act on the TDP.

Lastly, it should be noted that the variation of load cases in this thesis is limited. To yield defined results of the maximum stand-by times for various elements, one should also consider running more simulations. However, in this work the focus was primarily on a complete cross-sectional analysis and due to time constraints, no research into regular wave approximations of JONSWAP loads was done. For future research, it is recommended to include this study. The OrcaFlex manual [5] devotes a theoretical chapter to this, based on [39], which may be useful for further research.

9

Conclusions & Recommendations

In this chapter, the presented theory, models and analyses are used to answer the research questions that were defined in Chapter 1. Therefore, the structure of this chapter will be based on the main research question:

Which submarine power cable material properties are limiting from a fatigue point of view and how does this affect cable installation operations?

After conclusions are drawn, the chapter will conclude with recommendations for future work.

9.1. Conclusions

A fatigue assessment method for submarine power cable installation operations was presented in this report to find resistance limits of various cable elements, which was based on the rainflow counting algorithm, S-N curves and Miner's rule. These methods are widely established methods in fatigue analysis and frequently applied in fatigue assessment of offshore pipelines and umbilicals. However, non-specific S-N data yields a level of uncertainty, particularly for cable cross-section materials may lead to unstable fatigue behaviour for materials with steep Basquin slopes, which was the case for lead.

Furthermore, a structural model for cross-sectional stresses was developed and verified against existing cable test data. For bending behaviour, consistent results between the data and theory was shown. However, the sample size of test data for submarine power cables remains small and therefore a larger amount of cables should be analysed to yield scientific conclusions about the validity of the cross-sectional model. Consequently, many assumptions have to be made when analysing different types of cables. Upon implementation of the cross-sectional model, it was found that the tensile stresses in the cross-sectional cable components have negligible effect on fatigue life.

Based on a material S-N data analysis and the cross-sectional model that was developed, it was theoretically found that lead sheaths are the most critical component in cable cross-sections due to the combination of weak fatigue properties and relatively high elastic modulus. In the case that the protective sheath is not made of lead, it was shown that cable conductors are critical components.

Additionally, a fatigue assessment calculation tool was developed to calculate stresses and fatigue damage of various cables with input from the global modelling software OrcaFlex. From the global output of OrcaFlex, local stresses were calculated with the cross-sectional model and subsequently analysed by the aforementioned fatigue assessment methods. The model was applied to three cable types, subject to various load cases, and showed favourable fatigue results for mild loading conditions, yielding infinite fatigue life for wave loads with $H_s \leq 1.5$m. For severe load scenarios, fatigue life was shown to be minimal, and mitigation measures are required. Moreover, it was concluded that lead is indeed the weakest cable component from fatigue point of view. Due to its steep S-N curve and severe base cases, defining maximum stand-by times for lead sheaths accurately is difficult. For other

materials, such as HDPE, Aluminium, Copper and Stainless Steel, it was found that installation operations are not limited by their respective fatigue life, as long as the MBR of the cable is preserved. If the MBR is breached, plastic behaviour comes into play and one of the main model assumptions is broken.

Mitigation measures that were analysed in this report are: Vessel heading variation, layback increase, Lazy wave cable configuration and bend restrictors. It was shown that a variation in vessel heading or an increase of layback always have positive effect on the fatigue life of cable components. The lazy wave configuration, proved to be the most effective mitigation measure in deep water, as the motions at the TDP - which is most sensitive for fatigue - are damped through the lazy bend shape. However, its main drawback is that it cannot be used in shallow. In that case, the lazy bend is not free to move due to the nearby connections at the TDP and departure point and fatigue is becoming more apparent. The bend restrictor was found to provide insufficient mitigation to the cable response at the TDP and should not be used to counter fatigue in the touchdown zone. However, at the departure point, bending restrictors have some positive effect on fatigue life, although lesss significant than other mitigation measures.

No mitigation measure was found to independently decrease fatigue damage below the fatigue budget for severe load cases and thus combinations of favourable vessel headings with lazy wave configurations and increased laybacks were analysed for the different types of cables. The combination of increased tension in the cable with a favourable vessel heading proved to be the most effective mitigation measure, as it improves fatigue life independent of water depth and all load cases with $H_s = 2.5$ m were mitigated to have maximum standby time of $t_{sb} \geq 125$ days. In some cases, even the severe load cases with $H_s = 4$ m were mitigated to damage magnitudes below the fatigue budget. Therefore, it is recommended to always mitigate fatigue by favourable vessel headings in combination with a layback length increase.

Based on the above findings, it can be concluded that the weak fatigue properties of lead, used as cable sheathing material, is limiting from fatigue point of view and mitigation measures to counter lead sheath fatigue need to be put in place for wave loadings with $H_s \geq 2.5$ m. With the application of an increased layback length and favourable wave heading, the maximum stand-by time for lead sheaths was found to be 125 days. For load cases with $H_s \geq 4$, the researched mitigation measures were insufficient and fracture of the cable component occurs.

9.2. Recommendations

The single-most important recommendation of this research is the improvement of the validation of the cross-sectional model. Due to scarce cross-sectional cable data and/or test data, the model was only comparatively validated with bending data of four cables. More information from the manufacturers about material alloys and cross-sectional geometry of submarine power cable would be welcome for future research.

Additionally, developing in-house test methods to determine cable bending stiffness is recommended for an increased sample size of test data. In 2003, a first-order method for measuring the rigidity of a polymeric cable was proposed as an international standard, after which an improved second-order method was published in 2015 [40]. However, testing cables in-house requires testing equipment, which is often costly.

Furthermore, the S-N curve approach to fatigue calculation is decreasingly applicable for materials with steep S-N curves. In addition, S-N data corresponding to specific cable components is rare. Therefore, for future work it is recommended that strain-life based fatigue calculation methods are researched. Literature exists for strain-life curves that correspond to submarine power cables [32], [33], [38]. These texts can be used as a basis or as reference to test other fatigue calculation methods.

Since the cable components entered the plastic regime for some load cases, the assumption of linearity breaks down. However, this phenomenon occurred only in severe load cases where the MBR of the cable was breached. Therefore, additional research into mitigation measures for severe load cases

($H_s \geq 4$m) is recommended. Since the increase of tension in the cable yields promising mitigation results, it is interesting to study up to which wave heights this is effective, before violating the maximum allowable tension in the cable. As stated in Chapter 8, load cases should be selected such that cable integrity is not lost. In this text, the number of load cases was limited and therefore no accurate limit for fatigue was determined. If load cases are selected more carefully and varied, defining stand-by times is expected to become more accurate and precise. To accelerate this process, it is also recommended to analyse regular wave JONSWAP approximations. OrcaFlex running times are exponentially decreased when regular waves are modelled, making it possible to analyse a greater amount of load cases. Lastly, as was the case with the cross-sectional model, the fatigue assessment method that was developed in this research would benefit from comparative data of similar fatigue assessment tools. Gaining understanding in the internal fatigue calculation tool of OrcaFlex is therefore recommended.

Bibliography

[1] C. Bathias and A. Pineau. *Fatigue of Materials and Structures: Fundamentals*. ISTE, London, UK, 2010.

[2] Netherlands Aviation Safety Board. Aircraft accident report 92-11. Technical report, Government of the Netherlands, 1992.

[3] Westwood Global Energy Group. Subsea cable tracker 2018-2022. https://www.westwoodenergy.com/product/subsea-cable-tracker-2018-2022/, 2018.

[4] DEME Offshore Netherlands.

[5] Orcina. *OrcaFlex Help Manual 10.3d*. Ulverston, UK, 2019.

[6] DEME Offshore Netherlands. Guideline cable lay operations. Technical report, DEME, 2018.

[7] T Worzyk and S. Langström. Use of aluminium conductors in submarine power cables. 2015.

[8] T. Worzyk. *Submarine Power Cables*. Springer, 2009.

[9] J. Parmar. Cable construction & cable selection. https://electricalnotes.wordpress.com/2016/04/07/cable-construction-cable-selection-part1/, 2016.

[10] G. Skeie, N Sodahl, and O. Steinkjer. Efficient fatige analysis of helix elements in umbilicals and flexible risers: Theory and applications. *Journal of Applied Mathematics*, 246812, 2012.

[11] Cigré. Recommendations for mechanical testing of submarine cables. Technical report, Working Group B1.43, 2015.

[12] J. P. Kurt. Empirical Factors in the Prediction of Helically Armored Cable Axial Stiffness. *Journal of Energy Resources Technology*, 106(4):521–526, 12 1984.

[13] B. Loos. Operability limits based on vessel motions for submarine power cable installation, 2017.

[14] F.C. Campbell. *Fatigue and Fracture - Understanding the Basics*. ASM International, 2012.

[15] C. Lalanne. 1.1.1.2 stress-strain curve, 2014.

[16] R. G. Budynas, J. K. Nisbett, and J. E. Shigley. *Shigley's Mechanical Engineering Design, 9th ed.* McGraw-Hill, 2011.

[17] K. A. Zakaria, S. Abdullah, and M. Ghazali. A review of the loading sequence effects on the fatigue life behaviour of metallic materials. *Journal of Engineering Science and Technology Review*, 9:189–200, 10 2016.

[18] Altair eFatigue LLC. Rainflow counting technical background.

[19] H.J. Sutherland. On the fatigue analysis of wind turbines, 1999.

[20] I. Rychlik. A new definition of the rainflow cycle counting method. *International Journal of Fatigue, pp 119-121*, 1987.

[21] K. Inagaki, J. Ekh, and S. Zahrai. Mechanical analysis of second order helical structure in electrical cable. *International Journal of Solids and Structures 44, pp 1657-1679*, 2006.

[22] J.A. Witz and Z. Tan. On the axial-torsional structural behaviour of flexible pipes, umbilicals and marine cables. *Marine Structures 5, pp 205-227*, 1992.

[23] J.A. Witz and Z. Tan. On the flexural structural behaviour of flexible pipes, umbilicals and marine cables. *Marine Structures 5, pp 229-249*, 1992.

[24] DNV GL. Cross-section analysis of submarine power cables with focus on installation loads, 2017.

[25] I. Kraincanic and Kebadze. Slip initiation and progression in helical armouring layers of unbonded flexible pipes and its effect on pipe bending behaviour. *Journal of Strain analysis*, No 3. Vol. 36, 2001.

[26] A. Nyilas. Fatigue data compilation and evaluation of fatigue on design, 1985.

[27] N.J. Simon, E.S. Drexler, and R.P. Reed. *NIST Monograph 177 - Properties of Copper and Copper Alloys at Cryogenic temperatures*. United States Department of Commerce, Technology Asministration National Institute of Standards and Technology, 1993.

[28] J. Kaufman. *Properties of Aluminium Alloys - Fatigue Data and the Effects ot Temperature, Product From, and Processing*. ASM International, Materials Park, Ohio, 2008.

[29] AgileTek. [Cable name] bending stiffness. Technical report, AgiletTek Engineering Limited, 2017.

[30] J.L. Ocaña, J.A. Porro, M. Diaz, L. Ruiz de Lara, C. Correa, and D. Peral. Fatigue life enhancement of high reliabilit components by laser shock processing. 2015.

[31] Z. Qi, N. Hu, D. Zeng, and X. Su. A stress-based model for fatigue life prediction of high density polyethylene under complpicated loading conditions. *International Journal of Fatigue, pp 281-289*, 119, 2019.

[32] J. Johanson, L. M. Viespoli, A. Alvaro, and F. Berto. Small-and full-scale fatigue testing of lead cable sheathing, 2019.

[33] P. Anelli, D. Donazzi, and W. G. Lawson. The fatigue life of lead alloy e as a sheathing material for submarine power cables. *IEEE Transactions on Power Delivery*, 1988.

[34] Granta Design Limited. Ces edupack software, 2019.

[35] International Standards Organisation, Petroleum and Natural Gas Industries. Design and operation of subsea production systems, part 5: Subsea umbilicals, 2009.

[36] Yong Bai and Qiang Bai. *Subsea Pipelines and Risers*. Elsevier, 2005.

[37] Dr. Henk den Besten. Oe44085 fatigue strength of marine structures - fatigue fundamentals in materials, 2020.

[38] JPS. Cable handling procedure for [cable name] submarine cable. Technical report, J-Power Systems Corporation, 2018.

[39] N. D. P. Barltrop and A. J. Adams. *Dynamics of fixed marine structures*. Butterworth Heinemann for MTD., 3rd edition, 1991.

[40] Janislaw Tarnowski. Improved method of determining bending stiffness of underground cables, 2015.

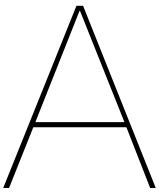

Overview of cable properties

The content of this chapter is confidential and will not be made public.

B

OrcaFlex Fatigue assessment methods

The software package OrcaFlex offers an internal fatigue calculation tool, with several methods of fatigue assessment in marine applications. As stated in the OrcaFlex manual [5], two of these methods are suitable for flexibles like submarine power cables. The following presents an overview of these two methods and their respective advantages over the other method. Furthermore, arguments are presented for why the analysis performed in this thesis does not utilise the fatigue calculation tool for a comparative study of fatigue assessment methods.

B.1. OrcaFlex Fatigue calculation tool: Stress Factors

As OrcaFlex models a power cable as a line of uniform, homogeneous material, the stress in the various components cannot be directly found from the line model. However, the stress factor method allows the calculation of fatigue for pre-defined, separate components of a cross-section of a flexible [5]. A component is defined by its stress factors for tension and bending. The equation to calculate the stresses by which the damage is calculated is given by

$$S = K_t T + K_c(\kappa_x \sin\theta + \kappa_y \theta) \tag{B.1}$$

where

- S Stress [MPa].
- K_t Stress factor for tension $\left[\frac{\text{MPa}}{\text{MN}}\right]$.
- K_c Stress factor for bending $\left[\frac{\text{MPa m}}{\text{rad}}\right]$.
- T Tension [MN].
- κ_x Curvature in x-direction [m^{-1}].
- σ_x Curvature in y-direction [m^{-1}].
- θ Circumferential location of the point where fatigue is to be calculated [rad].

The equation for a point in the cable which is in the plane of bending is thus given by

$$S = K_t T + K_c|\kappa| \tag{B.2}$$

where κ is the curvature of the cable. After defining the components by the stress factors, OrcaFlex performs rainflow counting and subsequently Miner's rule is applied based on user-input S-N curves for the components to yield cable fatigue damage.

It is evident that the stress factor approach is very similar to the external stress calculation method that was presented in this report: Likewise, the stress is defined as the sum of contributions due to tensile and bending strain. In fact, the two methods are theoretically exactly the same when the terms of the local stresses derived in Chapter 4 are used as stress factors in the fatigue calculation tool and hence the stress factor approach can theoretically be used to validate and verify the external stress calculation method.

However, the results obtained by performing the stress factor fatigue analysis, shown in Figure B.1, were questionable and unrealistic. It can be seen from the figure that the magnitude of the damage

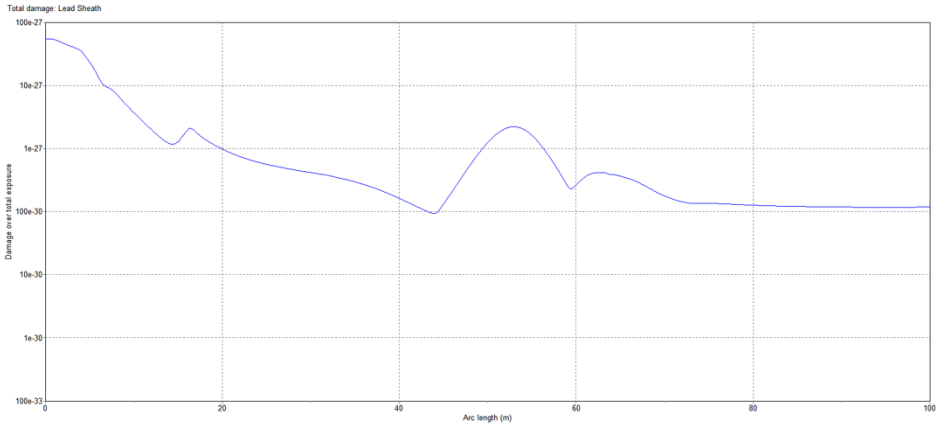

Figure B.1: Damage vs. cable arc length - results for the stress factor fatigue assessment of Cable 1 from Table **??**. Load case: 3 hour JONSWAP[$\Theta = 60°$, $H_s = 2.5$ m, $T_p = 7$ s].

of the lead protective sheath varies from 10^{-25} to 10^{-31}, depending on the cable arc length. The maximum stand-by time would in that case be $3E25$ hours. Moreover, these results were also found for more severe load cases and are very inconsistent with the expectations and results found in Chapter 6. Unfortunately, due to the many assumptions and calculation steps of the fatigue tool, it is difficult to retrace the cause of this. Therefore, it was decided to not use the stress factor method in this research.

B.2. OrcaFlex Fatigue calculation tool: Histograms

A different approach is the histograms method, which does not involve damage calculation. Instead, rainflow cycle counting is performed and the cycles are then arranged into histograms. The correct post-processing is then required to yield fatigue damage of the cable.

The rainflow counting for this method can be performed on a number of variables calculated by OrcaFlex. These variables are, among other:

- ZZ stress σ_{zz}
- Direct tensile stress σ_t
- Bending stress σ_b
- Primary membrane stress $P_m = \sigma_b(R_{mid}, \theta)$
- Primary bending stress $P_b = \sigma_b(R_{out}, \theta) - P_m$

where

(R, θ) Cross-sectional position in the cable ([m], [rad]).

Fatigue analyses in OrcaFlex are usually performed on the ZZ stress, which is the sum of bending and tensile stress, which is again consistent with the first assumption made in Chapter 4. However, it should be kept in mind that the stresses in this method are based on a cable that is modelled as a homogeneous line element. Therefore, contrary to the stress factor calculation method, the different components of a cable cross-section cannot be directly analysed with the fatigue calculation tool.

In this case it is also not possible to relate the bending stresses on the homogeneous cable as determined by OrcaFlex to the local bending stresses in the elements because the bending stress in OrcaFlex is not driectly calculated from the curvature, which is required as input for the local bending stresses.

Furthermore, the curvature cannot be derived from the histograms as the stress time-dependency of the stresses and curvature is lost in output. This is illustrated in Figure B.2.

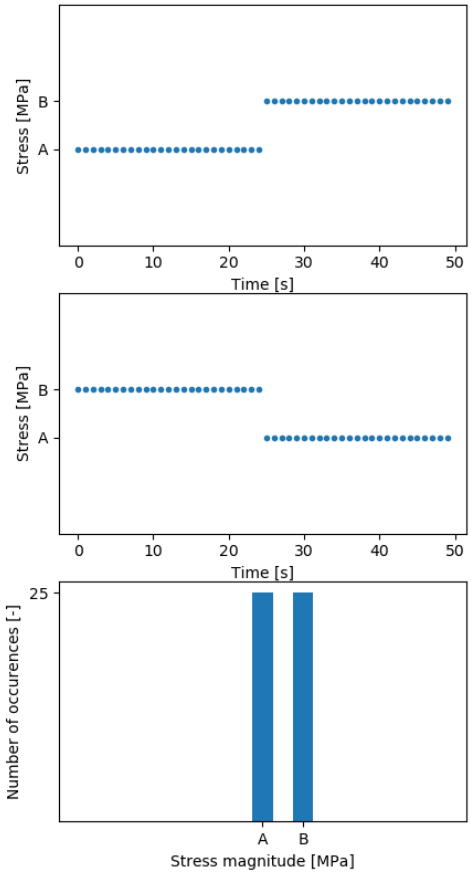

Figure B.2: Two distinctive stress time-histories for which the histogram output is the same. If only the output diagram is available, the stress magnitude cannot be linked to the corresponding time stamp and thus not to the curvature or axial strain occurring at that time stamp.

It can be seen in the figure that two distinctive stress time-histories have the same histogram output. When only this diagram is available, the time stamp corresponding to a certain stress magnitude is lost. Although the time dependency is not relevant for the fatigue analysis, to be able to relate stress magnitude to the corresponding curvature, the time-history is required, which in this case is not possible due to the histograms only tracking the amount of occurrences and not the time of occurrence.

As the histograms calculation method does not provide the possibility to analyse the stresses on the various cable components, its results cannot be compared to the external stress calculation method and thus it was not utilised in this thesis project.

C

Python implementation

The content of this chapter is confidential and will not be made public.

D

Mitigation results

In this appendix, an overview of the fatigue analysis results for loading scenarios with $H_s = 4$m is provided. The results are not further discussed, as they are nearly identical to the results of the load cases that are presented in Chapter 7 in terms of mitigation effectiveness.

D.1. Vessel heading

Infield power cable: Figure D.1
Export power cable: Figure D.2
Interconnector power cable: Figure D.3
Infield power cable: Figure D.4

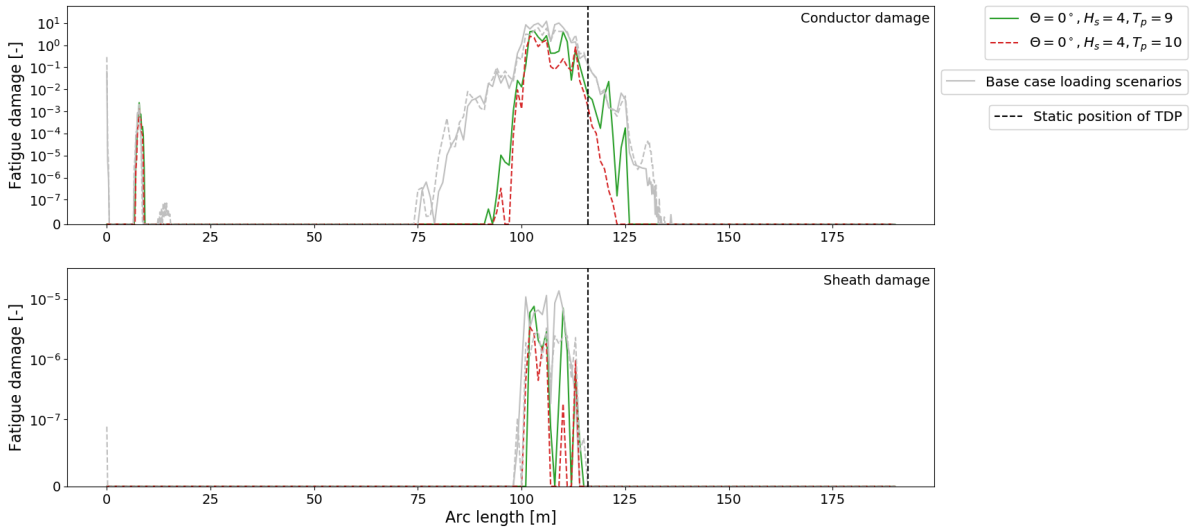

Figure D.1: Vessel heading: Fatigue damage vs. cable arc length for HVAC infield power cable Al conductor (top) and HDPE sheath (bottom). Wave loading direction $\Theta = 0°$. Grey lines correspond to base case damage curves.

Export power cable: D.5
Interconnector power cable: Figure D.6

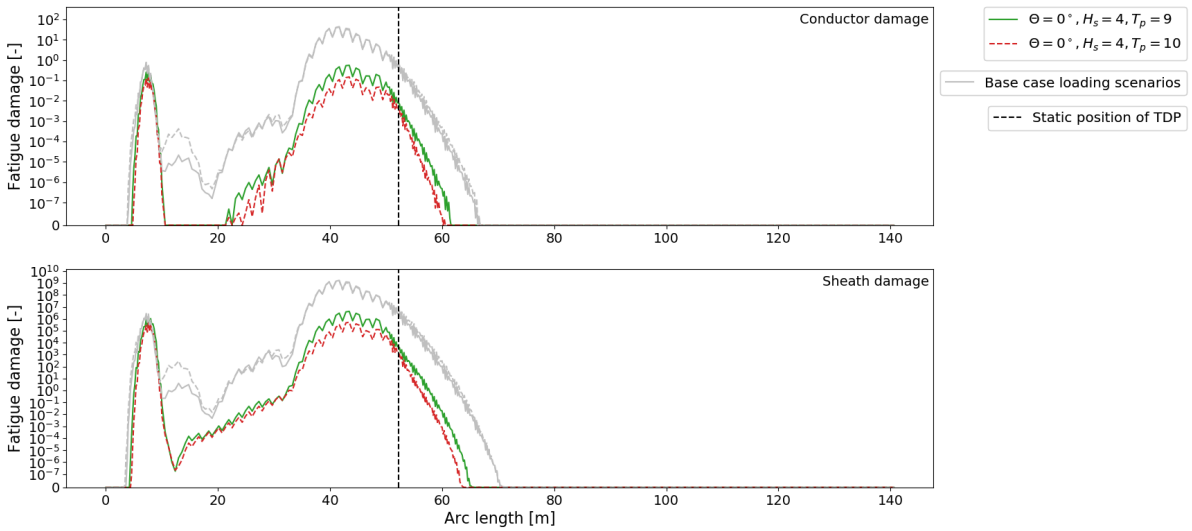

Figure D.2: Vessel heading: Fatigue damage vs. cable arc length for HVAC export power cable Al conductor (top) and Pb sheath (bottom). Wave loading direction $\Theta = 0°$. Grey lines correspond to base case damage curves.

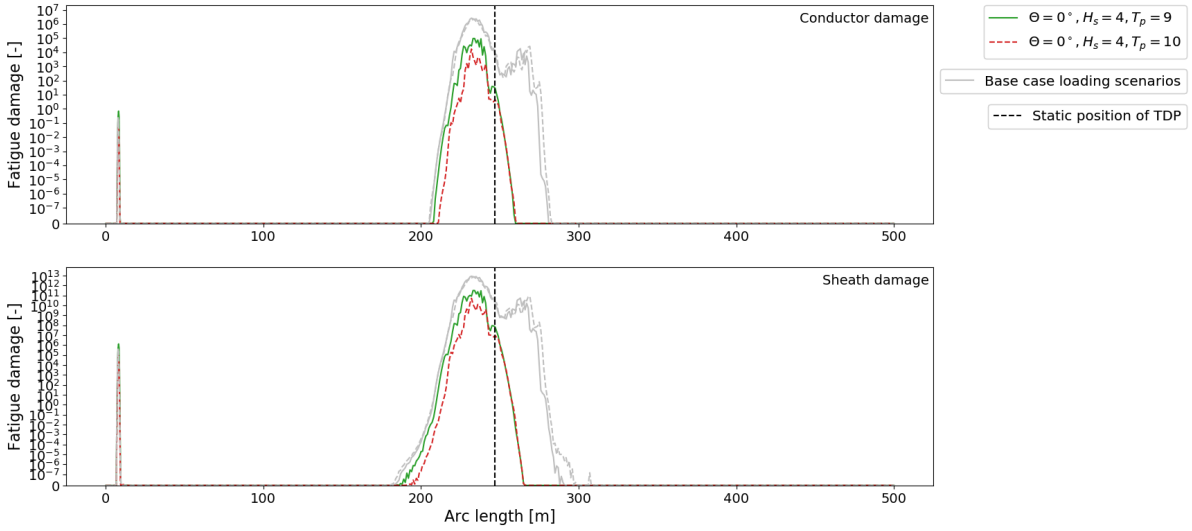

Figure D.3: Vessel heading: Fatigue damage vs. cable arc length for HVDC interconnector power cable Cu conductor (top) and Pb sheath (bottom). Wave loading direction $\Theta = 0°$. Grey lines correspond to base case damage curves.

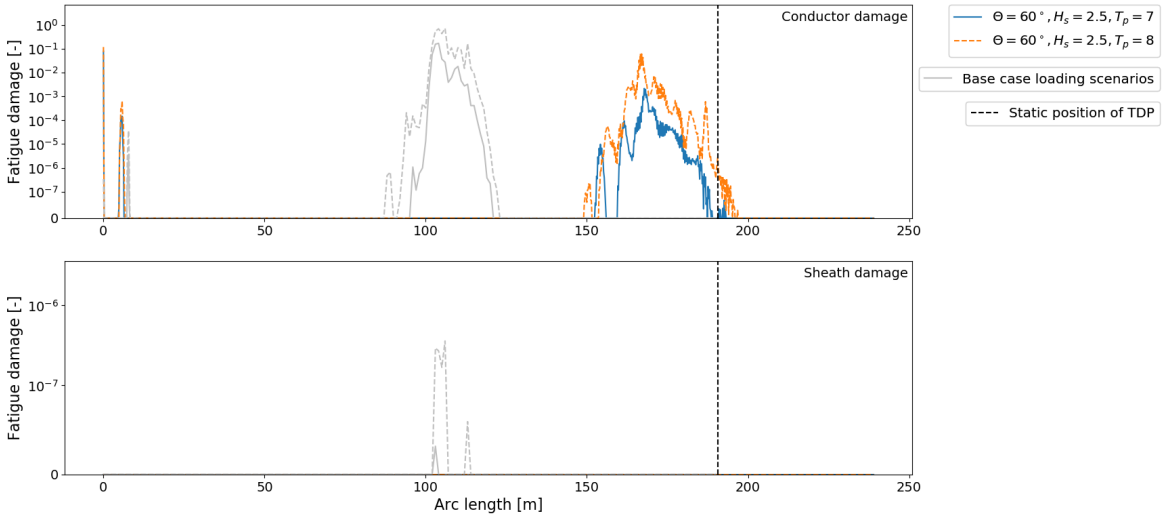

Figure D.4: Layback increase: Fatigue damage vs. cable arc length for HVAC infield power cable Al conductor (top) and HDPE sheath (bottom). Wave loading direction $\Theta = 60°$. Grey lines correspond to base case damage curves.

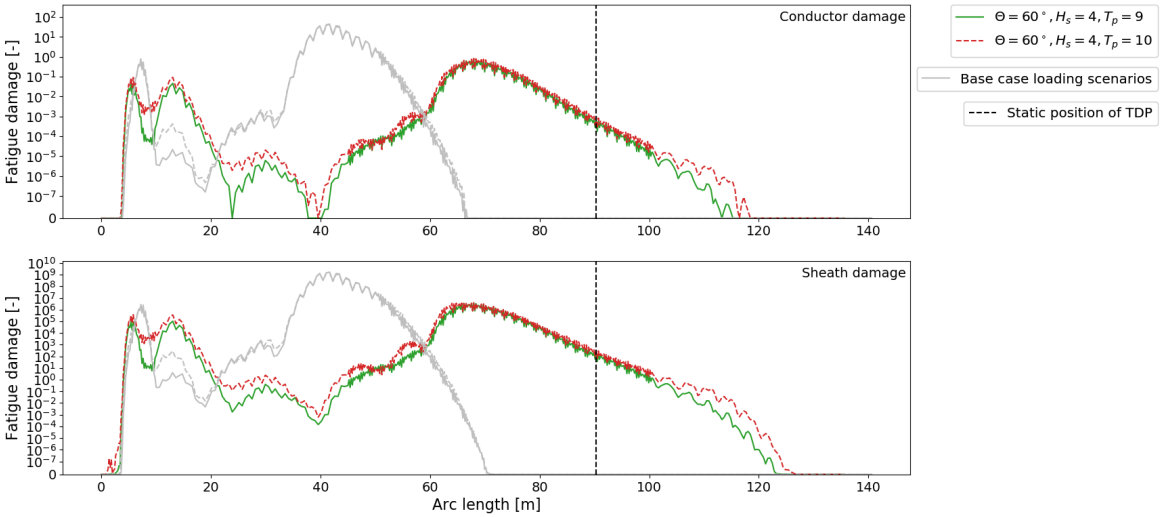

Figure D.5: Layback increase: Fatigue damage vs. cable arc length for HVAC export power cable Al conductor (top) and Pb sheath (bottom). Wave loading direction $\Theta = 60°$. Grey lines correspond to base case damage curves.

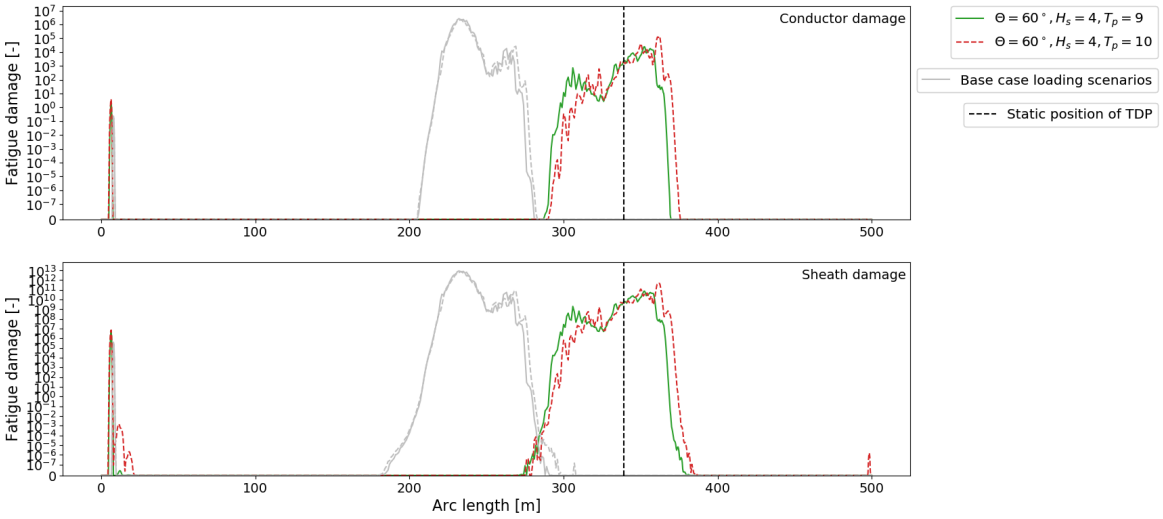

Figure D.6: Layback increase: Fatigue damage vs. cable arc length for HVDC interconnector power cable Cu conductor (top) and Pb sheath (bottom). Wave loading direction $\Theta = 60°$. Grey lines correspond to base case damage curves.

D.2. Lazy wave

Infield power cable: Figure D.7
Export power cable: D.8
Interconnector power cable: Figure D.9

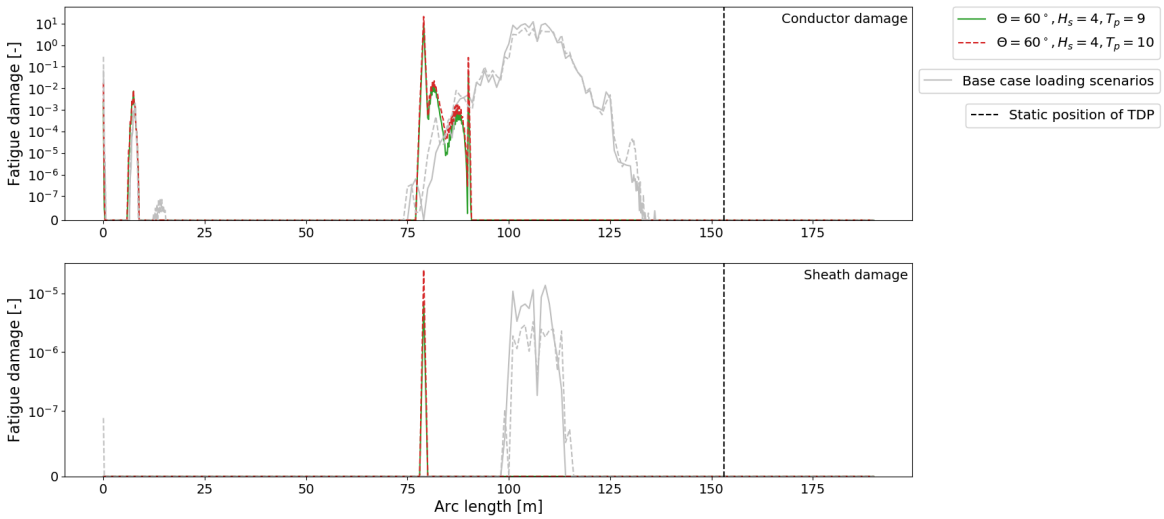

Figure D.7: Lazy wave: Fatigue damage vs. cable arc length for HVAC infield power cable Al conductor (top) and HDPE sheath (bottom). Wave loading direction $\Theta = 60^{\circ}$.

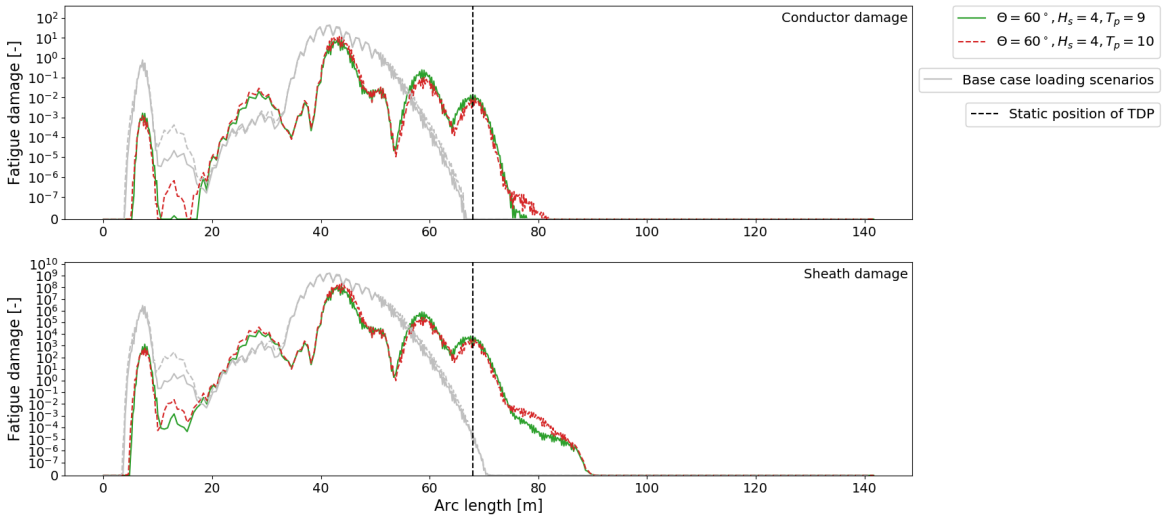

Figure D.8: Lazy wave: Fatigue damage vs. cable arc length for HVAC export power cable Al conductor (top) and Pb sheath (bottom). Wave loading direction $\Theta = 60^{\circ}$.

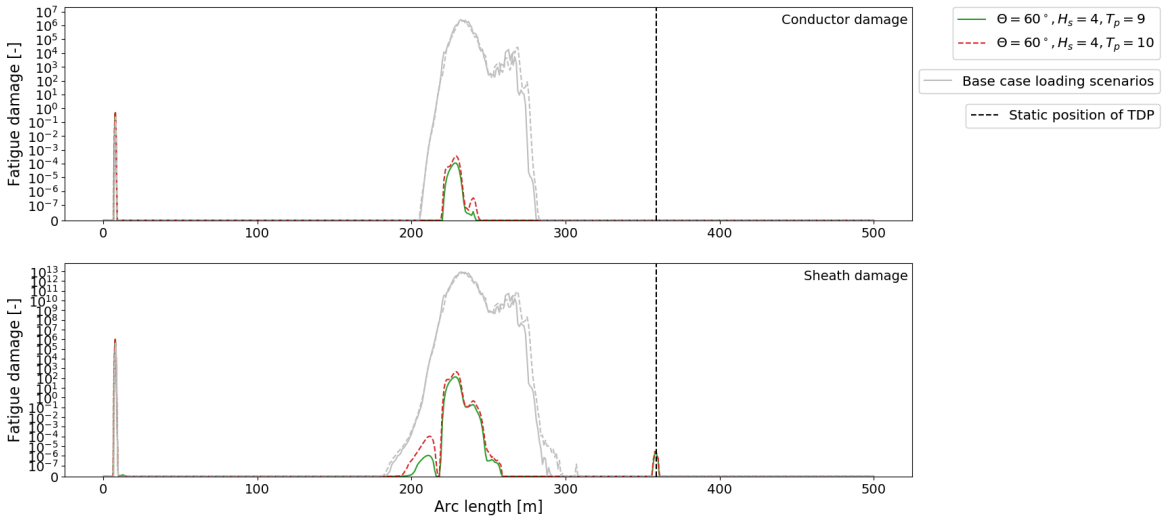

Figure D.9: Lazy wave: Fatigue damage vs. cable arc length for HVDC interconnecting power cable Cu conductor (top) and Pb sheath (bottom). Wave loading direction $\Theta = 60^{\circ}$.

D.3. Bend restrictor

Infield power cable: Figure D.10
Export power cable: D.11
Interconnector power cable: Figure D.12

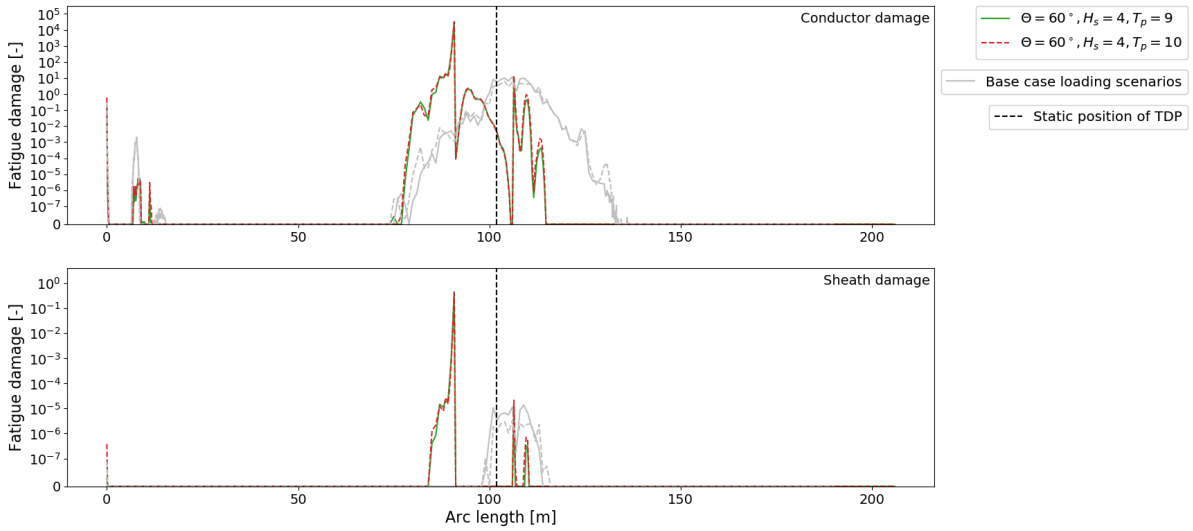

Figure D.10: Bend restrictor: Fatigue damage vs. cable arc length for HVAC infield power cable Al conductor (top) and HDPE sheath (bottom). Wave loading direction $\Theta = 60°$. Grey lines correspond to base case damage curves.

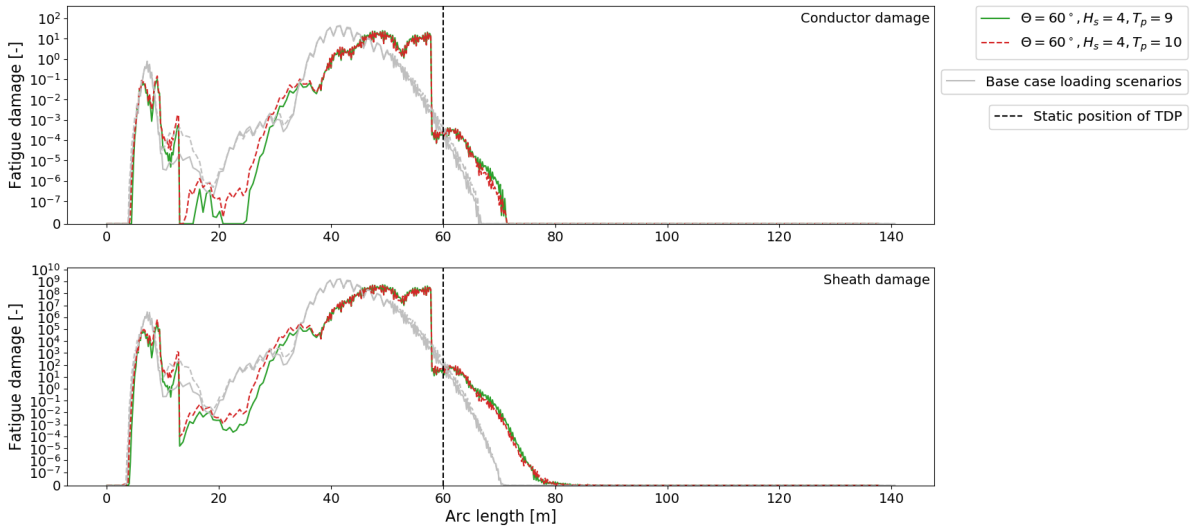

Figure D.11: Bend restrictor: Fatigue damage vs. cable arc length for HVAC export power cable Al conductor (top) and Pb sheath (bottom). Wave loading direction $\Theta = 60°$. Grey lines correspond to base case damage curves.

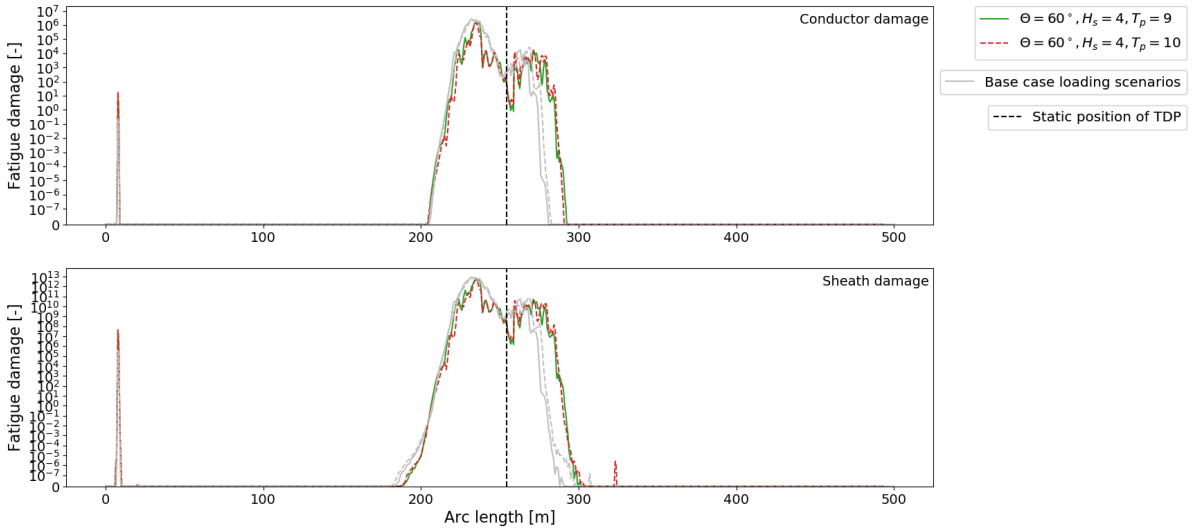

Figure D.12: Bend restrictor: Fatigue damage vs. cable arc length for HVDC interconnector power cable Cu conductor (top) and Pb sheath (bottom). Wave loading direction $\Theta = 60^{\circ}$. Grey lines correspond to base case damage curves.

D.4. Layback increase and vessel heading

3x300mm^2 Al HVAC infield power cable: Figure D.13
3x1800mm^2 Al HVAC export power cable: D.14
HVDC interconnector power cable: Figure D.15

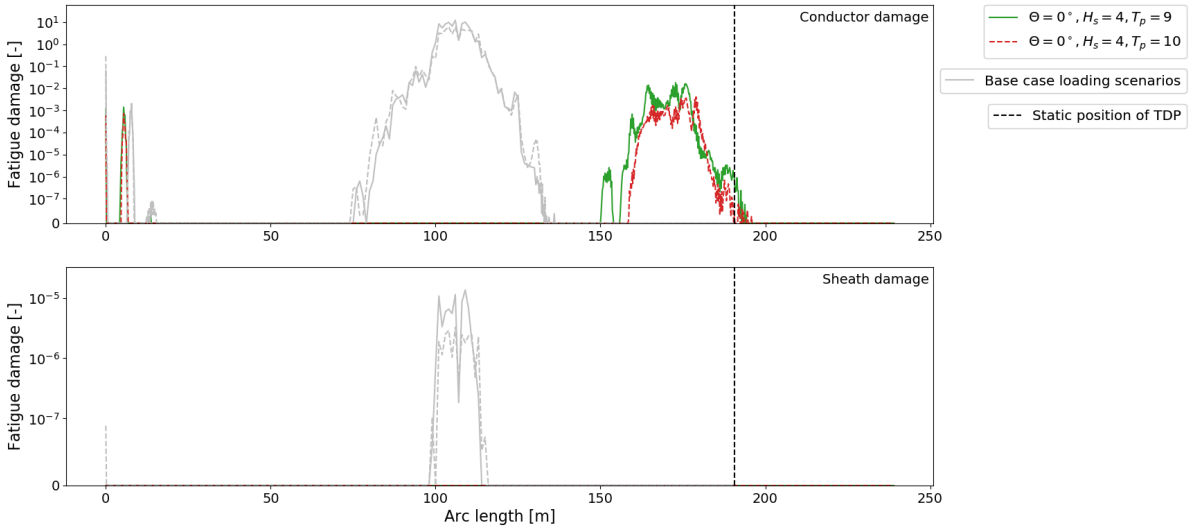

Figure D.13: Layback increase: Fatigue damage vs. cable arc length for HVAC infield power cable Al conductor (top) and HDPE sheath (bottom). Wave loading direction $\Theta = 0^{\circ}$.

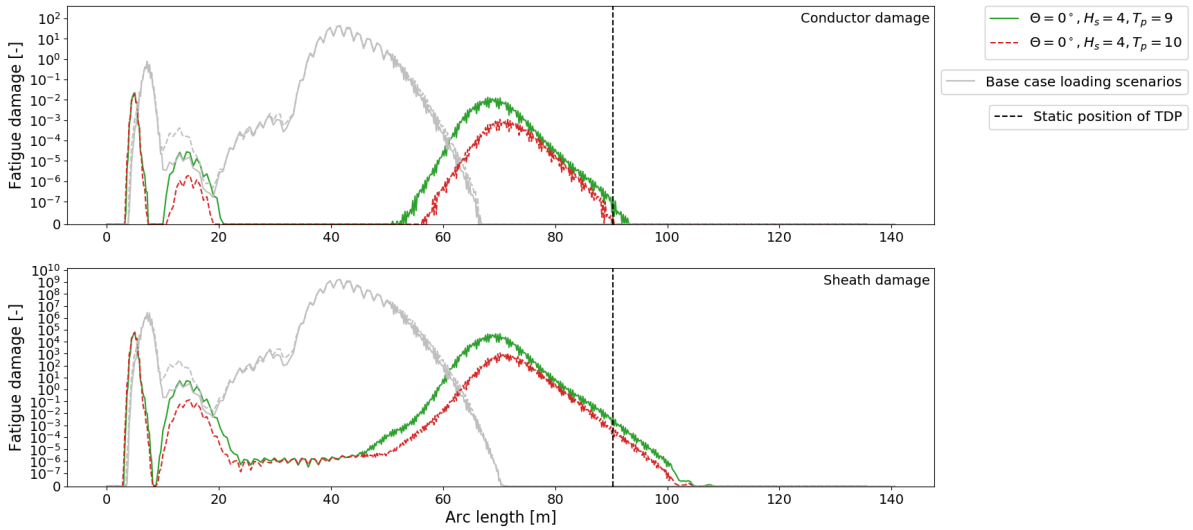

Figure D.14: Layback increase: Fatigue damage vs. cable arc length for HVAC export power cable Al conductor (top) and Pb sheath (bottom). Wave loading direction $\Theta = 0°$.

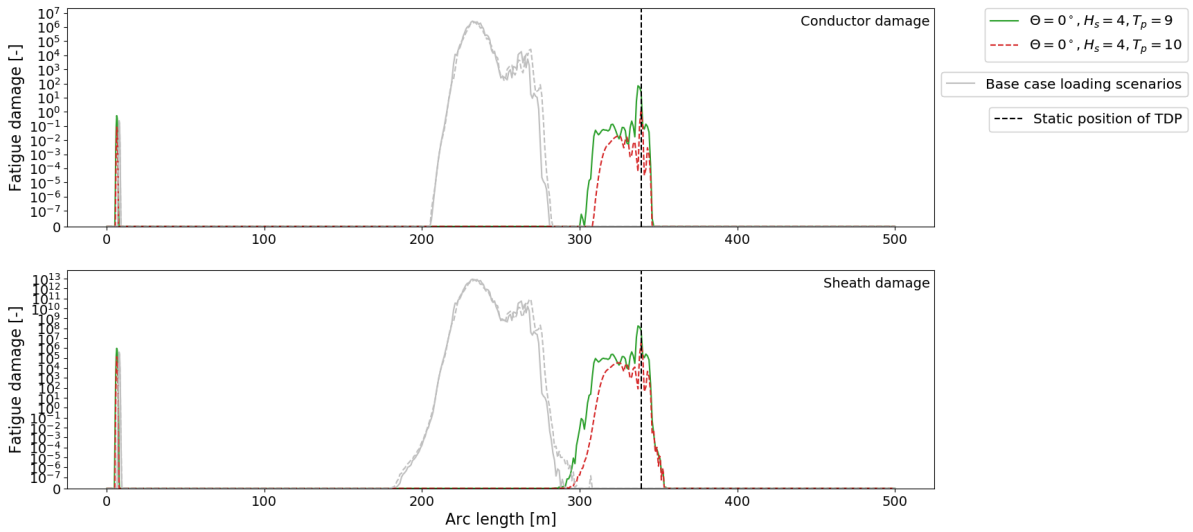

Figure D.15: Layback increase: Fatigue damage vs. cable arc length for HVDC interconnector power cable Cu conductor (top) and Pb sheath (bottom). Wave loading direction $\Theta = 0°$.